



HAL
open science

Comparison of Human and Experimental Pulmonary Veno-Occlusive Disease

Grégoire Manaud, Esther Nossent, Mélanie Lambert, Maria-Rosa Ghigna,
Angele Boet, Maria-Candida Vinhas, Benoît Ranchoux, Sébastien Dumas,
Audrey Courboulin, Barbara Girerd, et al.

► **To cite this version:**

Grégoire Manaud, Esther Nossent, Mélanie Lambert, Maria-Rosa Ghigna, Angele Boet, et al.. Comparison of Human and Experimental Pulmonary Veno-Occlusive Disease. *American Journal of Respiratory Cell and Molecular Biology*, 2020, Epub ahead of print. 10.1165/rcmb.2019-0015OC . inserm-02561102v2

HAL Id: inserm-02561102

<https://inserm.hal.science/inserm-02561102v2>

Submitted on 2 Feb 2024

HAL is a multi-disciplinary open access archive for the deposit and dissemination of scientific research documents, whether they are published or not. The documents may come from teaching and research institutions in France or abroad, or from public or private research centers.

L'archive ouverte pluridisciplinaire **HAL**, est destinée au dépôt et à la diffusion de documents scientifiques de niveau recherche, publiés ou non, émanant des établissements d'enseignement et de recherche français ou étrangers, des laboratoires publics ou privés.



HAL
open science

Comparison of Human and Experimental Pulmonary Veno-Occlusive Disease

Grégoire Manaud, Esther J Nossent, Mélanie Lambert, Maria-Rosa Ghigna,
Angèle Boët, Maria-Candida Vinhas, Benoit Ranchoux, Sébastien J Dumas,
Audrey Courboulin, Barbara Girerd, et al.

► **To cite this version:**

Grégoire Manaud, Esther J Nossent, Mélanie Lambert, Maria-Rosa Ghigna, Angèle Boët, et al..
Comparison of Human and Experimental Pulmonary Veno-Occlusive Disease. *American Journal of
Respiratory Cell and Molecular Biology*, 2020, 63 (1), pp.118 - 131. 10.1165/rmb.2019-0015oc .
hal-04433099

HAL Id: hal-04433099

<https://hal.science/hal-04433099>

Submitted on 1 Feb 2024

HAL is a multi-disciplinary open access archive for the deposit and dissemination of scientific research documents, whether they are published or not. The documents may come from teaching and research institutions in France or abroad, or from public or private research centers.

L'archive ouverte pluridisciplinaire **HAL**, est destinée au dépôt et à la diffusion de documents scientifiques de niveau recherche, publiés ou non, émanant des établissements d'enseignement et de recherche français ou étrangers, des laboratoires publics ou privés.

Comparison of Human and Experimental Pulmonary Veno-Occlusive Disease

Grégoire Manaud Msc^{1,2,3*}, Esther J. Nossent MD^{4*}, Mélanie Lambert PhD^{1,2,3}, Maria-Rosa Ghigna⁵, Angèle Boët, MD, PhD⁶, Maria-Candida Vinhas ⁶, Benoit Ranchoux PhD^{1,2,3}, Sébastien J. Dumas PharmD-PhD^{1,2,3}, Audrey Courboulin PhD^{1,2,3}, Barbara Girerd MD, PhD^{1,2,3}, Florent Soubrier MD-PhD⁷, Juliette Bignard MSc⁷, Olivier Claude PhD⁷, Florence Lecerf Msc^{1,2,3}, Aurélie Hautefort PhD^{1,2,3}, Monica Florio PhD⁸, Banghua Sun⁸, Sophie Nadaud PhD⁷, Stijn E. Verleden PhD⁹, Séverine Remy PhD¹⁰, Ignacio Anegón, MD¹⁰, Harm Jan Bogaard MD-PhD⁴, Olaf Mercier MD-PhD^{1,2,3,11} Elie Fadel MD-PhD^{1,2,3,11}, Gérald Simonneau MD-PhD^{1,2,3}, Anton Vonk Noordegraaf MD-PhD⁴, Katrien Grünberg MD-PhD⁴, Marc Humbert MD-PhD^{1,2,3}, David Montani MD-PhD^{1,2,3}, Peter Dorfmüller MD-PhD^{1,2,3,5,12}, Fabrice Antigny PhD^{1,2,3}§, and Frédéric Perros PhD^{1,2,3,13}§

1. *Univ Paris-Sud, Faculté de Médecine, Université Paris-Saclay, Le Kremlin-Bicêtre, France*
2. *AP-HP, Centre de Référence de l'Hypertension Pulmonaire, Département Hospitalo-Universitaire (DHU) Thorax Innovation, Service de Pneumologie et Réanimation Respiratoire, Hôpital de Bicêtre, Le Kremlin-Bicêtre, France.*
3. *UMRS 999, INSERM and Univ. Paris-Sud, Laboratoire d'Excellence (LabEx) en Recherche sur le Médicament et l'Innovation Thérapeutique (LERMIT), Centre Chirurgical Marie Lannelongue, Le Plessis Robinson, France.*
4. *Amsterdam UMC, Vrije Universiteit Amsterdam, Pulmonary Medicine, Amsterdam Cardiovascular Sciences, De Boelelaan 1117, Amsterdam, The Netherlands*
5. *Dept of Pathology, Hôpital Marie Lannelongue, Le Plessis-Robinson, France.*
6. *Dept of Research, Hôpital Marie Lannelongue, Le Plessis-Robinson, France.*
7. *INSERM UMR_S 956, Université Pierre and Marie Curie Université (Paris 06), Paris, France.*
8. *Cardio-Metabolic Disorders, Amgen Research, Amgen Inc, Thousand Oaks, USA.*
9. *BREATH-Department of CHROMETA- KU Leuven, Leuven Belgium*

10. INSERM UMR 1064-Center for Research in Transplantation and Immunology-ITUN et Transgenic Rats and Immunophenomic Platform, Nantes, France

11. Service de Chirurgie Thoracique, Centre Chirurgical Marie Lannelongue, Le Plessis-Robinson, France.

12. Department of Pathology, University of Giessen and Marburg Lung Center (UGMLC), Justus-Liebig University Giessen, German Center for Lung Research (DZL), Giessen, Germany.

13. Centre de Recherche de l'Institut Universitaire de Cardiologie et de Pneumologie de Québec, Laval University, QC, Canada

* and \$: equally contributed

Corresponding authors:

Fabrice Antigny, INSERM U999, Centre Chirurgical Marie Lannelongue, 133, Avenue de la Résistance, F-92350 Le Plessis Robinson, France. Fax: (33) 1 40 94 25 22, Tel: (33) 1 40 94 25 15, e-mail: fabrice.antigny@u-psud.fr

Frédéric Perros, INSERM U999, Centre Chirurgical Marie Lannelongue, 133, Avenue de la Résistance, F-92350 Le Plessis Robinson, France. Fax: (33) 1 40 94 25 22, Tel: (33) 1 40 94 25 33, e-mail: frederic.perros@inserm.fr

Authors' contributions :

Conception and design: E.J.N., I.A., D.M., P.D., F.A., and F.P.

Acquisition of data: G.M., E.J.N., M.L., M.R.G., M.C.V., A.B., B.R., S.J.D., A.C., J.B., O.C., F.L., A.H., M.F., B.S., S.E.V., S.R., F.A., and FP

Analysis and interpretation: G.M., E.J.N., M.L., M.R.G., A.B., B.R., S.J.D., A.C., F.L., A.H., M.F., B.S., P.D., F.A., and FP

Drafting the manuscript for important intellectual content: G.M., E.J.N., M.R.G., B.G., F.S., S.N., HJ. B, O.M., E.F., G.S., A.VN., K.G., M.H., D.M., P.D., F.A., and F.P.

Supports:

This work was funded the French National Research Agency (Agence Nationale de la Recherche, ANR; grant: ANR-13-JSV1-0011-01) and by Pulmonary Vascular Research Institute (PVRI) Bmpr2 Research Grant supported by the Dinosaur Trust (to F.P.), and by DHU TORINO (Département Hospitalo-Universitaire Thorax Innovation) and AP-HP. This work was also supported by INSERM, Université Paris-Sud, Université Paris-Saclay and Hôpital Marie Lannelongue. G.M. is 2017 Laureate of Fonds de Recherche en Santé Respiratoire et de la Fondation du Souffle. F.A. receives funding from the Fondation du Souffle et Fonds de Dotation Recherche en Santé Respiratoire, from the Fondation Lefoulon-Delalande and from the Fondation Legs Poix. F.A. also received funding from the National Funding Agency for Research: ANR-18-CE14-0023. M.L. is supported by Therapeutic Innovation Doctoral School (ED569). E.J.N. was supported by an ERS (European Respiratory Society) PAH Long-Term Research Fellowship. S.E.V is supported by a post-doctoral fellowship of FWO (12G8718N) and a grant from KU Leuven (C24/18/073).

Running title: Comparison of human and experimental PVOD

This article has an online data supplement, which is accessible from this issue's table of content online at www.atsjournals.org.

ABSTRACT

Pulmonary veno-occlusive disease (PVOD) occurs in humans either as heritable form (hPVOD) due to biallelic inactivating mutations of *EIF2AK4* (encoding GCN2), or as a sporadic form at older age (sPVOD). The chemotherapeutic agent Mitomycin C is a potent inducer of PVOD in humans and in rats (MMC-PVOD). Here we compared human hPVOD and sPVOD, and MMC-PVOD pathophysiology at the histological, cellular and molecular levels to unravel common altered pathomechanisms. MMC-exposure in rats was primarily associated with arterial and microvessels remodeling and secondarily followed by venous remodeling, when PVOD became symptomatic. In all forms of PVOD tested, there were convergent GCN2-dependent but eIF2 α -independent pulmonary protein overexpression of heme oxygenase 1 (HO-1) and CCAAT-enhancer-binding protein (C/EBP) homologous protein (CHOP), two downstream effectors of GCN2 signaling and endoplasmic reticulum (ER) stress. In human PVOD samples, CHOP immunohistochemical staining mainly labeled endothelial cells in remodeled veins and arteries. Strong HO-1 staining was observed only within capillary hemangiomatosis foci, where intense microvascular proliferation occurs. HO-1 and CHOP stainings were not observed in control and pulmonary arterial hypertension lung tissues, supporting the specificity for CHOP and HO-1 involvement in PVOD pathobiology. *In vivo* loss of GCN2 (*EIF2AK4* mutations carriers and *Eif2ak4*^{-/-} rats) or *in vitro* GCN2 inhibition in cultured pulmonary artery endothelial cells (PAECs) using pharmacological and siRNA approaches demonstrated that GCN2 loss-of-function negatively regulates BMP-dependent SMAD1/5/9 signaling. Exogenous BMP9 was still able to reverse GCN2 inhibition-induced PAECs proliferation. In conclusion, we identified CHOP and HO-1 inhibition, and BMP9 as potential therapeutic options for PVOD.

Keywords: Pulmonary hypertension, pulmonary veno-occlusive disease, GCN2, SMAD signaling, BMPR-II.

INTRODUCTION

Pulmonary Veno-Occlusive Disease (PVOD) is a rare form of pulmonary hypertension (PH) (1) characterized by widespread fibrous intimal proliferation and muscular hyperplasia of septal veins and preseptal venules, pulmonary capillary congestion and hemangiomas-like proliferation. PVOD is associated with a poor response to available therapy for pulmonary arterial hypertension and to date, lung transplantation remains the treatment of choice (1, 2).

The pathobiology of PVOD has been poorly explored. However, biallelic mutations in the eukaryotic initiation factor 2 alpha kinase 4 gene (*EIF2AK4*) cause autosomal recessive heritable PVOD (hPVOD) (3). Sporadic form of PVOD (sPVOD) are also described, in particular in a context of occupational exposure to organic solvents or treatment by specific chemotherapeutic agents (1, 2, 4).

The *EIF2AK4* gene codes for GCN2 (general control nonderepressible 2), a serine-threonine kinase described to change gene expression in response to amino acid deprivation and to play a key role in immune tolerance to cells undergoing apoptosis (5). GCN2 belongs to a family of 4 kinases phosphorylating the α -subunit of eukaryotic initiation factor 2 (eIF2 α). These 4 serine-threonine kinases including GCN2, PERK (PKR-like ER kinase), PKR (protein kinase double-stranded RNA-dependent) and HRI (heme-regulated inhibitor) are involved in the control of general translation in response to various cellular stresses (6). Phosphorylation of eIF2 α protects cells by reducing protein synthesis and regulating changes in expression of genes involved in stress response, defined as “integrated stress response” (ISR) (6). These genes are involved in a variety of cellular mechanisms, such as resistance to oxidative stress, inflammation, cell survival, autophagy or angiogenesis. However, the role of GCN2 and ISR in pulmonary vascular remodeling leading to PVOD still remains to be elucidated. Indeed, the lack of animal models recapitulating PVOD disease and the lack of molecular studies on human PVOD explain the lack of knowledge regarding this condition. Only Lathen C and colleagues identified that the suppression of the Ets family transcription factors (ERG), promotes the development of a PVOD-like disease in mice (7).

Our group has previously demonstrated the responsibility of mitomycin C (MMC) both in humans and in a rat model of the disease (MMC-PVOD) and other toxic compounds in human sPVOD (8).

Here we compared hPVOD, sPVOD and MMC-PVOD pathophysiology in order to obtain more insight into the histological, cellular and molecular alterations steering disease progression. This comparison should allow the discovery of common altered signaling pathways that could be targeted by novel therapeutic agents. Although most attention has been brought to post-capillary vascular remodeling, pulmonary arterial intimal fibrosis and thickening of the muscular media are always observed in PVOD and it is still unclear, whether these lesions represent primary changes, or whether they are the secondary cause of post-capillary remodeling. We clarified this point by quantifying and qualifying the progressive vascular remodeling occurring in the MMC-PVOD model.

METHODS

Methods section is provided in the Supplementary material.

RESULTS

Human data are exposed after animal data.

Analysis of the MMC-PVOD model.

Histopathology of PVOD induced by MMC exposure in rat

Morphometric analysis of all 5 groups (week 1, 2, 3, 4, and 5 after MMC-exposure) and controls showed initial narrowing within pulmonary arteries of a diameter between 70 and 250 μm , with an important and rather sudden reduction of the patent lumen area of approximately 50% from week 1 (after MMC-exposure) (Figure 1). These first changes were followed by mild, but significant muscularization of microvessels of under 70 μm in diameter from week 2 on, that intensified with moderate and severe remodeling from week 4 (Figure 1 and 2). Significant pulmonary venous patent lumen area reduction of approximately 20% was observed from week 3 and intensified with lumen reduction to 50% and more in the following 2 weeks (Figure 1 and 2).

Concerning the quality of pulmonary arterial remodeling media hyperplasia/hypertrophy was the prominent finding in early stages, while intimal fibrosis was observed only at week 5 (Figure 2C).

Disease progression

Compensatory RV hypertrophy due to increased pulmonary arterial pressures, as qualified by the Fulton index (RV/(LV+S)), was significantly increased as compared to controls at the 4th week of our kinetic study (Figure 2F), demonstrating that PH becomes symptomatic 4 weeks after the first MMC exposure.

Molecular characterization of the MMC-induced PVOD rat model

Overexpression of the integrated stress response (ISR) kinases and ISR effectors

Pulmonary GCN2 content was dramatically decreased as soon as 2 weeks after MMC exposure and was weakly expressed along the progression of the disease. More precisely, GCN2 expression was progressively decreased along the disease progression; by 40% after 1 week, 50% after 2 weeks of MMC-exposure and by 85-90% after 4 and 5 weeks after MMC-exposure (Figure 3A). Parallel to GCN2 loss of expression, we observed a progressive and sequential overexpression of PERK (1.7, 1.8, 1.6 and 1.9 fold increase respectively at W2, W3, W4 and W5), PKR (2.5, 5 and 6 fold increase respectively at W3, W4 and W5) and GCN1 (GCN2 coactivator) (2 and 2.5 fold increase respectively at W3, W4) (Figure 3A).

As illustrated in Figure 3, stress responses kinases are known to phosphorylate the α -subunit of eIF2 α which in turn should activate the activating transcription factor 4 (ATF4). Unexpectedly the phosphorylation state of eIF2 α was not significantly affected (Figure E1 in the data supplement) and paradoxically the downstream effector of eIF2 α , ATF4 was strongly increased 4 and 5 weeks after MMC-exposure (Figure 3B). ATF4 is known to induce expression of another transcription factor, CCAAT- enhancer-binding protein (C/EBP) homologous protein (CHOP) and to induce heme oxygenase 1 (HO-1) (9). As displayed in Figure 3B, CHOP and HO-1 expression were 3-4 fold increased 4 and 5 weeks after MMC-exposure.

BMPRII and TGF β imbalance in lung from MMC-exposed rats

Impaired BMPRII signaling is a common pathogenic mechanism of various forms of pulmonary arterial hypertension (PAH) (10). We showed that lung BMPRII expression was not modified in PVOD animals (Figure 3C) while the phosphorylation status of SMAD1/5/8 (downstream BMPRII signaling) was severely reduced 4 weeks and beyond after MMC-exposure (Figure 3C). The phosphorylation status of SMAD2/3 (TGF β signaling) was remarkably increased 4 and 5 weeks after MMC exposure (Figure 3C).

Upregulation of mitogenic, anti-apoptotic and differentiation pathways in MMC-exposed rats

The MAPK pathways play a critical role in the regulation of cell proliferation (11). We showed a progressive increased phosphorylation of P38 from the third week to the fifth week after MMC-exposure. We also observed an increase in ERK1/2-phosphorylation 4 and 5 after MMC-exposure (Figure E2 in the data supplement). This activation of the MAPK signaling pathway suggests that proliferation processes are ongoing at these time points and contribute to the pulmonary vascular remodeling observed in MMC- rats. Accordingly, expression of the Proliferating Cell Nuclear Antigen (PCNA, proliferation marker) was significantly increased at these time points (10 fold at W4 and W5) (Figure E2 in the data supplement), confirming the unleashed proliferation of pulmonary vascular cells in MMC-exposed lungs (12).

In addition, we demonstrated a strong increase in the expression of the anti-apoptotic protein survivin at 4 and 5 weeks after MMC-exposure (Figure E2 in the data supplement) that can participate in the obstructive accumulation of death-resistant pulmonary vascular cells in MMC-exposed rats.

In line with the upregulation of mitogenic and anti-apoptotic pathways, we found that microvascular and venous lesions were predominantly characterized by muscular hyperplasia; intimal fibrosis was generally not observed. Foci of alveolar wall thickening suggestive of pulmonary capillary hemangiomatosis became just perceivable at week 3 and showed obvious progression at week 4 and 5 (Figure E3 in the data supplement). In relation to the aberrant growth and accumulation of pulmonary

mesenchymal cells we demonstrated that the mesenchymal transition-promoting transcription factor Twist1 was severely increased 4 and 5 weeks after MMC-exposure (Figure E4 in the data supplement). The expression of p120-catenin, which maintains cell-cell junction, was dramatically decreased during the 3 last weeks of disease induced by MMC exposure (W3, W4 and W5) (Figure E5 in the data supplement).

Late apoptosis and inflammation

Despite pulmonary upregulation of mitogenic and anti-apoptotic pathways 4 and 5 after MMC-exposure, we also showed that the active form of Caspase 3 (cleaved caspase 3), which is a critical executioner of apoptosis, was dramatically increased in lungs from MMC-exposed rats at the same time points (Figure E6). Cleaved Caspase 9 expression was not significantly affected by MMC-exposure (data not shown). This apoptosis could be related to the pulmonary inflammation (high leukocyte turnover) that is detected through the pan-leukocyte marker CD45 protein quantification in the same time points in MMC-PVOD rats. Significant pulmonary inflammation was also detected in sPVOD (Figure E7 in the data supplement).

Down regulation of KCNK3 current in PASMC isolated from MMC-exposed rats

Mutations in the *KCNK3* gene have been recognized as a new genetic cause of PAH (13). We recently demonstrated that loss *KCNK3* function is a hallmark of PAH (14) and that *Kcnk3* loss-of-function mutation in rat predisposes to the development of PH (15). *KCNK3* function was evaluated at two time points (week 3 and week 5 post-MMC exposure and in controls) by whole-cell patch-clamp experiments on freshly isolated rat PASMCs. *KCNK3* current (I_{KCNK3}) was evaluated using the selective *KCNK3* blocker A293 (Figure 4A). At 200 nmol/L, A293 reduced approximately K^+ current by 30-40% in control PASMC and represent the I_{KCNK3} (or A293-sensitive current) (Figure 4A). At 3 and 5 weeks after MMC-exposure, I_{KCNK3} was significantly reduced by 80% compared to control conditions (Figure 4B, left panel).

Moreover, the global K^+ current was reduced in PASMC isolated from MMC-rats by 50% (Figure 4B, Middle panel) and the A293-Insensitive- K^+ current by 40% (Figure 4B, right panel), indicating that voltage- K^+ current (K_v channels) were also significantly reduced in MMC-rats.

Late increase in pulmonary serotonin content

Serotonin, an old actor of PH pathogenesis is considered to be a key driver of pulmonary arterial remodeling in PAH (16). However, in our PVOD model, pulmonary serotonin content was only increased at the very end of PVOD development (W5) (Figure E8 in the data supplement) when PH and pulmonary vascular remodeling are already established, arguing for a late role and/or a marker of PH severity.

Downregulation of Ets transcription factor ERG in experimental PVOD and in human PVOD.

Lathen and colleagues demonstrated that the loss of ERG is crucial for endothelial homeostasis in pulmonary veins in mice (7). We showed that lung protein expression of ERG was lost 4 and 5 weeks after MMC-exposure when PH became symptomatic (Figure E9A in the data supplement) and drastically reduced in hPVOD and sPVOD patients (Figure E9B in the data supplement).

Human data.

Upregulation of CHOP and HO-1, p-SMAD2/3 and downregulation of p-SMAD1/5/9 in hPVOD and sPVOD patients

We measured the protein expression of ISR kinases in the lungs from hPVOD and sPVOD patients and non PVOD patients (Figure 5A and Figure E10 in the data supplement). We found that GCN2 expression was abolished in hPVOD patients as compared with controls. We found a great heterogeneity for GCN2 expression in the sporadic forms of the disease, from total loss to nearly normal expression (Figure 5A and Figure E10 in the data supplement). It must reflect the very diverse etiologies of these idiopathic PVODs. Unlike MMC-PVOD, the lung expression of GCN1, PERK and PKR were not significantly modified in hPVOD and sPVOD patients compared to controls patients (Figure 5A). As observed in experimental PVOD, the phosphorylation status of eIF2 α was unchanged as compared to control patients (Figure E1 in the data supplement).

Regarding ISR kinase effectors, we found that ATF4 expression was unaffected in hPVOD and sPVOD (Figure 5B). However, the expression of downstream effectors CHOP and HO-1 was significantly increased in hPVOD patients (2-fold increase) and in sPVOD patients (3.6-fold increase) (Figure 5B), as we observed in rat MMC-PVOD.

We found that p-SMAD1/5/8 was significantly reduced in hPVOD patients (60% decrease) while BMPRII expression was unchanged (Figure 5C). Moreover, SMAD2/3 phosphorylation was higher in

sPVOD patients as compared to control patients (3-fold increase when expression normalized to β -actin, no significant difference when normalized to total SMAD2/3) (Figure 5C).

Specific CHOP and HO-1 expression in pulmonary vascular lesions of PVOD

Since we highlighted an overexpression of HO-1 and CHOP, two downstream important effectors of GCN2 signaling, in both human and experimental PVOD, we decided to focus on those factors and to localize the sites of their expression by immunohistochemistry. We challenged the PVOD specificity of CHOP and HO-1 expression by comparing their expression in PVOD as compared to non-PH and PAH samples.

We observed no convincing HO-1 nor CHOP staining in control and PAH lung tissues (Figures E11, E12 and E13 in the data supplement). However, we found both in sporadic (Figure E14 in the data supplement) and heritable PVOD (Figure 6), that CHOP staining labels endothelial cells in remodeled veins and arteries, whereas the staining becomes faint in smooth muscle cells. Strong HO-1 staining is observed only within capillary hemangiomatosis foci (Figure 6). Outside these foci no staining is observed. The endothelial cells from arteries or veins do not express HO-1. Capillary hemangiomatosis foci strongly stains for the endothelial marker CD31 and display scant to high number of Ki67 positive cells (Figure E14 in the data supplement and Figure 6).

GCN2 loss-of-function negatively regulates BMP-dependent SMAD1/5/9 signaling and exogenous BMP9 reverses GCN2 inhibition-induced PAECs proliferation.

To confirm *in vivo* the possible link between loss of GCN2 and BMP signaling, we quantified GCN2 and SMAD1/5/9 phosphorylation by Western blot in the lungs of a newly created transgenic rat model knock out (KO) for *Eif2ak4* ($\Delta 152\text{Ex1}/\Delta 152\text{Ex1}$) as compared to wild type animals. We found a 4 fold decrease in SMAD1/5/9 phosphorylation in KO rats (Figure 7A). Since those rats did not have increased pulmonary arterial pressure, as measured by right heart catheterization (data not shown), the decrease in SMAD1/5/9 phosphorylation in these rats is not the mere consequence of PH. It appears in this “pure” background (same genetic background, same environment) that loss of GCN2 decreases robustly SMAD1/5/9 phosphorylation.

Using a specific GCN2 inhibitor (2662034 compound) and a dual GCN2/PERK inhibitor (2712911 compound), we demonstrated that specific GCN2 inhibition preferentially decreases BMP9-induced SMAD1/5/8 phosphorylation in human PAEC rather than in PASMC (Figure 7B and figures E15A-B in the data supplement). We confirmed the consequence of GCN2 invalidation in both cell types through a siRNA strategy. This strategy significantly reduced complete medium (with Fetal Calf Serum)-induced phosphorylation of SMAD1/5/8 in PAEC but not in PASMC (Figure 7C and figure E15C in the data supplement). The loss of GCN2 strongly enhanced complete medium-induced PAEC proliferation (by 2-fold increase) (Figure 7D) but decreased PASMC proliferation rate (Figure E15D in the data supplement). siRNA against GCN2 also increased the expression of the anti-apoptotic protein survivin in PAEC (Figure E16 in the data supplement). The specific GCN2 inhibitor (2662034 compound) also almost tripled complete medium-induced PAECs proliferation, an effect that was blunted by exogenous BMP9 treatment (Figure 7E) suggesting that the proliferative effects of GCN2 depend upon its effects on BMP2/SMAD.

Since GCN2 inhibits Target of Rapamycin Complex 1 (mTORC1) in response to amino acid starvation (17), since mTORC1 signaling negatively affects BMP signaling (18), and since rapamycin (mTORC1 inhibitor) has already been shown to potentiate BMP signaling (19), we hypothesized that GCN2 may increase SMAD signaling through the downstream inhibition of mTORC1. As expected, 2662034 compound decreased and rapamycin increased BMP9-induced SMAD1/5/9 phosphorylation. However, GCN2 inhibition with 2662034 compound strongly reduced BMP9+rapamycin-induced SMAD1/5/9 phosphorylation (Figure 7F). This led us to envision that GCN2 may be rather downstream of mTORC1.

Since mTORC1 is upstream of GCN2, we still couldn't explain the potentiating effect of GCN2 on BMP2 signaling. To try deciphering the link between GCN2 and BMP signaling, we analyzed the effect of GCN2 activation by histidinol (0.5 mM) on the transcriptional expression of the genes involved in the BMP signaling (Human BMP Signaling Pathway– Anygene QPCR array) in pulmonary endothelial cells. GCN2 activation was associated with an almost 5 times decrease in chordin expression (Fold change (FC): -4.76, P=0.0065) (Table E1 in the data supplement).

We also wondered whether BMP signaling can also feedback on ISR signaling activation, therefore effect of BMPR2 activation by BMP9 (20 ng/ml) on the transcriptional expression of the genes involved in the ISR signaling (Human ISR Signaling Pathway– Anygene QPCR array) in pulmonary endothelial cells was further investigated. Our results suggest a negative feedback of BMP signaling to the ISR with downregulation of several genes involved in response to endoplasmic reticulum stress (BCL2L11, FC: -1.39, P=0.0014), apoptotic process (PMAIP1, FC: -2.27, P=0.0029), regulation of translation (RPL7, FC: -1.82, P=0.0029) and autophagy (SQSTM1, FC: -2.00, P=0.0193) (Table E2 in the data supplement).

Note: A transcriptional mechanism alters levels of total protein, with proportional change in phospho-protein, whereas a post-translational mechanism leads to an increase or decrease in phosphorylation in the presence of steady state protein level. Most of the phospho-protein shown in this result section were only normalized to β -Actin, which does not discriminate transcriptional and post-translational mechanisms.

DISCUSSION

Extensive pulmonary venous lesions and capillary remodeling are the hallmark of PVOD whereas the pathology in PAH is classically described as constrictive remodeling of the pre-capillary pulmonary vasculature (20). However, our group has recently reported significant remodeling in pulmonary veins and venules of patients with heritable PAH (21). Inversely, we recently highlighted that pulmonary arterial remodeling is also an important feature of PVOD (22). This last observation concurs with the early and massive arterial narrowing in our rat model of PVOD. The early reduction of pulmonary arterial patency, which may be initially caused by vasoconstriction, could rely on the observed loss of KCNK3 function that controls pulmonary arterial tone in humans (23).

MMC has been linked to PVOD, but also to cardiomyopathy. Coupled with the recent idea that pulmonary venous remodeling can be seen in PH secondary to left heart disease (24), we also had to confirm that the MMC model used here is truly representative of PVOD and not Group 2 PH. Indeed, MMC has been associated with cardiotoxicity (25); the most common cardiac event associated with

MMC being chronic heart failure (CHF). However, almost all patients who experienced a cardiac event had received prior doxorubicin therapy. This strongly suggests that MMC probably enhanced the cardiac damage incurred by prior doxorubicin therapy, thus exhibiting a synergistic cardiotoxic effect. MMC-related cardiac failure is not an acute event; it exhibits a trend towards a cumulative dose effect and occurs weeks after multiple doses of MMC (25). In the series of MMC-induced PVOD in human we described recently (8), all patients had left cardiac evaluation by echocardiography with no finding of left ventricular dysfunction, and none received prior doxorubicin therapy. In addition, the left cardiac catheterization found normal pulmonary artery wedge pressure (PawP \leq 15 mmHg) in all patients eliminating left cardiac involvement in the mechanism of PVOD occurrence. We carried over an echocardiographic follow-up of MMC-exposed rat and analyzed parameters that could inform us about potential alterations of left ventricle (LV) function like LV fractional shortening (LVFS). Pulmonary artery acceleration time (PAAT), a validated index of pulmonary vascular resistance, arterial pressure, and compliance, was also used to assess pulmonary hemodynamics at the same time points. Lower PAAT is indicative of pulmonary vascular disease (26, 27). Our observations suggest a rather limited and transient effect of MMC on the left heart in contrast to the very early and constant decrease in PAAT (Figure E17 in the data supplement), indicative of pulmonary vascular disease. Moreover, histologically confirmed venous remodeling occurred late in the development of our MMC-PVOD model, at a time LVFS value returned to control values. This argues against LV dysfunction-induced pulmonary venous remodeling

The imbalance of BMP/TGF β signaling contributes to endothelial dysfunction, vascular remodeling, inflammation and disordered angiogenesis in PAH (28). We wondered whether this axis could be altered in PVOD. Specific GCN2 inhibition with 2662034 compound or with siRNA reduced SMAD1/5/9 signaling but not abrogates it in PAECs. Moreover, SMAD1/5/9 activation is decreased but not abolished in the lungs from *EIF2AK4*^{-/-} PVOD patients and *Eif2ak4* KO rats. We showed that BMP9 is able to reverse GCN2-inhibition-induced PAEC proliferation, a pathway that could contribute to the characteristic foci of capillary hemangiomatosis, a highly typical histologic finding in PVOD. This supports that the hypothesis that the proliferative effects of GCN2 depends upon its effects on

BMP9-dependent signaling, probably the canonical SMAD1/5/9 signaling, but we did not investigate the other non- canonical SMAD-independent signaling p38, ERK, JNK (MAPK), PI3K/Akt, LIMK, Rho, ROCK and TAK1 (29). Actually, many other gene modifiers regulate the BMPR2/SMAD1/5/9 axis (30, 31). Hence, there are many factors that can explain the heterogeneity of phospho-SMAD levels in human PVOD samples, especially those from sporadic PVOD: different etiologies, different genetic background, differences in expression of gene modifiers, different disease evolution, etc. Moreover, the relation between the GCN2 and the SMAD1/5/9-dependent signalings is difficult to decipher for several reasons. First, the roles of BMP9 in vascular homeostasis remain controversial and context-dependent. On the one hand, it was reported that BMP9 induces proliferation and migration of endothelial cells by triggering the expression of VEGFR2 and TIE-2, both of which stimulate blood endothelial cell proliferation (32). By contrast, BMP-9 inhibits bFGF-induced endothelial cell proliferation and VEGF-stimulated angiogenesis, when signaling through ALK1 (33). In our proliferation experiments, all performed in complete medium (with Fetal Calf Serum), BMP9 alone had no effect on the PAEC proliferation whereas it abolished GCN2 inhibition-induced PAECs overproliferation. This selectivity suggests that the proliferative effects of GCN2 depend upon its effects on BMPR2/SMAD. Second, to confirm this dependence, interventional studies with knock-down of the receptors (BMPR2, ALK1) or downstream BMP-regulated effectors may be envisioned. However, BMPR2 siRNA silencing, for instance, results in a proliferative, promigratory PAEC phenotype (34) that may hide the upstream regulatory effect of GCN2 on this pathway. As a result of an interaction screen performed with the luminescence-based mammalian interactome mapping technique, GCN2 was found to directly interact with SMAD4 and SMAD1 (35) and also with ALK-1, endoglin (ENG) and transforming growth factor- β receptor-2 (TGFB2) (36). To study further the physical interactions that exist between GCN2 and members of the TGF- β -BMP superfamily and modulate them through site-directed mutagenesis of GCN2 may be a way to circumvent the aforementioned issues and dissect the interplay between GCN2 and BMP signalings.

Our results suggest that GCN2 may be downstream of mTORC1 in the regulation cascade which modulates SMAD1/5/9 phosphorylation, but further work is needed to dissect this regulatory

axis. It has to be recognized that the two best established responses to amino acid deprivation are inhibition of the mammalian target of rapamycin (mTOR) kinase and phosphorylation of eukaryotic initiation factor 2 α (eIF2 α) (37). Recent data showed that inhibition of mTORC1 leads to activation of GCN2 and phosphorylation eIF2 α in a mechanism dependent on the PP6C phosphatase (37). This mechanism fit with and can explain our results with mTORC1 being a negative regulator of GCN2. *In vitro* activation of GCN2 with histidinol was associated with a dramatic decrease in chordin expression. Extracellular antagonists, such as chordin, are essential regulators of BMP signaling. Chordin binds to BMPs blocking interaction with BMP receptors (38). Interventional studies are now required to confirm and investigate the role of chordin in the GCN2-mediated BMP signaling potentiation. We also showed that BMP signaling activation with BMP9 can also negatively feedback on ISR signaling activation, potentially dampening the deleterious effects of chronic ISR activation.

Two of the representative factors involved in the ISR response which are CHOP (39) and HO-1 (9) are overexpressed in both sPVOD and hPVOD patients as well as in experimental PVOD, suggesting that loss of GCN2 is associated to a paradoxical overexpression of its downstream effectors. Our immunohistochemical experiments support the specificity for CHOP and HO-1 involvement in PVOD pathobiology, with HO-1 appearing as a specific marker of capillary hemangiomatosis foci, which are pathognomonic lesions of PVOD and the place of intense microvascular endothelial cell proliferation. Relevantly, extensive study has revealed a context-dependent effect of HO-1 activity in angiogenesis (40). HO-1 over-expression promotes endothelial cell proliferation and enhances development of endothelial tubules on Matrigel (41). HO-1-deficient mice exhibit reduced endothelial proliferative responses to growth factors, attenuated tube formation and impaired wound healing (42). These observations suggest that CHOP and/or HO-1 inhibition may be valuable targets for specific therapeutic development of PVOD. Since HO-1 is very often upregulated in tumors in comparison to healthy tissues, its inhibition, with metalloporphyrins for instance, is under investigation for anticancer treatment (43). The results of this research field may be translated to PAH therapeutic innovation. Inhibition of CHOP is hypothesized to enhance cell survival by preventing Unfolded Protein Response (UPR) programmed cell death, but there are currently no known small molecule CHOP inhibitors either

for laboratory or clinical use. However, sodium 4-phenylbutyrate (4-PBA), an ER stress inhibitor also considered as a CHOP inhibitor, has been demonstrated to alleviate monocrotaline-induced pulmonary hypertension in rats (44). Monocrotaline, a pyrrolizidine alkaloid, causes veno-occlusive disease of the liver and pulmonary lesions in a dose-dependent manner in a similar fashion as alkylating agents like MMC (45). This also highlights the therapeutic potential of CHOP inhibition in PVOD.

The molecular hub for all ISR kinases, and GCN2 in particular, is the eukaryotic translation initiation factor 2 (eIF2 α) which is phosphorylated upon ISR activation (46). Surprisingly, the loss of GCN2 in human and experimental PVOD, or in PAEC and PASMC though siRNA knock down (not shown) and at the opposite, the concomitant CHOP- and HO-1-mediated ISR response, are not associated with alterations in the phosphorylation status of eIF2 α . This highlights that a GCN2-dependent but eIF2 α -independent pathway is making the bridge between opposing observations. Although ATF4 induction without increased phosphorylation of eIF2 α is atypical for most ISRs, there are other examples of ISRs that can induce ATF4 or CHOP without increased phosphorylation of eIF2 α in macrophages, fibroblasts, and solid tumor cells (47–49). Indeed, ATF4 can also be induced without an increase in eIF2 phosphorylation, through the inhibition of eIF2B, a guanine nucleotide exchange factor (47–49). In hepatic cells eIF2 α phosphorylation by dietary methionine restriction was uncompromised in *Gcn2*^{-/-} mice. Instead, the ISR kinase PERK was activated in both intact and *Gcn2*^{-/-} mice (50). PERK activation corresponded with induction of the ISR and the nuclear respiratory factor 2 (NRF2) program. Relevantly, the PERK/NRF2 axis is described to mediate also the induction of CHOP (51) and to up-regulate HO-1 (52). The apparent mystery of the GCN2-dependent but eIF2 α -independent pathway occurring in PVOD that emanates from the results of our study will have to be elucidated in the future.

At last, we showed that ERG protein expression is abolished in hPVOD and sPVOD patients as well as in MMC-exposed rats. ERG has been identified as a key modulator of endothelial cell differentiation (53), and hematopoiesis (54). Recently, ERG was demonstrated to be essential for endothelial homeostasis in pulmonary venules (7). Homozygous deletion of ERG in mice die prematurely due to the loss of pulmonary venules and the concomitant development of PVOD (7). ERG

expression was also significantly reduced in chronically hypoxic mice and PAH patients (55). Here, we highlighted that ERG loss of expression is a hallmark of PVOD (human forms and animal models of PVOD), an observation that suggests that ERG dysfunction may indeed be a central player of pulmonary veinular remodeling.

Conclusion

Our study paints a picture of the histological and molecular alterations present in experimental and human PVOD. It paves the way for future studies aiming at understanding and curing this orphan disease. We demonstrated that MMC exposure is primarily associated with arterial and microvessel remodeling and only secondary followed by severe venous remodeling, suggesting that precapillary and capillary alterations may be initial events in PVOD. In all forms of PVOD tested, there were convergent GCN2-dependent but eIF2 α -independent pulmonary protein overexpression of HO-1 and CHOP, two downstream effectors of GCN2 signaling and ER stress. In human PVOD samples, immunohistochemical staining supported the specificity for CHOP and HO-1 involvement in PVOD pathobiology, especially in pulmonary endothelial cells and pulmonary capillary hemangiomatosis foci. Our work shows that GCN2 loss-of-function negatively regulates SMAD1/5/9 phosphorylation. Despite this dampened BMP signaling, exogenous BMP9 was still able to reverse GCN2 inhibition-induced PAECs proliferation. CHOP and HO-1 inhibition, and BMP9 may hence be considered as potential therapeutic options for PVOD.

NOTE ADDED IN PROOF

Although no change in phosphorylation of Eif2a was detected, transient activation of the pathway might still be possible via minute changes in phosphorylation that cannot be detected by the methodology we employed.

REFERENCES

1. Montani D, Lau EM, Dorfmüller P, Girerd B, Jaïs X, Savale L, Perros F, Nossent E, Garcia G, Parent F, Fadel E, Soubrier F, Sitbon O, Simonneau G, Humbert M. Pulmonary veno-occlusive disease. *Eur Respir J* 2016;47:1518–1534.
2. Montani D, Girerd B, Jaïs X, Levy M, Amar D, Savale L, Dorfmüller P, Seferian A, Lau EM, Eyries M, Le Pavec J, Parent F, Bonnet D, Soubrier F, Fadel E, Sitbon O, Simonneau G, Humbert M. Clinical phenotypes and outcomes of heritable and sporadic pulmonary veno-occlusive disease: a population-based study. *Lancet Respir Med* 2017;5:125–134.
3. Eyries M, Montani D, Girerd B, Perret C, Leroy A, Lonjou C, Chelghoum N, Coulet F, Bonnet D, Dorfmüller P, Fadel E, Sitbon O, Simonneau G, Tregouët D-A, Humbert M, Soubrier F. EIF2AK4 mutations cause pulmonary veno-occlusive disease, a recessive form of pulmonary hypertension. *Nat Genet* 2014;46:65–69.
4. Montani D, Lau E, Descatha A, Humbert M. Pulmonary veno-occlusive disease as an occupational lung disease. *Lancet Respir Med* 2017;5:e19.
5. Ravishankar B, Liu H, Shinde R, Chaudhary K, Xiao W, Bradley J, Koritzinsky M, Madaio MP, McGaha TL. The amino acid sensor GCN2 inhibits inflammatory responses to apoptotic cells promoting tolerance and suppressing systemic autoimmunity. *Proc Natl Acad Sci U S A* 2015;112:10774–10779.
6. Santos-Ribeiro D, Godinas L, Pilette C, Perros F. The integrated stress response system in cardiovascular disease. *Drug Discov Today* 2018;23:920–929.
7. Lathen C, Zhang Y, Chow J, Singh M, Lin G, Nigam V, Ashraf YA, Yuan JX, Robbins IM, Thistlethwaite PA. ERG-APLNR axis controls pulmonary venule endothelial proliferation in pulmonary veno-occlusive disease. *Circulation* 2014;130:1179–1191.

8. Perros F, Günther S, Ranchoux B, Godinas L, Antigny F, Chaumais M-C, Dorfmueller P, Hautefort A, Raymond N, Savale L, Jais X, Girerd B, Cottin V, Sitbon O, Simonneau G, Humbert M, Montani D. Mitomycin-Induced Pulmonary Veno-Occlusive Disease: Evidence From Human Disease and Animal Models. *Circulation* 2015;132:834–847.
9. Dey S, Sayers CM, Verginadis II, Lehman SL, Cheng Y, Cerniglia GJ, Tuttle SW, Feldman MD, Zhang P, Fuchs SY, Diehl JA, Koumenis C. ATF4-dependent induction of heme oxygenase 1 prevents anoikis and promotes metastasis. *J Clin Invest* 2015;125:2592–2608.
10. Ma L, Chung WK. The genetic basis of pulmonary arterial hypertension. *Hum Genet* 2014;133:471–479.
11. Zhang W, Liu HT. MAPK signal pathways in the regulation of cell proliferation in mammalian cells. *Cell Res* 2002;12:9–18.
12. Fabrice A, Benoît R, Valérie N, Lau E, Sébastien B, Frédéric P. A simple method to assess in vivo proliferation in lung vasculature with EdU: the case of MMC-induced PVOD in rat. *Anal Cell Pathol Amst* 2015;2015:326385.
13. Lambert M, Capuano V, Olschewski A, Sabourin J, Nagaraj C, Girerd B, Weatherald J, Humbert M, Antigny F. Ion Channels in Pulmonary Hypertension: A Therapeutic Interest? *Int J Mol Sci* 2018;19:.
14. Antigny F, Hautefort A, Meloche J, Belacel-Ouari M, Manoury B, Rucker-Martin C, Pechoux C, Potus F, Nadeau V, Tremblay E, Ruffenach G, Bourgeois A, Dorfmueller P, Breuils-Bonnet S, Fadel E, Ranchoux B, Jourdon P, Girerd B, Montani D, Provencher S, Bonnet S, Simonneau G, Humbert M, Perros F. Potassium Channel Subfamily K Member 3 (KCNK3) Contributes to the Development of Pulmonary Arterial Hypertension. *Circulation* 2016;133:1371–1385.
15. Lambert M, Capuano V, Boet A, Tesson L, Bertero T, Nakhleh MK, Remy S, Anegon I, Pechoux C, Hautefort A, Rucker-Martin C, Manoury B, Domergue V, Mercier O, Girerd B, Montani D,

- Perros F, Humbert M, Antigny F. Characterization of Kcnk3-Mutated Rat, a Novel Model of Pulmonary Hypertension. *Circ Res* 2019;125:678–695.
16. Eddahibi S, Guignabert C, Barlier-Mur A-M, Dewachter L, Fadel E, Dartevelle P, Humbert M, Simonneau G, Hanoun N, Saurini F, Hamon M, Adnot S. Cross talk between endothelial and smooth muscle cells in pulmonary hypertension: critical role for serotonin-induced smooth muscle hyperplasia. *Circulation* 2006;113:1857–1864.
17. Yuan W, Guo S, Gao J, Zhong M, Yan G, Wu W, Chao Y, Jiang Y. General Control Nonderepressible 2 (GCN2) Kinase Inhibits Target of Rapamycin Complex 1 in Response to Amino Acid Starvation in *Saccharomyces cerevisiae*. *J Biol Chem* 2017;292:2660–2669.
18. Deng Z, Lei X, Zhang X, Zhang H, Liu S, Chen Q, Hu H, Wang X, Ning L, Cao Y, Zhao T, Zhou J, Chen T, Duan E. mTOR signaling promotes stem cell activation via counterbalancing BMP-mediated suppression during hair regeneration. *J Mol Cell Biol* 2015;7:62–72.
19. Spiekerkoetter E, Tian X, Cai J, Hopper RK, Sudheendra D, Li CG, El-Bizri N, Sawada H, Haghghat R, Chan R, Haghghat L, de Jesus Perez V, Wang L, Reddy S, Zhao M, Bernstein D, Solow-Cordero DE, Beachy PA, Wandless TJ, Ten Dijke P, Rabinovitch M. FK506 activates BMPR2, rescues endothelial dysfunction, and reverses pulmonary hypertension. *J Clin Invest* 2013;123:3600–3613.
20. Pietra GG, Capron F, Stewart S, Leone O, Humbert M, Robbins IM, Reid LM, Tuder RM. Pathologic assessment of vasculopathies in pulmonary hypertension. *J Am Coll Cardiol* 2004;43:25S-32S.
21. Ghigna M-R, Guignabert C, Montani D, Girerd B, Jaïs X, Savale L, Hervé P, Thomas de Montpréville V, Mercier O, Sitbon O, Soubrier F, Fadel E, Simonneau G, Humbert M, Dorfmueller P. BMPR2 mutation status influences bronchial vascular changes in pulmonary arterial hypertension. *Eur Respir J* 2016;48:1668–1681.

22. Nossent EJ, Antigny F, Montani D, Bogaard HJ, Ghigna MR, Lambert M, Thomas de Montpréville V, Girerd B, Jais X, Savale L, Mercier O, Fadel E, Soubrier F, Sitbon O, Simonneau G, Noordegraaf AV, Humbert M, Perros F, Dorfmüller P. Pulmonary vascular remodeling patterns and expression of general control nonderepressible 2 (GCN2) in pulmonary veno-occlusive disease. *J Heart Lung Transplant Off Publ Int Soc Heart Transplant* 2017;doi:10.1016/j.healun.2017.09.022.
23. Olschewski A, Veale EL, Nagy BM, Nagaraj C, Kwapiszewska G, Antigny F, Lambert M, Humbert M, Czirják G, Enyedi P, Mathie A. TASK-1 (KCNK3) channels in the lung: from cell biology to clinical implications. *Eur Respir J* 2017;50:.
24. Fayyaz AU, Edwards WD, Maleszewski JJ, Konik EA, DuBrock HM, Borlaug BA, Frantz RP, Jenkins SM, Redfield MM. Global Pulmonary Vascular Remodeling in Pulmonary Hypertension Associated with Heart Failure and Preserved or Reduced Ejection Fraction. *Circulation* 2018;137:1796–1810.
25. Pai VB, Nahata MC. Cardiotoxicity of chemotherapeutic agents: incidence, treatment and prevention. *Drug Saf* 2000;22:263–302.
26. Naing P, Kuppusamy H, Scalia G, Hillis GS, Playford D. Non-Invasive Assessment of Pulmonary Vascular Resistance in Pulmonary Hypertension: Current Knowledge and Future Direction. *Heart Lung Circ* 2017;26:323–330.
27. Levy PT, Patel MD, Choudhry S, Hamvas A, Singh GK. Evidence of Echocardiographic Markers of Pulmonary Vascular Disease in Asymptomatic Infants Born Preterm at One Year of Age. *J Pediatr* 2018;197:48-56.e2.
28. Tielemans B, Delcroix M, Belge C, Quarck R. TGF β and BMPRII signalling pathways in the pathogenesis of pulmonary arterial hypertension. *Drug Discov Today* 2019;24:703–716.

29. Bach D-H, Park HJ, Lee SK. The Dual Role of Bone Morphogenetic Proteins in Cancer. *Mol Ther Oncolytics* 2018;8:1–13.
30. Dannewitz Prosseda S, Tian X, Kuramoto K, Boehm M, Sudheendra D, Miyagawa K, Zhang F, Solow-Cordero D, Saldivar JC, Austin ED, Loyd JE, Wheeler L, Andruska A, Donato M, Wang L, Huebner K, Metzger RJ, Khatri P, Spiekerkoetter E. FHIT, a Novel Modifier Gene in Pulmonary Arterial Hypertension. *Am J Respir Crit Care Med* 2019;199:83–98.
31. West J, Cogan J, Geraci M, Robinson L, Newman J, Phillips JA, Lane K, Meyrick B, Loyd J. Gene expression in BMPR2 mutation carriers with and without evidence of pulmonary arterial hypertension suggests pathways relevant to disease penetrance. *BMC Med Genomics* 2008;1:45.
32. Suzuki Y, Ohga N, Morishita Y, Hida K, Miyazono K, Watabe T. BMP-9 induces proliferation of multiple types of endothelial cells in vitro and in vivo. *J Cell Sci* 2010;123:1684–1692.
33. Scharpfenecker M, van Dinther M, Liu Z, van Bezooijen RL, Zhao Q, Pukac L, Löwik CWGM, ten Dijke P. BMP-9 signals via ALK1 and inhibits bFGF-induced endothelial cell proliferation and VEGF-stimulated angiogenesis. *J Cell Sci* 2007;120:964–972.
34. Awad KS, Elinoff JM, Wang S, Gairhe S, Ferreyra GA, Cai R, Sun J, Solomon MA, Danner RL. Raf/ERK drives the proliferative and invasive phenotype of BMPR2-silenced pulmonary artery endothelial cells. *Am J Physiol Lung Cell Mol Physiol* 2016;310:L187-201.
35. Barrios-Rodiles M, Brown KR, Ozdamar B, Bose R, Liu Z, Donovan RS, Shinjo F, Liu Y, Dembowy J, Taylor IW, Luga V, Przulj N, Robinson M, Suzuki H, Hayashizaki Y, Jurisica I, Wrana JL. High-throughput mapping of a dynamic signaling network in mammalian cells. *Science* 2005;307:1621–1625.

36. Xu G, Barrios-Rodiles M, Jerkic M, Turinsky AL, Nadon R, Vera S, Voulgaraki D, Wrana JL, Toporsian M, Letarte M. Novel protein interactions with endoglin and activin receptor-like kinase 1: potential role in vascular networks. *Mol Cell Proteomics MCP* 2014;13:489–502.
37. Wengrod J, Wang D, Weiss S, Zhong H, Osman I, Gardner LB. Phosphorylation of eIF2 α triggered by mTORC1 inhibition and PP6C activation is required for autophagy and is aberrant in PP6C-mutated melanoma. *Sci Signal* 2015;8:ra27.
38. Troilo H, Zuk AV, Tunncliffe RB, Wohl AP, Berry R, Collins RF, Jowitt TA, Sengle G, Baldock C. Nanoscale structure of the BMP antagonist chordin supports cooperative BMP binding. *Proc Natl Acad Sci U S A* 2014;111:13063–13068.
39. Pakos-Zebrucka K, Koryga I, Mnich K, Ljujic M, Samali A, Gorman AM. The integrated stress response. *EMBO Rep* 2016;17:1374–1395.
40. Kim Y-M, Pae H-O, Park JE, Lee YC, Woo JM, Kim N-H, Choi YK, Lee B-S, Kim SR, Chung H-T. Heme oxygenase in the regulation of vascular biology: from molecular mechanisms to therapeutic opportunities. *Antioxid Redox Signal* 2011;14:137–167.
41. Deramaudt BM, Braunstein S, Remy P, Abraham NG. Gene transfer of human heme oxygenase into coronary endothelial cells potentially promotes angiogenesis. *J Cell Biochem* 1998;68:121–127.
42. Deshane J, Chen S, Caballero S, Grochot-Przeczek A, Was H, Li Calzi S, Lach R, Hock TD, Chen B, Hill-Kapturczak N, Siegal GP, Dulak J, Jozkowicz A, Grant MB, Agarwal A. Stromal cell-derived factor 1 promotes angiogenesis via a heme oxygenase 1-dependent mechanism. *J Exp Med* 2007;204:605–618.
43. Podkalicka P, Mucha O, Józkowicz A, Dulak J, Łoboda A. Heme oxygenase inhibition in cancers: possible tools and targets. *Contemp Oncol Poznan Pol* 2018;22:23–32.

44. Wu Y, Adi D, Long M, Wang J, Liu F, Gai M-T, Aierken A, Li M-Y, Li Q, Wu L-Q, Ma Y-T, Hujiaaihemaiti M. 4-Phenylbutyric Acid Induces Protection against Pulmonary Arterial Hypertension in Rats. *PloS One* 2016;11:e0157538.
45. Günther S, Perros F, Rautou P-E, Girerd B, Ghigna M-R, Cazals-Hatem D, Lau EM, Dorfmüller P, Sitbon O, Valla DC, Humbert M, Montani D. Understanding the Similarities and Differences between Hepatic and Pulmonary Veno-Occlusive Disease. *Am J Pathol* 2019;189:1159–1175.
46. Ron D. Translational control in the endoplasmic reticulum stress response. *J Clin Invest* 2002;110:1383–1388.
47. A novel mechanism for the control of translation initiation by amino acids, mediated by phosphorylation of eukaryotic initiation factor 2B. - PubMed - NCBI. at <<https://www.ncbi.nlm.nih.gov/pubmed/?term=18160716>>.
48. Woo CW, Kutzler L, Kimball SR, Tabas I. Toll-like receptor activation suppresses ER stress factor CHOP and translation inhibition through activation of eIF2B. *Nat Cell Biol* 2012;14:192–200.
49. Lehman SL, Ryeom S, Koumenis C. Signaling through alternative Integrated Stress Response pathways compensates for GCN2 loss in a mouse model of soft tissue sarcoma. *Sci Rep* 2015;5:11781.
50. Wanders D, Stone KP, Forney LA, Cortez CC, Dille KN, Simon J, Xu M, Hotard EC, Nikonorova IA, Pettit AP, Anthony TG, Gettys TW. Role of GCN2-Independent Signaling Through a Noncanonical PERK/NRF2 Pathway in the Physiological Responses to Dietary Methionine Restriction. *Diabetes* 2016;65:1499–1510.
51. Zong Z-H, Du Z-X, Li N, Li C, Zhang Q, Liu B-Q, Guan Y, Wang H-Q. Implication of Nrf2 and ATF4 in differential induction of CHOP by proteasome inhibition in thyroid cancer cells. *Biochim Biophys Acta* 2012;1823:1395–1404.

52. Chen Y, Yuan T, Zhang H, Yan Y, Wang D, Fang L, Lu Y, Du G. Activation of Nrf2 Attenuates Pulmonary Vascular Remodeling via Inhibiting Endothelial-to-Mesenchymal Transition: an Insight from a Plant Polyphenol. *Int J Biol Sci* 2017;13:1067–1081.
53. Nikolova-Krsteovski V, Yuan L, Le Bras A, Vijayaraj P, Kondo M, Gebauer I, Bhasin M, Carman CV, Oettgen P. ERG is required for the differentiation of embryonic stem cells along the endothelial lineage. *BMC Dev Biol* 2009;9:72.
54. Loughran SJ, Kruse EA, Hacking DF, de Graaf CA, Hyland CD, Willson TA, Henley KJ, Ellis S, Voss AK, Metcalf D, Hilton DJ, Alexander WS, Kile BT. The transcription factor Erg is essential for definitive hematopoiesis and the function of adult hematopoietic stem cells. *Nat Immunol* 2008;9:810–819.
55. Looney AP, Han R, Stawski L, Marden G, Iwamoto M, Trojanowska M. Synergistic Role of Endothelial ERG and FLI1 in Mediating Pulmonary Vascular Homeostasis. *Am J Respir Cell Mol Biol* 2017;57:121–131.

FIGURES LEGENDS

Figure 1: MMC induces remodeling of the pulmonary arteries, veins and microvessels in rats. **A**, Pulmonary artery adjacent to a bronchus showing progressive hyperplasia/hypertrophy of the media with narrowing of the lumen at week 1,2,3,4, and 5 (Trichrome/Weigert staining). **B**, Pulmonary vein displaying progressive muscularization of the wall and narrowing of the lumen at week 1,2,3,4 and 5 (α -SMA IHC). **C**, Microvessels showing progressive remodeling with muscularization of the wall and progressive obstruction of the lumen at week 1,2,3,4 and 5 (α -SMA IHC). Scale bars: A and B: 100 μ m, C: 50 μ m.

Figure 2: MMC induces pulmonary vascular remodeling in rats. **A**, Surface open lumen/total area (%) of pulmonary arteries showing a significant change ($p < 0.0001$) at week 1 with progressive narrowing of the lumen in comparison with controls. **B**, Surface open lumen/total area (%) of pulmonary veins display a significant change ($p < 0.005$) at week 3 with progressive narrowing of the lumen in comparison with controls. **C**, Pulmonary artery at week 5 with intimal fibrosis (arrow) (HE staining)/Pulmonary artery with pronounced adventitial fibrosis (*) (HES staining). **D**, Non remodeled microvessels are significantly reduced from week 2 ($p < 0.00001$). Mild remodeling of microvessel is already observed at week 1, but becomes more pronounced every week with a significant change in week 2 ($p < 0.00001$). Moderate remodeling of the microvessels becomes abundant at week 4 ($p < 0.005$) and severe remodeling later on in week 5 ($p < 0.005$) **E**, Remodeling of microvessels over time at week 1,2,3,4 and 5 showing that moderate (orange) and severe (red) remodeling of microvessels is a late feature of disease development. **F**, The Fulton index ($RV/(LV+S)$) was significantly increased ($p < 0.0001$) at week 4 in comparison with controls. ** $P < 0.005$. **** $P < 0.0001$

Figure 3: ISR and SMADs phosphorylation are affected in lungs from MMC exposed rat. **A**, Pulmonary levels of GCN2 (A1), GCN1 (A2), PERK (A3), PKR(A4) were analyzed by Western blotting during the development of PVOD in control and MMC exposed-rats. **B**, Pulmonary levels of ATF4 (B1), HO-1 (B2), CHOP (B3) were analyzed by Western blotting during the development of PVOD in control and MMC exposed-rats. **C**, BMPRII (C1), p-SMAD1/5/8 (C2) and p-SMAD2/3 (C3)

measured by Western blot analysis in control and MMC-exposed rats. Analyses were performed 1, 2, 4 and 5 weeks after MMC-exposure; week 3 is displayed in Figures E18-E19 in the data supplement). β -Actin was used as loading control. * $P < 0.05$; ** $P < 0.005$. *** $P < 0.0005$. **** $P < 0.0001$

Figure 4: KCNK3 is functionally reduced in PASMC isolated from MMC-exposed rats. A, Representative traces of the whole cell currents in PASMCs in the control (top, left traces) and MMC (5 weeks) (bottom, left traces) rats before and after treatment with A293 (200nM) (right traces) **B,** Current-voltage relationship of the A293- K^+ sensitive current (I_{KCNK3}) (top left panel), of global K^+ current (top middle panel) and A293-Insensitive K^+ current (top right panel) in control and MMC-exposed rats (3 and 5 weeks after MMC exposure) PASMCs. Corresponding quantification of the A293-sensitive current, global- K^+ current and A293-Insensitive K^+ current (3 different rats, n=7-12 cells). * $P < 0.05$; ** $P < 0.005$. *** $P < 0.0005$. **** $P < 0.0001$.

Figure 5: ISR and SMADs phosphorylation are affected in lungs from hPVOD and sPVOD patients. A, Pulmonary levels of GCN2 (A1), GCN1 (A2), PERK (A3), PKR (A4) were analyzed by Western blotting in hPVOD and sPVOD patients. β -Actin was used as loading control. **B,** Pulmonary levels of ATF4 (B1), HO-1 (B2), CHOP (B3) were analyzed by Western blotting in hPVOD and sPVOD patients. β -Actin was used as loading control. **C,** BMPRII (C1), p-SMAD1/5/8 (C2, C3) and p-SMAD2/3 (C4, C5) measured by Western blot analysis in hPVOD and sPVOD patients. β -Actin was used as loading control in C1, C2 and C4; p-SMAD1/5/8 is normalized to SMAD1/5/8 in C3, p-SMAD2/3 is normalized to SMAD2/3 in C5. * $P < 0.05$; ** $P < 0.005$. *** $P < 0.0005$. **** $P < 0.0001$

hPVOD samples are originating from patients with nonsense/frameshift mutations in *EIF2AK4* and therefore were expected to show complete absence of GCN2 protein.

Figure 6: CHOP and HO-1 are expressed in typical pulmonary vascular lesions of hPVOD. A. CHOP immunostaining in lungs from hPVOD: endothelial staining is visible in both remodeled veins (A2, blue arrow) and arteries (A3, blue arrow). The staining becomes faint in smooth muscle cells whereas it is well observed in cytoplasm of bronchial cells, alveolar cells and macrophages (A1, A2, A3 black arrows). **B.** HO-1 staining in PVOD lungs is observed in interstitial cells within alveolar septa in

capillary hemangiomas foci (B1, B2). The labelling is strong and highlights interstitial cells with cytoplasmic extensions. Outside these foci no staining is observed. Arterial and venous endothelial cells do not express HO-1(B3, B4). **C.** Ki67 staining highlights cells engaged in proliferation. Scant interstitial cells are labelled within capillary hemangiomas foci and in bronchial basal layer (C1). There is no significant Ki67 staining in end-stage remodeled arteries and veins (C2 and C3). **D.** CD31 staining underlines endothelial cells within alveolar septa (D1, D2) and of pulmonary vessels (D3, D4). **E,F.** Ki67 and HO-1 staining are focused within capillary hemangiomas foci (black arrows). Remodeled small pulmonary artery (blue arrow) does not display significant staining.

Figure 7: GCN2 loss-of-function negatively regulates SMAD1/5/9 phosphorylation and exogenous BMP9 reverses GCN2 inhibition-induced PAECs proliferation.

A, Pulmonary levels of p-SMAD1/5/8 analyzed by Western blot in wild type (WT) and *Eif2ak4* knock out (KO) rats. β -Actin was used as loading control. **B,** Effect of GCN2 or PERK/GCN2 dual inhibitor on SMAD1/5/8 phosphorylation induced in huPAEC by rhBMP9 (20ng/ml). 2712991 is PERK/GCN2 dual inhibitor, 2662034 is specific GCN2 inhibitor. β -Actin was used as loading control. Right panels represent the quantification of the Western blots (Left panels). **C,** Human PAEC cultured in complete medium (with Fetal Calf Serum) were transfected with siRNA against GCN2. GCN2 knockdown efficiency and SMAD1/5/8 phosphorylation was assessed by western blots; Amido Black (AB) and β -Actin stainings were respectively used as a loading control. **D,** Quantification of the consequence of the si-RNA-mediated silencing of GCN2 on PAEC cell proliferation measured by BrdU incorporation. **E,** Quantification of the PAEC cell proliferation measured by BrdU incorporation in serum-activated proliferating PAEC treated with BMP9 (20ng/ml), with the specific GCN2 inhibitor (2662034 compound, inhGCN2), with the combination BMP9+inhGCN2, or not treated (NT). **F,** Quantification of p-SMAD1/5/8 levels analyzed by Western blot in basal medium cultured-PAEC treated with BMP9 (20ng/ml), the specific GCN2 inhibitor (2662034 compound, inhGCN2), the combination BMP9+inhGCN2, the combination BMP9+rapamycin (Rapa, 10ng/ml), the combination BMP9+Rapa+inhGCN2, or not treated (NT). β -Actin was used as loading control. *P<0.05; **P<0.005. ***P<0.0005. **** P < 0.0001

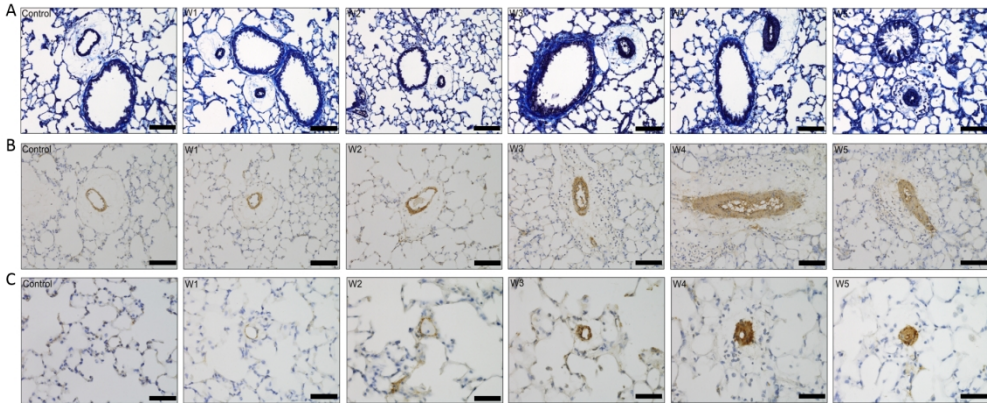


Figure 1

529x221mm (96 x 96 DPI)

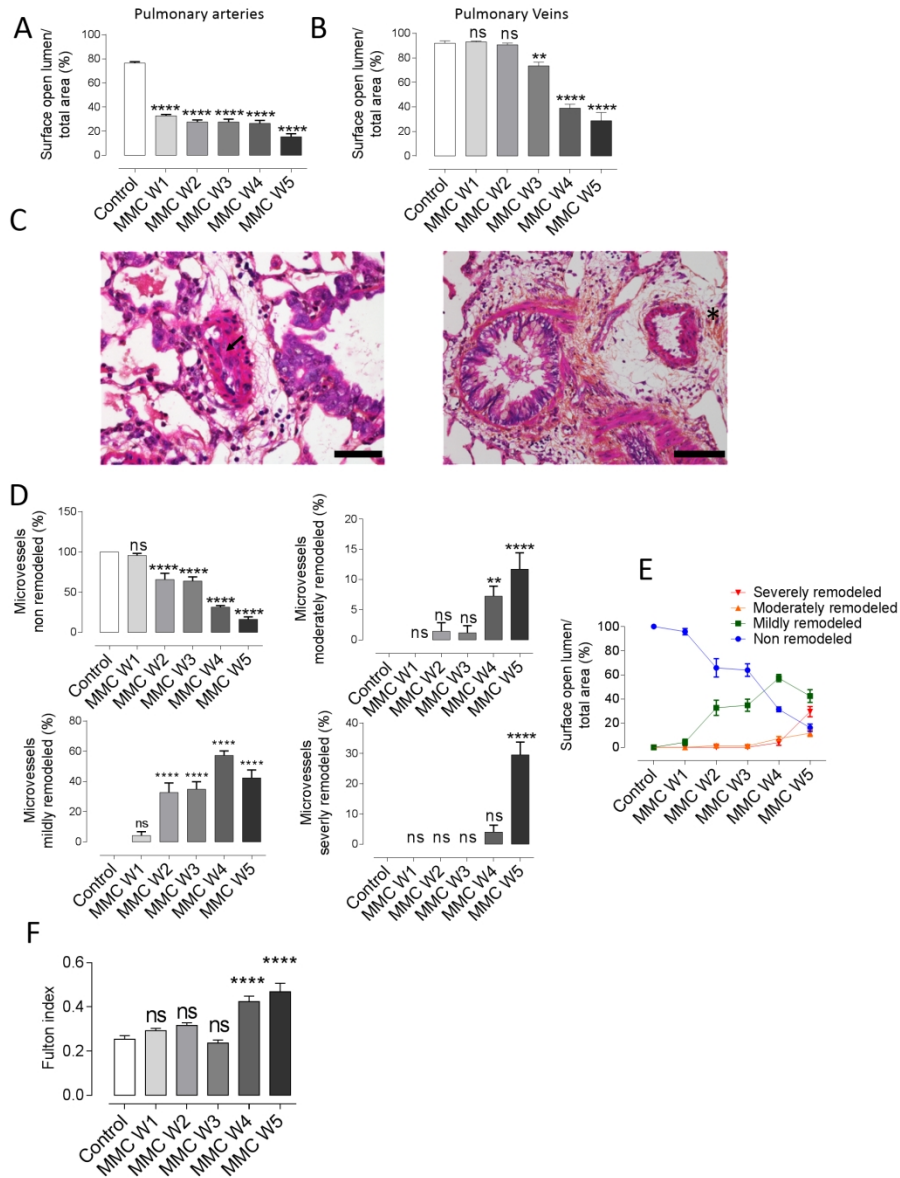


Figure 2

543x709mm (96 x 96 DPI)

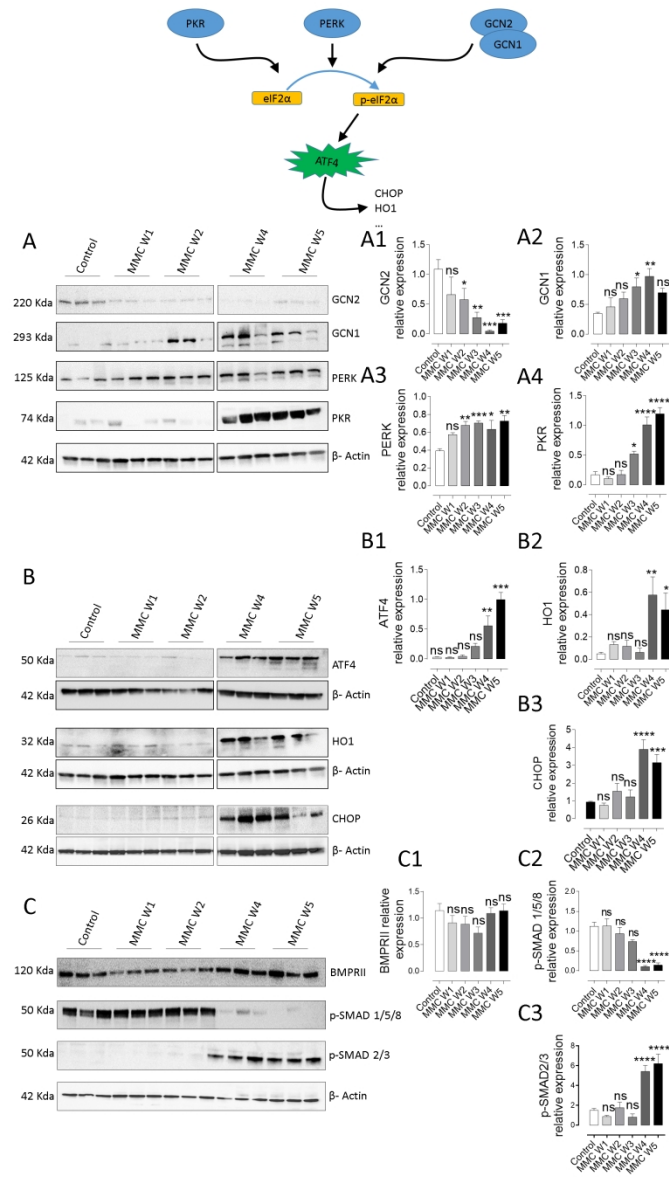


Figure 3

559x960mm (96 x 96 DPI)

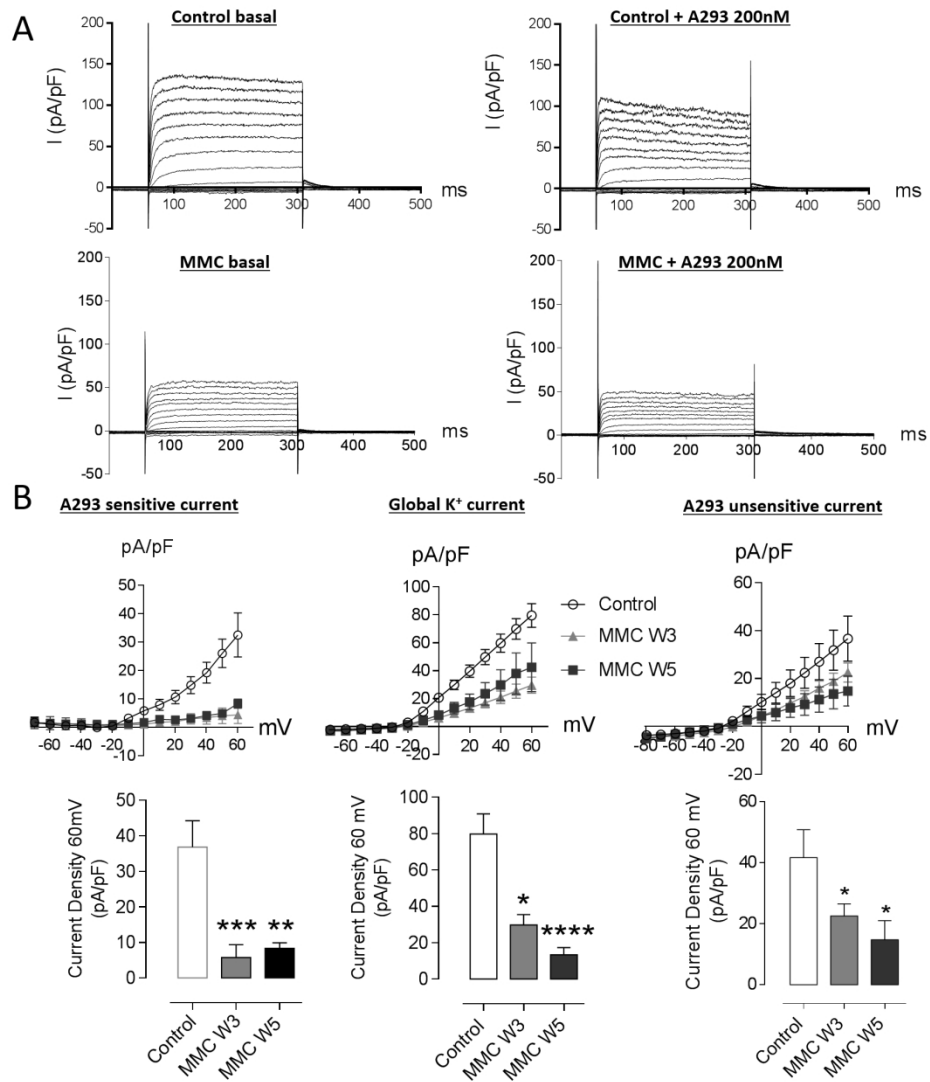


Figure 4

512x570mm (96 x 96 DPI)

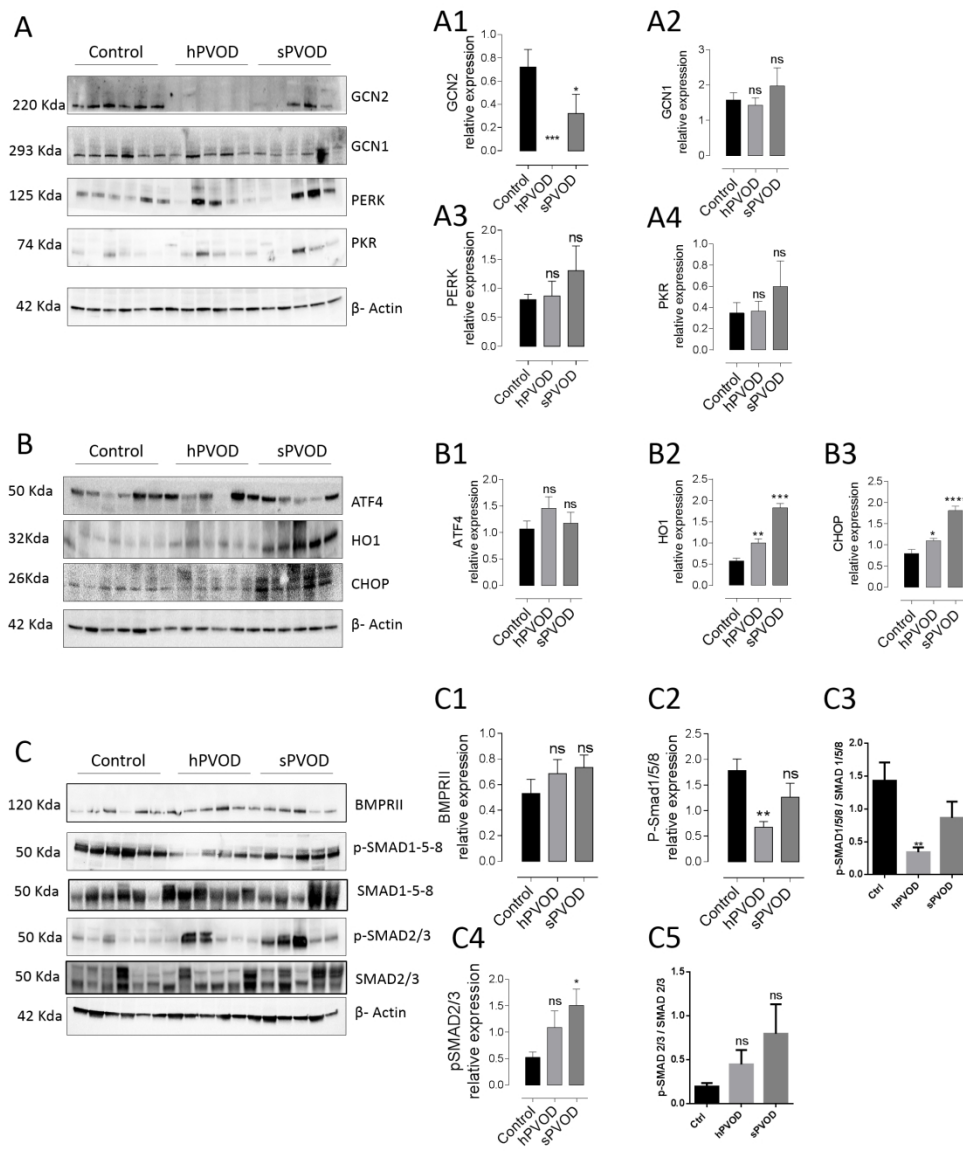


Figure 5

603x711mm (96 x 96 DPI)

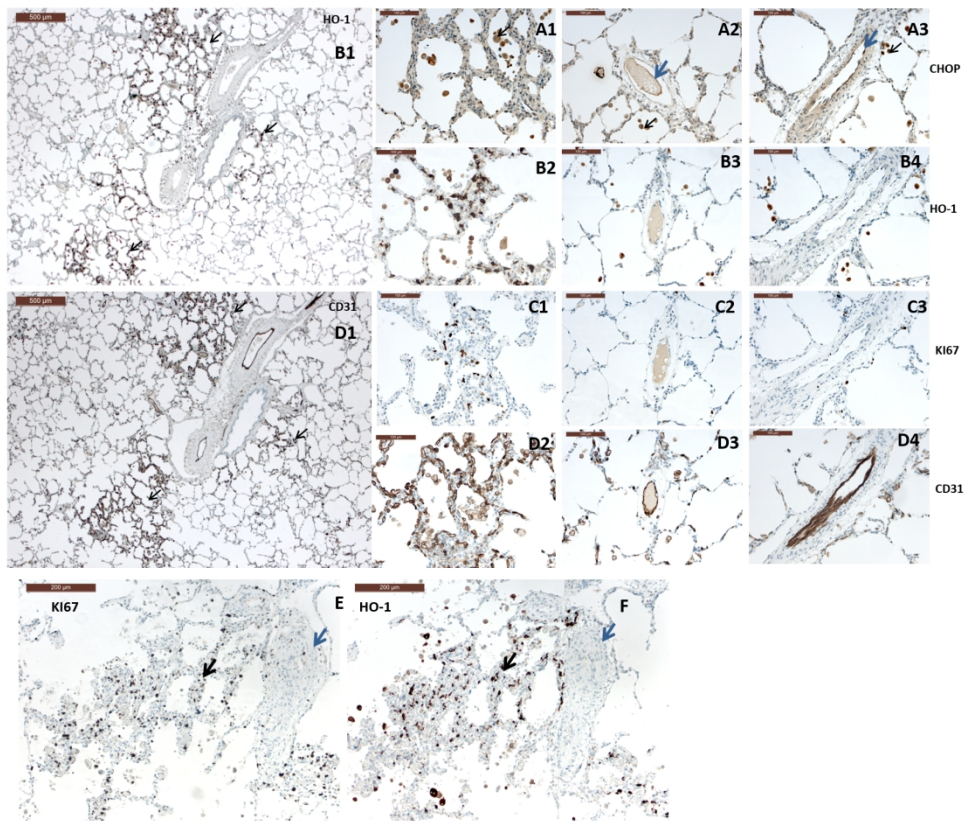


Figure 6

326x273mm (150 x 150 DPI)

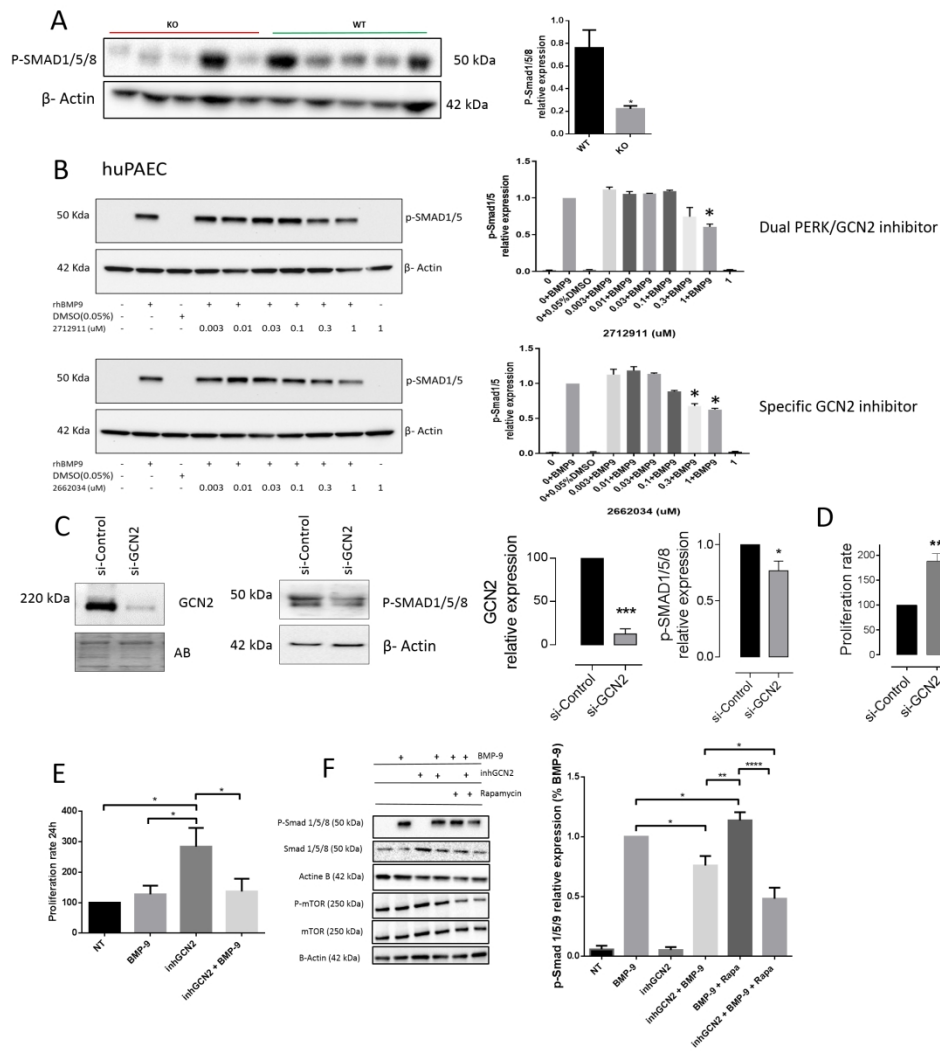


Figure 7

416x456mm (150 x 150 DPI)

Online Supplemental Data

Comparison of Human and Experimental Pulmonary Veno-Occlusive Disease

Grégoire Manaud Msc, Esther J. Nossent MD, Mélanie Lambert PhD, Maria-Rosa Ghigna, Angèle Boët, MD, PhD, Maria-Candida Vinhas , Benoit Ranchoux PhD, Sébastien J. Dumas PharmD-PhD, Audrey Courboulin PhD, Barbara Girerd MD, PhD, Florent Soubrier MD-PhD, Juliette Bignard MSc, Olivier Claude PhD, Florence Lecerf Msc, Aurélie Hautefort PhD, Monica Florio PhD, Banghua Sun, Sophie Nadaud PhD, Stijn E. Verleden PhD, Séverine Remy PhD, Ignacio Anegón, MD, Harm Jan Bogaard MD-PhD, Olaf Mercier MD-PhD Elie Fadel MD-PhD, Gérald Simonneau MD-PhD, Anton Vonk Noordegraaf MD-PhD, Katrien Grünberg MD-PhD, Marc Humbert MD-PhD, David Montani MD-PhD, Peter Dorfmüller MD-PhD, Fabrice Antigny PhD, and Frédéric Perros PhD

Methods

Patients - We retrospectively reviewed clinical data and histological samples from 12 PVOD patients (6 with biallelic mutations in the *EIF2AK4* gene (hPVOD) and 6 non-carriers (sPVOD)) who were transplanted between 2004 and January 2015. Clinical diagnosis of PVOD had been established during interdisciplinary meetings with pulmonologists, radiologists and pathologists. Study patients were part of the French Network on Pulmonary Hypertension, a program approved by our institutional Ethics Committee, and had given written informed consent (Protocol N8CO-08-003, ID RCB: 2008-A00485-50, approved on June 18, 2008). Pulmonary arterial hypertension (PAH) samples used in immunohistochemistry (see hereafter) were originating from the same cohort.

For control patients, unused donor lungs were matched to the study cohort as close as possible using age and gender. These donor lungs were collected under existing Belgian law which releases the lungs for research if the quality is not sufficient for transplantation (Ethical number S59648 S61653 S61987). The methodology is explained before and in brief included air-inflation till 30cm of H₂O and fixation at 10 Cm H₂O in the fumes of liquid nitrogen and storage at -80°C. After CT scan (Siemens Somatom), lungs are sliced using a bandsaw in 2cm slices and systematically sampled using a core bore (1).

Clinical assessment - Patient demographics, pulmonary function testing and hemodynamics at diagnosis were obtained from the pulmonary hypertension database of the French Referral Center for Pulmonary Hypertension, Department of Pulmonology and Intensive Care Unit for Respiratory Diseases, Hôpital Bicêtre, AP-HP, Université Paris-Sud, Le Kremlin-Bicêtre, France.

In vivo study design - Rats were housed at the Faculty of Pharmacy of Châtenay-Malabry (ANIMEX platform, Châtenay Malabry, France). Animal studies were approved by the administrative panel on animal care at the Université Paris-Sud, Le Plessis-Robinson, France. The animal facility is licensed by the French Ministry of Agriculture (agreement N° B92-019-01). This study was approved by the Committee on the Ethics of Animal Experiments CEEA26 CAP Sud. Rat experiments were supervised by Dr. Frédéric Perros (agreement delivered by the French Ministry of Agriculture for animal experiment N° A92-392). All efforts were made to minimize animal suffering.

Generation of *GCN2-deficient rats* – sgRNA was designed, produced and tested in vitro in rat C6 cells by T7 endonuclease I mismatch detection as previously described (2). The sgRNA targeted the following sequence: GGACTTCCAGGATCTGCGGC CGG. Zygote microinjection were performed as previously described (3). Briefly, zygotes were collected from pre-pubescent (4–5-wk-old) SD superovulated donor female rats (SD/Crl, Charles River, L'Arbresle, France) and then mated with fertile males. sgRNA (10ng/μl) and Cas9mRNA (50ng/μl) were co-microinjected into the cytoplasm of one-cell-stage fertilized embryos. Surviving embryos were implanted on the same day in the oviduct of pseudopregnant females (0.5 dpc). Newborn rats were genotyped using microcapillary electrophoresis as previously described (4). Our strategy was to induce a reading frame shift in the first exon of *Eif2ak4* in order to disrupt the gene. We developed a strain with a biallelic deletion of 152 bp in the first exon of *Eif2ak4* ($\Delta 152\text{Ex1}/\Delta 152\text{Ex1}$).

All animal care and procedures performed in this study were approved by the Animal Experimentation Ethics Committee of the Pays de la Loire region, France, in accordance with the guidelines from the French National Research Council for the Care and Use of Laboratory Animals (Permit Number: Apafis 692). All efforts were made to minimize suffering. The rats were housed in a controlled environment (temperature $21\pm 1^\circ\text{C}$, 12-h light/dark cycle).

Rat Genotyping - After genomic DNA extraction from rats' ear punches, PCR were performed using 5X Herculase and primers (DNA bases: UPTE71-EIF2AK4: 5'-GAGGTCCCGTTTTTCAGAGC-3' and LoTE71-EIF2AK4: 5'-AAGTCGAGGTGGGGAAGAAT-3') encompassed mutant sequences. The PCR product were loaded on 1.5% agarose gels and stained with SYBR Safe (Invitrogen; cat. no. S33102). The amplicon size is 619 pb for wild-type allele and 467 pb for $\Delta 152\text{Ex1}$ allele.

Mitomycin C-induced PVOD-model - To evaluate the kinetics of PH development after MMC exposure, female Wistar rats (5 weeks old, Janvier Labs, Saint Berthevin, France) received two regimens of MMC as previously described (5) (3 mitomycin-C Kyowa $\text{mg}\cdot\text{kg}^{-1}\cdot\text{wk}^{-1}$ once a week for 2 weeks, IP). Rats were randomly assigned to a control group (n=5) or MMC exposed groups (n=30). Rats were sacrificed at week 1 (n=5), week 2 (n=5), week 3 (n=5), week 4 (n=5) and week 5 (n=5). To

minimize suffering, necropsy order at each time point was determined by the clinical condition of individual animals.

Evaluation of right ventricle hypertrophy and collection of tissue - Rats were anesthetized with isoflurane (2L/min O₂/3% isoflurane; Minerve, Esternay, France). Following exsanguination, the hilum of the left lung was ligated and the right lung was distended by infusion of formalin via the trachea, and then embedded in paraffin. The non-inflated left lungs were snap frozen in liquid nitrogen and used for protein and RNA quantification. For Fulton's index of right ventricle hypertrophy (RVH), the ratio of the right ventricular weight to left ventricular plus septal weight (RV/LV+S) was calculated.

Echocardiographic measurement – To rule out the possibility that MMC-induced LV dysfunction participates in the pulmonary venous and arteriolar alterations seen with mitomycine, we carried over an Trans-thoracic echocardiography (TTE) follow-up of MMC-exposed rat (3 mg MMC/kg i.p. at day 0 and day 7) and analyzed parameters that could inform us about potential alterations of left ventricle (LV) function: calculated aortic cardiac output (CO), LV fractional shortening (LVFS), LV End Systolic Diameter (LVESD), LV End Diastolic Diameter (LVEDD) and Interventricular septum thickness at end-diastole (IVSd), at day 0 (before MMC exposure), then day 2, 8, 10, 17, 22 and 28 post first MMC exposure. Pulmonary artery acceleration time (PAAT), a validated index of pulmonary vascular resistance, arterial pressure, and compliance, was used to assess pulmonary hemodynamics at the same time points. Lower PAAT is indicative of pulmonary vascular disease (6) (7). Evaluation by TTE was performed with a digital ultrasound system (Vivid E9, GE Healthcare) by using a high-frequency phased array transducer (12 S-D 4-12MHz, GE Healthcare). Echocardiographic evaluation procedure was performed under general anesthesia and spontaneous breathing with an Isoflurane Rodent Anesthesia 21 System (Minerve, Esternay, France) (maintenance: isoflurane 2% at room air). Rats were shaved and body temperature was controlled during experiments. All analyses were performed in a blinded fashion way: rats' experimental conditions were unknown by the operator during TTE examination and data interpretation. All measurement were performed as previously described (8).

Histopathology - Lung samples from all rats were retrospectively analyzed in a blinded fashion by conventional light microscopy using quantitative semi-automated software (NIS-BR, Nikon, Champigny sur Marne, France). Of each rat at each time point 5-micrometer thick sections were stained with hematoxylin-eosin (HE) or hematoxylin-eosin-saffron (HES) and Trichrome/Weigert staining (cytoplasm/smooth muscle cells in red, fibrin/erythrocytes in magenta, collagen/fibrosis in blue, elastic fibres in black and nuclei in brown/black). Additional α -smooth-muscle actin (α -SMA) immunohistochemical (IHC) stains were performed.

Quantifying remodeling pulmonary arteries and veins – All pulmonary vessels were topographically recognized: pulmonary arteries were always accompanied by an adjacent airway; pulmonary veins were identified within interlobular septa, or in pre-septal position. Also, when septa were not visible due to sectional hazard, vessels between to transversally sectioned and clearly identified PAs were identified as pulmonary veins. Vessels beneath $<70\ \mu\text{m}$ in diameter are referred to as microvessels, since their pre- or post-capillary origin cannot be clearly determined. The surface of the lumen, intima, media and adventitia of 5 concentric pulmonary arteries (Trichrome/Weigert staining) of each rat was measured, as was the lumen and total wall thickness of 5 veins (diameter between 70 and 250 μm) (α -SMA, IHC). The ratio between the surface of the lumen and total vessel wall was calculated.

Quantifying remodeling of microvessels - Microvessels (arterioles and venules) were counted in 10 fields (objective 20x) on 1 paraffin slide (α -SMA, IHC) of each rat. The degree of remodeling was assessed semi-quantitatively: not remodeled (α -SMA negative), mildly remodeled (α -SMA positive but without loss of the lumen), moderate remodeled (α -SMA positive with loss of the lumen $\leq 50\%$) and severely remodeled (α -SMA positive with loss of the lumen $>50\%$).

Immunohistochemistry - Paraffin-embedded 5 μm thick sections of lung samples were mounted on SuperFrostPlus slides (Thermoscientific, Villebon sur Yvette, France). The immunostainings using CHOP (rabbit polyclonal, reference number: HPA058416, Sigma-Aldrich), HO-1 (rabbit polyclonal, reference number: HPA000635, Sigma-Aldrich), CD31 (EP78, rabbit monoclonal), Ki67 (SP6, rabbit monoclonal) antibodies were performed according the facility automated protocol (benchmark GX

autostainer, Ventana Medical System, Roche). Positive and negative controls of HO-1 and CHOP stainings were used to validate the specificity of the primary antibodies (Figure E20).

Western blots - Rat lung tissue samples were prepared as described (9). 80 µg of protein were separated on SDS-PAGE and transferred to PVDF membrane. After blocking, membranes were incubated in TBS and 5% nonfat milk overnight at 4°C with primary antibodies described in the Table E1. Blots were incubated with horseradish peroxidase (HRP)-conjugated goat anti-mouse diluted 1:10000 (Cell Signaling) or with HRP-conjugated goat anti-rabbit diluted 1:5000 (Cell Signaling), respectively. Antibodies were revealed using ECL reagents (Perkin Elmer). Image-J Software was used to quantify the level of protein expression.

Electrophysiological recordings - Hearts and lungs were rapidly excised into ice-cold physiological Ca^{2+} -free Hank's media. First- to third-order intrapulmonary arteries, with diameters between 2 and 0.2 mm, were dissected, the endothelium of vessels was disrupted by rubbing the luminal surface with a cotton swab, the fibroblast-containing adventitial layer was removed, and the media containing PASMC was dissociated with a cocktail containing papain, DTT, and BSA, as previously described (10). K^+ currents were recorded using the whole-cell patch-clamp technique at room temperature (22–24°C) in normoxic conditions, with an Axopatch 200B amplifier, a Digidata 1440A, and pClamp 10 software (Molecular Devices, Sunnyvale, CA, USA). Borosilicate glass pipettes (Harvard Apparatus) were pulled with a Sutter puller, fired polished, and had a resistance of 3–5 MΩ. The pipette solution contained (in mM): 130 KCl, 1 MgCl₂, 10 HEPES, 1 EGTA, at pH 7.2 (adjusted with KOH). The bath solution contained (in mM): 124 NaCl, 5 KCl, 0.5 NaH₂PO₄, 0.5 KH₂PO₄, 1 MgCl₂, 1 CaCl₂, 10 HEPES, 10 glucose, at pH 7.4 (adjusted with NaOH). Cell capacitances (9–15 pF for PASMC and 4–5 pF for PAEC) were obtained for each cell measured, and the current was normalized to the cell's capacitance. I_{KV} was elicited by applying a 400-ms voltage step to 0 mV, from a holding potential of –40 mV. I_{KCNK3} current was elicited by addition of specific KCNK3 blocker, A293 compound (provided by Sanofi). I_{KCNK3} correspond to the A293 sensitive current. To minimize any nonspecific effects, we used A293 at

200 $\mu\text{mol/L}$ (10, 11). The junction potential of ~ 4.6 mV between the pipette and bath solution was corrected off-line.

Determination of pulmonary serotonin levels using Liquid chromatography/tandem mass spectrometry (LC-MS/MS)

1. Preparation of standards

Stock solutions of serotonin (Sigma-Aldrich, Lyon, France) and serotonin-D4 used as internal standards (Cluzeau Info Labo, Sainte-Foy-La-Grande, France) were prepared at a concentration of 10mg/ml in distilled water. They were then diluted as working solutions in ammonium formate 100mM (buffered with formic acid at pH=3.5) at concentrations of 1 $\mu\text{g/ml}$ and 3 $\mu\text{g/ml}$, respectively. The internal standard was included in the sample before extraction.

2. Sample preparation for LC-MS/MS

The extraction solution was composed of 10% ammonium formate 100 mM pH 3.5, 10% serotonin-D4 solution 3 $\mu\text{g/ml}$ and 80% acetonitrile allowing metabolite extraction and protein precipitation. Pieces of frozen lungs from rats were weighed (about 50mg) and homogenized into 1ml of extraction solution using GentleMACS™ dissociator (Miltenyi Biotech, Paris, France). The homogenates were then centrifuged at 1500g for 5 min at 4°C in order to discard macroscopic residues. The supernatants were collected and submitted to two successive centrifugations at 15000g for 10 min at 4°C to further eliminate small residues. Supernatants were collected after each centrifugation to achieve a clear solution and then stored at -20°C until use.

3. LC-MS/MS

10 μL each standard (serotonin and serotonin-D4 solutions) and extracts were injected in a HPLC instrument Ultimate 3000 DGP3600 (Dionex, Sunnyvale, CA, USA) with an automatic injector WPS 3000 set at 4°C. Separation of metabolites was performed using a Nucleoshell® HILIC column (100mmx2mm, 2.7 μm , Macherey-Nagel, Hoerd, France). The mobile phase composed of acetonitrile/100mM ammonium formate (pH=3.5): 80/20 (V/V), was used at a flow rate of 400 $\mu\text{L/min}$.

The run time was 4,5min for each sample. The retention time was 1 min for both serotonin and serotonin-D4.

Detection of serotonin was achieved with a triple quadrupole mass spectrometer (Waters, Milford, Massachusetts, USA) using an electrospray ionization source. The source and desolvation gas temperatures were set to 120°C and 350°C respectively. Desolvation gas flow was set to 479L/h, capillary and cone voltages to 2,5kV and 35V respectively. Multiple reaction monitoring (MRM) was used in positive mode to detect precursor ions of serotonin at m/z 177 and serotonin-D4 at m/z 181. Applying collision energies of 10eV and 11eV, product ions were obtained at m/z 160 and 164 for serotonin and serotonin-D4 respectively.

4. Semi-quantitative analysis

Peaks of serotonin and internal standard serotonin-D4 were integrated and the variability of extraction rates was corrected calculating the ratio between peak areas of serotonin and serotonin-D4. Then, these ratios were divided by the weight of lung pieces.

Effect of GCN2 and PERK/GCN2 dual inhibitor on BMP-9 signaling in huPAEC and huPASMC cells

Experiments displayed on Figure 7B, E15A and E15B were performed in Amgen Laboratories (Dr Monica Florio and Dr Banghua Sun) following the above protocols:

Cells and Reagents

Human pulmonary artery endothelial cells (huPAEC), human pulmonary artery smooth muscle cells (huPASMC) and culture medium were obtained from Lonza Bioscience (Walkersville, MD). Antibodies for phospho-SMAD1/5 was from Cell Signaling (Cat# 13820S); Phospho-PERK was from BioLegend (Cat# 6494) and β -Actin was from Sigma (Cat# A3854). Compound 2712991 and 2662034 were from Amgen compound bank. Recombinant human BMP9 was from R&D Systems (Cat# 3209-BP-010/CF).

Cell Treatment

huPAEC and huPASC cells were cultured on 6-well plates at 1×10^6 cells/ml in 2ml culture medium for 24 hours. Cells were typically about 70% confluent at the time of treatments. Cells were exposed to 0.003–1 μ M GCN2 inhibitory compounds or 0.05%DMSO in basal medium (without serum and any supplements) for 3 hours, followed by adding BMP9 at 20ng/ml for 30 minutes.

p-Smad1/5 and p-PERK Detection

Treated huPAEC and huPASC were harvested on ice in phosphate-buffered saline (PBS) and centrifuged. Cell lysates were made by adding an appropriate volume of lysis buffer (50 mM Tris-HCl [pH 7.4], 50 mM NaCl, 5 mM EDTA, 1% Triton X-100, 0.05% SDS, 50 mM NaF, 10 mM β -glycerophosphate, 10 mM sodium pyrophosphate, 100 μ M NaVO₄, protease inhibitor cocktail; Roche Applied Science, Indianapolis, IN) and vortexed for 2 seconds. After centrifugation at 4°C, the supernatant was removed and the protein concentration determined (BCA protein assay reagent; Pierce, Rockford, IL). An equal amount of total protein of each sample was resolved by SDS-PAGE and transferred onto nitrocellulose membrane (Invitrogen). Blots were blocked for 2 hours in PBST (PBS plus 0.1% Tween-20) containing 5% milk (blocking buffer) before incubation with primary antibodies. For p-Smad1/5 and p-PERK detection, blots were incubated with primary antibodies at 1:1,000 and 2 μ g/ml separately for 2 hours at room temperature. After three washes with PBST, blots were incubated with peroxidase-conjugated secondary antibodies (Cell Signaling, Cat# 7074S). Blots were developed using SuperSignal Pico Chemiluminescent substrate (Thermo Scientific, Cat# 34080). To detect β -Actin on the same blots, the blots were stripped with Western blot stripping buffer (Pierce) for 15 minutes with shaking. Blots were blocked for 1 hour, followed by incubation with β -Actin antibody (1 hour) and secondary antibody (1 hour) and developed. Western blot signal was detected using Bio-Rad ChemiDoc MP Image System.

Experiments displayed on Figure 7C, 7D, 7 E, E15C, E15D, E16 and E21 were performed at Inserm U999 following the above protocols:

Human PAEC culture

Human PAECs were cultured as previously described (12) and were used for the study between passages 3 and 5. Patients studied were part of a program approved by our institutional Ethics Committee and had given written informed consent (ID RCB: 2018-A01252-53, approved on June 18, 2006). Single and co-treatment of PAECs were made in 60mm dishes in 3ml of MCDB131 media (Gibco). At 70-80% of confluence, cells were treated with GCN2 inhibitory compound (2662034) at 1 μ M (Amgen), Rapamycin at 10 ng/ml (Sigma-Aldrich) in basal media (Serum and supplements free) for 4h, followed by adding BMP-9 (R&D Biosystems) for 30' at 20 ng/ml (13). We used rapamycin at 10 ng/ml, as previously described to potentiate BMP signaling in endothelial cells (14).

PAECs were treated with 0.5 mM of His during 4 hours because it induced a robust activating phosphorylation of GCN2 (Thr 899) as compared to other time points (10 and 24 hours) and other doses (0.05, 1, 2 and 5 mM) (Figure E21A) of the revised manuscript). At 0.5 mM His, 2662034 compound was also able to almost completely abrogate GCN2 phosphorylation whereas it couldn't at higher dose (1 mM) Figure E21B).

Human qPCR Array

Total RNA was extracted using TRIzol reagent according to standard procedures. RNA quantity and quality was assessed using the Nanodrop-ND-1000 (Nanodrop Technologies, Wilmington, USA). One microgram of total RNA was reverse-transcribed using a QuantiTect Reverse Transcription Kit (Qiagen, Valencia, CA, USA; cat. no. 205311). Gene expression of BMP pathway (Ref PZ36A1H1) and ISR pathway (ISR1H1) were determined using SignArray96, (Reference numbers: ISR1H1 and PZ36A1H1, Anygenes, and Paris, France) on a StepOne + Real-Time PCR System (Life Technologies). Briefly, each qPCR reaction contains 10 μ l of PMS, 2 μ l of Validated qPCR Primer Sets (Reverse + Forward, 10 μ M each; AnyGenes, Paris, France), 4 μ l of diluted cDNA and 4 μ l nuclease-free water for a final volume of 20 μ l. PCR amplification was conducted following cycling conditions : pre-incubation at 95 °C for 10 min, followed by 35 cycles of 10 s at 95 °C, 20 s at 60 °C, and 1 s at 72 °C. The mRNA expression for each gene was normalized using the housekeeping gene transcripts of actin beta (ACTB).

All the primer sets and associated fold change and p-value are described in the supplementary table E2 (BMP pathway) and E3 (ISR pathway).

Statistical Analyses –

All data were checked for normal distributions. Quantitative variables are presented as means \pm standard errors of the means (SEMs). Data were analyzed using Student's t-tests or one-way analysis of variance and Bonferroni multiple comparisons tests. P values less than 0.05 were considered to reflect statistical significance.

References

1. Verleden SE, Vasilescu DM, Willems S, Ruttens D, Vos R, Vandermeulen E, Hostens J, McDonough JE, Verbeken EK, Verschakelen J, Van Raemdonck DE, Rondelet B, Knoop C, Decramer M, Cooper J, Hogg JC, Verleden GM, Vanaudenaerde BM. The site and nature of airway obstruction after lung transplantation. *Am J Respir Crit Care Med* 2014;189:292–300.
2. Jung CJ, Ménoret S, Brusselle L, Tesson L, Usal C, Chenouard V, Remy S, Ouisse L-H, Poirier N, Vanhove B, de Jong PJ, Anegon I. Comparative Analysis of piggyBac, CRISPR/Cas9 and TALEN Mediated BAC Transgenesis in the Zygote for the Generation of Humanized SIRPA Rats. *Sci Rep* 2016;6:31455.
3. Ménoret S, De Cian A, Tesson L, Remy S, Usal C, Boulé J-B, Boix C, Fontanière S, Crénéguy A, Nguyen TH, Brusselle L, Thinard R, Gauguier D, Concordet J-P, Cherifi Y, Fraichard A, Giovannangeli C, Anegon I. Homology-directed repair in rodent zygotes using Cas9 and TALEN engineered proteins. *Sci Rep* 2015;5:14410.
4. Chenouard V, Brusselle L, Heslan J-M, Remy S, Ménoret S, Usal C, Ouisse L-H, NGuyen TH, Anegon I, Tesson L. A Rapid and Cost-Effective Method for Genotyping Genome-Edited Animals: A Heteroduplex Mobility Assay Using Microfluidic Capillary Electrophoresis. *J Genet Genomics* 2016;43:341–348.
5. Perros F, Günther S, Ranchoux B, Godinas L, Antigny F, Chaumais M-C, Dorfmueller P, Hautefort A, Raymond N, Savale L, Jaïs X, Girerd B, Cottin V, Sitbon O, Simonneau G, Humbert M, Montani D. Mitomycin-Induced Pulmonary Veno-Occlusive Disease: Evidence From Human Disease and Animal Models. *Circulation* 2015;132:834–847.
6. Levy PT, Patel MD, Choudhry S, Hamvas A, Singh GK. Evidence of Echocardiographic Markers of Pulmonary Vascular Disease in Asymptomatic Infants Born Preterm at One Year of Age. *J Pediatr* 2018;197:48-56.e2.

7. Naing P, Kuppusamy H, Scalia G, Hillis GS, Playford D. Non-Invasive Assessment of Pulmonary Vascular Resistance in Pulmonary Hypertension: Current Knowledge and Future Direction. *Heart Lung Circ* 2017;26:323–330.
8. Lambert M, Boet A, Rucker-Martin C, Mendes-Ferreira P, Capuano V, Hatem S, Adão R, Brás-Silva C, Hautefort A, Michel J-B, Dorfmueller P, Fadel E, Kotsimbos T, Price L, Jourdon P, Montani D, Humbert M, Perros F, Antigny F. Loss of KCNK3 is a hallmark of RV hypertrophy/dysfunction associated with pulmonary hypertension. *Cardiovasc Res* 2018;114:880–893.
9. Ranchoux B, Günther S, Quarck R, Chaumais M-C, Dorfmueller P, Antigny F, Dumas SJ, Raymond N, Lau E, Savale L, Jaïs X, Sitbon O, Simonneau G, Stenmark K, Cohen-Kaminsky S, Humbert M, Montani D, Perros F. Chemotherapy-induced pulmonary hypertension: role of alkylating agents. *Am J Pathol* 2015;185:356–371.
10. Antigny F, Hautefort A, Meloche J, Belacel-Ouari M, Manoury B, Rucker-Martin C, Péchoux C, Potus F, Nadeau V, Tremblay E, Ruffenach G, Bourgeois A, Dorfmueller P, Breuils-Bonnet S, Fadel E, Ranchoux B, Jourdon P, Girerd B, Montani D, Provencher S, Bonnet S, Simonneau G, Humbert M, Perros F. Potassium Channel Subfamily K Member 3 (KCNK3) Contributes to the Development of Pulmonary Arterial Hypertension. *Circulation* 2016;133:1371–1385.
11. Putzke C, Wemhöner K, Sachse FB, Rinné S, Schlichthörl G, Li XT, Jaé L, Eckhardt I, Wischmeyer E, Wulf H, Preisig-Müller R, Daut J, Decher N. The acid-sensitive potassium channel TASK-1 in rat cardiac muscle. *Cardiovasc Res* 2007;75:59–68.
12. Dumas SJ, Bru-Mercier G, Courboulin A, Quatredeniens M, Rucker-Martin C, Antigny F, Nakhleh MK, Ranchoux B, Gouadon E, Vinhas M-C, Vocelle M, Raymond N, Dorfmueller P, Fadel E, Perros F, Humbert M, Cohen-Kaminsky S. NMDA-Type Glutamate Receptor Activation Promotes Vascular Remodeling and Pulmonary Arterial Hypertension. *Circulation* 2018;137:2371–2389.
13. Long L, Ormiston ML, Yang X, Southwood M, Gräf S, Machado RD, Mueller M, Kinzel B, Yung LM, Wilkinson JM, Moore SD, Drake KM, Aldred MA, Yu PB, Upton PD, Morrell NW. Selective

enhancement of endothelial BMPR-II with BMP9 reverses pulmonary arterial hypertension. *Nat Med* 2015;21:777–785.

14. Spiekerkoetter E, Tian X, Cai J, Hopper RK, Sudheendra D, Li CG, El-Bizri N, Sawada H, Haghghat R, Chan R, Haghghat L, de Jesus Perez V, Wang L, Reddy S, Zhao M, Bernstein D, Solow-Cordero DE, Beachy PA, Wandless TJ, Ten Dijke P, Rabinovitch M. FK506 activates BMPR2, rescues endothelial dysfunction, and reverses pulmonary hypertension. *J Clin Invest* 2013;123:3600–3613.
15. Watson LE, Sheth M, Denyer RF, Dostal DE. Baseline echocardiographic values for adult male rats. *J Am Soc Echocardiogr* 2004;17:161–167.
16. Hayward R, Hydock DS. Doxorubicin cardiotoxicity in the rat: an in vivo characterization. *J Am Assoc Lab Anim Sci* 2007;46:20–32.

Supplemental legends

Figure E1: Analysis of p-eiF2 α in lung from hPVOD, sPVOD patients and MMC-exposed rats.

A, p-eiF2 α expression measured by Western blot analysis in control and MMC-exposed rats (1, 2, 4 and 5 weeks after MMC-exposure). **B**, p-eiF2 α in lung from hPVOD and spVOD. β -Actin was used as loading control ns = non-significant.

Figure E2: Upregulation of mitogenic and anti-apoptotic pathways in MMC-exposed rats:

Pulmonary levels of P-P38, p-ERK1/2, PCNA and Survivin in control and MMC-exposed rats (1, 2, 4 and 5 weeks after MMC-exposure, week 3 is displayed in supplemental figure E19). β -Actin was used as loading control. *P<0.05, **P<0.005, ***P<0.0005, ****P<0.0001

Figure E3: MMC induces progressive development of foci of alveolar wall thickening suggestive of pulmonary capillary hemangiomas in rats.

HE stained paraffin embedded lung sections in control and MMC-exposed rats (1, 2, 3, 4 and 5 weeks after MMC-exposure) with foci of alveolar wall thickening (arrows) suggestive of pulmonary capillary hemangiomas developing overtime and becoming manifest at week 3 and progressive at week 4 and 5.

Figure E4: Analysis of protein Twist-1 expression in MMC-exposed rats.

Twist1 measured by Western blot analysis (WB) in control and MMC-exposed rats (1, 2, 4 and 5 weeks after MMC-exposure, week 3 is displayed in supplemental figure E19). β -Actin was used as loading control. Quantification of the Western blots are shown close to Western blots image *P<0.05; ***P<0.0005.

Figure E5: Analysis of protein p120-catenin expression in lung from sPVOD, hPVOD patients and in MMC-exposed rats.

Pulmonary levels of p120-catenin was analyzed by Western blotting during the development of PVOD in control and MMC exposed-rats (A) (1, 2, 4 and 5 weeks after MMC-exposure, week 3 is displayed in supplemental figure E19) and in Human (B). β -Actin was used as loading control. Quantification of Western blots is shown near Western blot image. *P<0.05; ***P<0.0005.

Figure E6: Apoptosis is enhanced in MMC-induced PVOD.

Pulmonary levels of cleaved-Caspase 3 measured by Western blot analysis (WB) in control and MMC-exposed rats (1, 2, 4 and 5 weeks after MMC-exposure, week 3 is displayed in supplemental figure E19). β -Actin was used as loading control. Right panel represent the quantification of the Western blots. **P<0.005. ***P<0.0005.

Figure E7: Inflammation is enhanced in lung from hPVOD, sPVOD patients and in MMC-induced PVOD.

Pulmonary levels of CD45 measured by Western blot analysis (WB) in control and MMC-exposed rats (A) (1, 2, 4 and 5 weeks after MMC-exposure, week 3 is displayed in supplemental figure E19) and in lung from hPVOD and sPVOD (B). β -Actin was used as loading control. Right panel represent the quantification of the Western blots. *P<0.05.

Figure E8: Dysregulation of serotonin pathway in MMC-induced PVOD.

Pulmonary serotonin (5-HT) content was significantly increased at week 5. ***P<0.0005.

Figure E9: Analysis of ERG expression in lung from hPVOD, sPVOD patients and MMC-exposed rats. **A**, ERG expression measured by Western blot analysis in control and MMC-exposed rats (1, 2, 3, 4 and 5 weeks after MMC-exposure). **B**, ERG in lung from hPVOD and sPVOD. β -Actin was used as loading control *P<0.05; **P<0.005.

Figure 10: Additional analysis of GCN2 expression in lung from hPVOD, sPVOD patients

A, GCN2 lung expression measured by Western blot analysis in sPVOD patients. **B**, GCN2 lung expression hPVOD. β -Actin was used as loading control.

hPVOD samples are originating from patients with nonsense/frameshift mutations in *EIF2AK4*.

Figure E11: Analysis of Ki67, HO-1 and CHOP expression in control lung patients.

Lung tissue control. No KI67 staining within the alveolar septa (A). HO-1 (B) and CHOP (C) are not expressed in lung control.

Figure E12: Analysis of HO-1 expression in PAH lung patients

HO-1 staining in lungs with pulmonary arterial hypertension. Pulmonary arteries (A, C) and pulmonary veins (B, D) do not express HO-1 staining is not found in lung explants of PAH patients.

Figure E13: Analysis of CHOP expression in PAH lung patients

DDIT3 (CHOP) staining in lungs with pulmonary arterial hypertension. Pulmonary arteries do not express DDIT3, while in plexiform lesion a very faint staining become visible within the endothelial cells (B). No staining is observed in small muscular arteries (C). A very faint staining is observed in endothelial cells of small veins (D).

Figure E14: Analysis of Ki67, HO-1 and CD31 expression in sPVOD lung patients

PVOD without *EIF2AK4* mutation. DDIT3 (CHOP) staining in PVOD lung; endothelial staining is visible in both remodeled veins (1B, blue arrow) and arteries (1C, blue arrow). The staining becomes faint in smooth muscle cells whereas it is well observed in cytoplasm of bronchial cells, alveolar cells and macrophages (1A, 1B, 1C black arrows). HO-1 staining in PVOD lungs is observed in interstitial cells within alveolar septa in capillary hemangiomatosis foci (2A). The labelling is strong and highlights interstitial cells with cytoplasmic extensions. Outside these foci no staining is observed. The endothelial cells do not express HMOX. Ki67 staining highlights cells engaged in proliferation. Scant interstitial

cells are labelled within capillary hemangiomas foci and in bronchial basal layer. CD31 staining underlines endothelial cells within alveolar septa (4A) and of pulmonary vessels (4B, 4C).

Figure E15: Effect of GCN2 and PERK/GCN2 dual inhibitor on BMP-9 signaling in huPASM cells.

2712991 is PERK/GCN2 dual inhibitor, 2662034 is GCN2 inhibitor.

A, Effect of PERK/GCN2 dual inhibitor on BMP-9 signaling and PERK phosphorylation level in huPASM. **B**, Effect of specific GCN2 inhibitor on BMP-9 signaling and PERK phosphorylation in huPASM. **C**, Effect of siGCN2 on p-SMAD 1/5/8 phosphorylation in huPASM. **D**, Effect of siGCN2 on PASM proliferation. β -Actin (A, B) and Amido Black (C) was used as loading control. Right panels represent the quantification of the Western blots (Left panels). *P<0.05.

Figure E16: Knockdown of GCN2 in human pulmonary endothelial cells increases survivin expression.

Consequence of GCN2 knockdown on Survivin expression in human PAEC (n=4)

Figure E17: Effect of MMC on cardiac function in rats

Echocardiographic measurement of MMC exposed and control rats (J0, J2, J8, J10, J17, J22 and J28) of Weight (A), PAAT (B), Aortic Cardiac Output (C), Normalized Cardiac Output (D), LV Fractional Shortening (E), LV ESD (F), LV EDD (G) and IVDS (H).

Strikingly, PAAT was significantly lower in MMC exposed-rats as compared to controls, as soon as day 2 after the first MMC injection and remained lower for the whole follow-up. This was followed by a lower CO from day 8 to day 28. If normalized to the body weight, decreased CO was transient from day 8 to day 22. Interestingly, LVFS decreased following the same kinetic. Decreased LVFS was mainly attributable to lower LVEDD. IVSD was unchanged for the whole follow up indicating the absence of LV hypertrophy.

It has been shown that the use of echocardiography for assessment of cardiac anatomy, function, and hemodynamics can be consistently applied to the rat and replicates much of the information used routinely in human echocardiography. In this context, the LVFS are similar to those reported for healthy human beings (15). LVFS > 25% being the normal range, the LVFS values while decreased in MMC-exposed rat are not pathologic. Decreased CO could be linked to LV function alteration but can equally be attributed to right ventricular dysfunction. Moreover, toxicities of chemotherapy like MMC can result in clinically significant diarrhea leading to hypovolemia, another relevant trigger of low CO. At last, cardiotoxicity of chemotherapy like doxorubicin are associated to dilated cardiomyopathy (16) that doesn't fit with the lower LVEDD we measured in MMC exposed rat.

Figure E18: Pulmonary levels of p-P38, p-ERK1/2, PCNA, Survivin, GCN-1, PERK, HO-1, PKR, ATF4, CHOP, p-SMAD2/3 and Survivin in MMC-exposed rats.

A, Pulmonary levels of p-P38, p-ERK1/2, PCNA and Survivin expression in controls and MMC exposed rats (week 1, 2, 4 and 5). B Pulmonary levels of GCN1, PERK, HO-1, PKR, ATF4, CHOP, p-SMAD2/3 and Survivin in control and 3 weeks after MMC-exposure in rats. β -Actin was used as loading control. *P<0.05 **P<0.005 ***P<0.0005 ****P<0.0001.

Figure E19: Pulmonary levels of P-120-Catenin, p-SMAD1/5/8, Twist 1, P-P38, p-ERK1/2, cleaved Caspase 3, BMPRII, CD45, PCNA, GCN2 and p-eiF2 α three weeks after MMC-exposure. A, Pulmonary levels of P-120-Catenin, p-SMAD1/5/8, Twist 1, P-P38, p-ERK1/2, cleaved Caspase 3, BMPRII, CD45, PCNA, GCN2 and p-eiF2 α in control and 3 weeks after MMC-exposure in rats. β -Actin was used as loading control. *P<0.05.

Figure E20: Positive and negative controls of HO-1 and CHOP in human lung patients.

HO-1 positive and negative controls. HO-1 is expressed in membranes and cytoplasm of clear cells renal carcinoma (1A). The negative control has been performed on the same tissue by withdrawing the primary antibody (1B). HO-1 is not expressed in colorectal carcinoma [(1C) negative control]. DDIT3 (CHOP) staining appears strong within the cytoplasm of neoplastic cells (mediastinal seminoma (2A).

Endothelial staining is visible in tumor associated vessels (arrow). Negative control has been assessed on the same tissue by primary antibody withdrawal. No staining is found in colorectal cancer tissue, we used as additional negative control (2C).

Figure E21: Determination of the histidinol concentration in in vitro experiments.

Human PAEC levels of **A**, p-GCN2 (Thr 899) and GCN2 were analyzed by Western Blotting after treatment with several doses of Histidinol (0.05 mM, 0.5 mM and 1 mM) at several times (4h, 10h and 24h). β -Actin was used as loading control. **B**, p-GCN2 (Thr 899) and GCN2 were analyzed by Western Blotting after treatment with Histidinol 0.5 mM and 1 mM alone and co-treated with the GCN2 inhibitor 1 μ M (2662034) (left panel) with the quantification data (right panel).

Target	Host specie	Clone	Supplier	Reference	Concentration
GCN2	Rabbit	-	Cell Signaling	3302	1/1000
p-GCN2 (T899)	Rabbit	EPR2320Y	Abcam	ab75836	1/1000
ATF4	Rabbit	QC0913	Sigma-Aldrich	SAB2108090	1/1000
CHOP	Mouse	L63F7	Cell Signaling	2895	1/1000
p-eif2 α (Ser51)	Rabbit	-	Cell Signaling	9721	1/1000
BMPRII	Mouse	3F6	ThermoScientific	MA5-15827	1/1000
p-SMAD 1 (Ser463/465)/5 (Ser463/465)/8 (Ser465/467)	Rabbit	D5B10	Cell Signaling	13820	1/1000
SMAD 1/5/8	Rabbit	-	Abcam	ab80255	1/1000
p-SMAD2 (Ser465/467) /3 (Ser423/425)	Rabbit	D27F4	Cell Signaling	8828	1/1000
SMAD 2/3	Rabbit	-	Cell Signalling	3102	1/1000
TWIST1	Mouse	12A3	Santa Cruz Biotechnology	sc-81417	1/1000
p120-Catenin / Delta 1 Catenin	Mouse	6H11	Abcam	ab11508	1/10000
Cleaved Caspase 3	Rabbit	5A1E	Cell Signaling	9604	1/1000
CD45	Mouse	69/CD45	BD Transduction Laboratories	610266	1/1000
p-P38 (Thr180/Tyr182)	Rabbit	-	Cell Signaling	9211	1/1000
p-ERK1(Thr202)/2 (Thr204)	Rabbit	-	Cell Signaling	9101	1/1000
PCNA	Mouse	PC10	Dako	M0879	1/500
β -Actin	Mouse	AC-74	Sigma-Aldrich	A5316	1/10000
GCN1	Rabbit	-	Abcam	ab86139	1/5000
PERK	Rabbit	C33E10	Cell Signaling	3192	1/1000
p-PERK (Ser713)	Rabbit	Poly6494	BioLegend	649401	1/1000
PKR	Rabbit	-	Abcam	ab187883	1/1000
HO-1	Rabbit	-	Abcam	ab13243	1/2000
Survivin	Rabbit	71G4B7	Cell Signaling	2808	1/1000
ERG	Rabbit	EPR3864	Abcam	ab92513	1/1000
p-mTOR (Ser2448)	Rabbit	D9C2	Cell Signaling	5536	1/1000
mTOR	Rabbit	-	Cell Signaling	2972	1/1000
CD31	Rabbit	EP78	Sigma-Aldrich	131R-2	1/200

Table E2: Effect of histidinol treatment on the transcriptional activity related to the BMP signaling pathway in PECs

Page 59 of 87

Human BMP Signaling Pathway						Ref: PZ36A1H1			
Gene name	RefSeq	Symbol	sub-pathways	Ch. Location	Forward Primer location	Reverse Primer location	Amplicon size (bp)	Fold Change	p-value
activin A receptor like type 1	NM_000020.2	ACVRL1	Activin receptor signaling pathway	12q13.13	exon 8	exon 9	121	4,04	0,3768
activin A receptor type 1B	NM_020328.3	ACVR1B	Activin receptor signaling pathway	12q13.13	exon 3	exon 4	141	1,49	0,5542
activin A receptor type 1C	NM_145259.2	ACVR1C	Activin receptor signaling pathway	2q24.1	exon 8	exon 9	134	14,71	0,369
activin A receptor type 2A	NM_001278579.1	ACVR2A	Activin receptor signaling pathway	2q22.3-q23.1	exon 11	exon 12	137	27,58	0,3643
activin A receptor type 2B	NM_0011106.3	ACVR2B	Activin receptor signaling pathway	3p22.2	exon 9	exon 10	148	1,82	0,5445
follistatin	NM_006350.3	FST	Activin receptor signaling pathway	5q11.2	exon 1		128	13,84	0,1645
SMAD family member 3	NM_005902.3	SMAD3	Activin receptor signaling pathway	15q21-q22	Junction 6-7	exon 7	111	1,50	0,5177
transforming growth factor beta receptor 1	NM_004612.2	TGFBR1	Activin receptor signaling pathway	9q22	exon 4	exon 5	150	7,47	0,3902
cAMP-dependent protein kinase inhibitor alpha	NM_006823.4	PKIA	cAMP-mediated signaling	8q21.13	exon 3	Junction 3-4	97	14,00	0,3703
follistatin like 1	NM_007085.4	FSTL1	Cellular protein metabolism	3q13.33	exon 8	exon 9	78	3,90	0,3984
ornithine decarboxylase antizyme 1	NM_004152.2	OAZ1	Cellular protein metabolism	19p13.3	exon 5	exon 6	93	2,53	0,3458
activin A receptor type 1	NM_0011105.4	ACVR1	Cellular response to BMP stimulus	2q23-q24	exon 3	exon 4	130	2,34	0,4239
runt related transcription factor 2	NM_001024630.3	RUNX2	Cellular response to BMP stimulus	6p21	exon 4	exon 5	109	1,98	0,5209
SMAD family member 9	NM_001127217.2	SMAD9	Cellular response to BMP stimulus	13q13.3	exon 5	exon 6	149	1,23	0,7756
transmembrane protein 100	NM_001099640.1	TMEM100	Cellular response to BMP stimulus	17q23.1	exon 4	exon 4	131	17,41	0,283
growth factor receptor bound protein 2	NM_002086.4	GRB2	MAPK Signaling	17q24-q25	exon 6	exon 6	78	2,51	0,3463
Jun proto-oncogene, AP-1 transcription factor subunit	NM_002228.3	JUN	MAPK Signaling	1p32-p31	exon 1	exon 1	99	-1,14	0,809
mitogen-activated protein kinase kinase 1	NM_002755.3	MAP2K1	MAPK Signaling	15q22.1-q22.33	exon 3	exon 4	99	4,07	0,3747
mitogen-activated protein kinase kinase 2	NM_030662.3	MAP2K2	MAPK Signaling	19p13.3	exon 3	exon 4	141	-1,09	0,8342
mitogen-activated protein kinase kinase kinase 7	NM_145331.1	MAP3K7	MAPK Signaling	MAP3K7	exon 2	exon 3	91	7,20	0,3816
mitogen-activated protein kinase 1	NM_002745.4	MAPK1	MAPK Signaling	22q11.2	exon 1	exon 2	168	2,71	0,3343
mitogen-activated protein kinase 14	NM_001315.2	MAPK14	MAPK Signaling	6p21.3-p21.2	exon 1	exon 2	150	2,13	0,497
mitogen-activated protein kinase 3	NM_002746.2	MAPK3	MAPK Signaling	16p11.2	Junction 4-5	exon 5	108	-1,79	0,0968
mitogen-activated protein kinase 8	NM_139049.1	MAPK8	MAPK Signaling	10q11	exon 9	exon 10	92	14,03	0,3773
Raf-1 proto-oncogene, serine/threonine kinase	NM_002880.3	RAF1	MAPK Signaling	3p25	exon 2	exon 3	73	-2,70	0,0139
SOS Ras/Rac guanine nucleotide exchange factor 1	NM_005633.3	SOS1	MAPK Signaling	2p21	exon 20	Junction 20-21	129	1,41	0,6112
TGF-beta activated kinase 1 (MAP3K7) binding protein 1	NM_006116.2	TAB1	MAPK Signaling	22q13.1	exon 1	exon 2	77	1,66	0,4387
caveolin 1	NM_001753.4	CAV1	Negative regulation of BMP signaling pathway	7q31	exon 2	exon 3	106	7,64	0,3496

chordin	NM_003741.3	CHRD	Negative regulation of BMP signaling pathway	3q27.1	exon 11	exon 12	94	-4,76	0,0065
chordin like 1	NM_001143981.1	CHRD1	Negative regulation of BMP signaling pathway	Xq23	exon 3	exon 4	137	2,10	0,4995
follistatin like 3	NM_005860.2	FSTL3	Negative regulation of BMP signaling pathway	19p13.3	exon 4	exon 4	96	2,25	0,4592
gremlin 1, DAN family BMP antagonist	NM_013372.6	GREM1	Negative regulation of BMP signaling pathway	15q13.3	exon 2	exon 2	132	1,12	0,8067
homeodomain interacting protein kinase 2	NM_022740.4	HIPK2	Negative regulation of BMP signaling pathway	7q32-q34	exon 6	exon 7	106	3,97	0,3909
LDL receptor related protein 2	NM_004525.2	LRP2	Negative regulation of BMP signaling pathway	2q31.1	exon 34	exon 35	126	-1,38	0,4681
NBL1, DAN family BMP antagonist	NM_182744.3	NBL1	Negative regulation of BMP signaling pathway	1p36.13	exon 3	exon 4	142	1,35	0,6612
noggin	NM_005450.4	NOG	Negative regulation of BMP signaling pathway	17q22	exon 1	exon 1	115	-1,06	0,8985
SKI proto-oncogene	NM_003036.3	SKI	Negative regulation of BMP signaling pathway	1p36.33	exon 4	exon 5	83	-1,41	0,236
SMAD family member 6	NM_005585.4	SMAD6	Negative regulation of BMP signaling pathway	15q22.31	exon 2	exon 3	104	7,21	0,3978
SMAD family member 7	NM_005904.3	SMAD7	Negative regulation of BMP signaling pathway	18q21.1	exon 4	exon 4	144	4,51	0,3697
SMAD specific E3 ubiquitin protein ligase 1	NM_020429.2	SMURF1	Negative regulation of BMP signaling pathway	7q22.1	exon 18	exon 19	86	2,90	0,2766
SMAD specific E3 ubiquitin protein ligase 2	NM_022739.3	SMURF2	Negative regulation of BMP signaling pathway	17q23.3-q24.1	exon 18	exon 19	78	53,43	0,3654
sclerostin domain containing 1	NM_015464.3	SOSTDC1	Negative regulation of BMP signaling pathway	7p21.2	exon 1	exon 2	101	1,00	0,9944
transducer of ERBB2, 1	NM_005749.4	TOB1	Negative regulation of BMP signaling pathway	17q21.33	exon 2	exon 2	140	8,68	0,2854
eukaryotic translation initiation factor 4E binding protein 1	NM_004095.3	EIF4EBP1	Negative regulation of translational initiation	8p11.23	exon 1	exon 2	70	1,85	0,2618
eukaryotic translation initiation factor 4E binding protein 2	NM_004096.4	EIF4EBP2	Negative regulation of translational initiation	10q22.1	exon 1	exon 2	110	3,67	0,4453
eukaryotic translation initiation factor 4E binding protein 3	NM_003732.3	EIF4EBP3	Negative regulation of translational initiation	8p11.23	exon 1	exon 2	88	1,34	0,6775
endoglin	NM_001114753.1	ENG	Positive regulation of BMP signaling pathway	9q33-q34.1	exon 3	exon 4	110	2,03	0,3112
F-box and leucine rich repeat protein 15	NM_024326.3	FBXL15	Positive regulation of BMP signaling pathway	10q24.32	exon 3	exon 3	68	1,17	0,8097
forkhead box D1	NM_004472.3	FOXD1	Positive regulation of BMP signaling pathway	5q13.2	exon 1	exon 1	121	2,98	0,2593
hes family bHLH transcription factor 5	NM_001010926.3	HESS	Positive regulation of BMP signaling pathway	1p36.32	exon 2	exon 2	62	1,84	0,5854
notch receptor 1	NM_017617.3	NOTCH1	Positive regulation of BMP signaling pathway	9q34.3	exon 10	exon 11	80	-1,45	0,1963
nuclear mitotic apparatus protein 1	NM_006185.3	NUMA1	Positive regulation of BMP signaling pathway	11q13.4	exon 8	exon 9	130	1,66	0,415
SMAD family member 2	NM_005901.4	SMAD2	Positive regulation of BMP signaling pathway	18q21	exon 8	exon 9	149	14,35	0,3521
SMAD family member 4	NM_005359.5	SMAD4	Positive regulation of BMP signaling pathway	18q21.1	exon 9	exon 10	146	7,88	0,3346
SRY-box 11	NM_003108.4	SOX11	Positive regulation of BMP signaling pathway	2p25.2	exon 1	exon 1	112	1,44	0,5257
ubiquitin conjugating enzyme E2 O	NM_022066.4	UBE2O	Positive regulation of BMP signaling pathway	17q25.1	exon 15	exon 16	135	1,32	0,6745
zinc finger protein 423	NM_015069.4	ZNF423	Positive regulation of BMP signaling pathway	16q12.1	exon 7	Junction 7-8	130	4,22	0,3582
anti-Mullerian hormone	NM_000479.4	AMH	Positive regulation of NF-kappaB transcription factor activity	19p13.3	exon 4	exon 5	139	3,11	0,4831
nuclear factor kappa B subunit 1	NM_003998.3	NFKB1	Positive regulation of NF-kappaB transcription factor activity	4q24	exon 7	exon 7	67	2,06	0,2904
ubiquitin conjugating enzyme E2 D1	NM_003338.5	UBE2D1	Protein ubiquitination	10q21.1	exon 4	exon 5	147	107,95	0,3686
ubiquitin conjugating enzyme E2 D3	NM_003340.5	UBE2D3	Protein ubiquitination	4q24	exon 6	exon 7	102	14,43	0,3553

family with sequence similarity 83 member G	NM_001039999.3	FAM83G	Regulation of BMP signaling pathway	17p11.2	exon 4	exon 5	132	-1,25	0,6253
gremlin 2, DAN family BMP antagonist	NM_022469.4	GREM2	Regulation of BMP signaling pathway	1q43	exon 2	exon 2	135	3,35	0,4134
integrin subunit alpha 3	NM_002204.3	ITGA3	Regulation of BMP signaling pathway	17q21.33	exon 4	exon 5	136	1,16	0,8385
secreted frizzled related protein 4	NM_003014.4	SFRP4	Regulation of BMP signaling pathway	7p14.1	exon 1	exon 2	147	4,84	0,2909
solute carrier family 39 member 5	NM_173596.3	SLC39A5	Regulation of BMP signaling pathway	12q13.3	exon 8	exon 9	100	3,58	0,4675
transcription factor AP-2 beta	NM_003221.4	TFAP2B	Regulation of BMP signaling pathway	6p12.3	exon 5	exon 6	129	3,47	0,4736
X-linked inhibitor of apoptosis	NM_001167.3	XIAP	Regulation of BMP signaling pathway	Xq25	exon 3	exon 4	138	14,69	0,3583
LIM domain kinase 1	NM_002314.3	LIMK1	Signal transduction	7q11.23	exon 9	exon 10	85	-1,08	0,8005
solute carrier family 33 member 1	NM_004733	SLC33A1	Signal transduction	3q25.31	exon 5	exon 6	100	14,28	0,3526
SMAD family member 1	NM_005900.2	SMAD1	Signal transduction	4q31	Junction 4-5	exon 5	150	1,48	0,5489
SMAD family member 5	NM_001001419.2	SMAD5	Signal transduction	5q31	exon 3	exon 4	149	7,66	0,3646
signal transducer and activator of transcription 3	NM_139276.2	STAT3	Signal transduction	17q21	exon 19	exon 20	112	1,92	0,3542
activating transcription factor 2	NM_001880.3	ATF2	Transcription	2q32	exon 8	exon 8	93	7,39	0,3738
calcium/calmodulin dependent protein kinase IV	NM_001744.6	CAMK4	Transcription	5q22.1	exon 5	exon 6	103	7,63	0,3904
cAMP responsive element binding protein 1	NM_134442.3	CREB1	Transcription	2q34	exon 2	exon 3	147	7,86	0,3503
CREB binding protein	NM_004380.2	CREBBP	Transcription	16p13.3	exon 3	exon 4	88	2,94	0,2627
homeobox C9	NM_006897.2	HOXC9	Transcription	12q13.13	exon 1	exon 1	135	5,15	0,3116
MAGE family member D1	NM_001005333.1	MAGED1	Transcription	Xp11.22	exon 12	exon 13	133	3,61	0,138
NK2 homeobox 5	NM_004387.3	NKX2-5	Transcription	5q35.1	exon 2	exon 2	104	5,40	0,2387
paired like homeodomain 2	NM_000325.5	PITX2	Transcription	4q25	exon 3	exon 3	126	3,25	0,4368
scleraxis bHLH transcription factor	NM_001080514.3	SCX	Transcription	8q24.3	exon 1	exon 2	79	1,89	0,3759
T cell leukemia homeobox 2	NM_016170.5	TLX2	Transcription	2p13.1	exon 1	exon 1	69	6,43	0,4232
transducer of ERBB2, 2	NM_016272.4	TOB2	Transcription	22q13.2	exon 2	exon 2	113	-1,27	0,609
anti-Mullerian hormone receptor type 2	NM_020547.3	AMHR2	Transforming growth factor beta receptor signaling pathway	12q13.13	exon 11	exon 11	97	1,40	0,5759
forkhead box H1	NM_003923.2	FOXH1	Transforming growth factor beta receptor signaling pathway	8q24.3	exon 2	exon 2	86	-1,52	0,4048
ubiquitin specific peptidase 15	NM_001252078.2	USP15	Transforming growth factor beta receptor signaling pathway	12q14.1	exon 1	exon 2	148	27,86	0,3628
ubiquitin specific peptidase 9 X-linked	NM_001039590.2	USP9X	Transforming growth factor beta receptor signaling pathway	Xp11.4	exon 9	exon 10	95	8,58	0,3669
ubiquitin specific peptidase 9 Y-linked	NM_004654.3	USP9Y	Transforming growth factor beta receptor signaling pathway	Yq11.221	exon 26	exon 27	136	1,68	0,4104
peptidylprolyl isomerase A (cyclophilin A)	NM_021130	PPIA	House-keeping genes	7p13	exon 1	exon 2	97		
actin, beta	NM_001101	ACTB	House-keeping genes	7p22	exon 6	exon 6	106		
TATA box binding protein	NM_001172085	TBP	House-keeping genes	6q27	exon 5	exon 6	88		
beta-2-microglobulin	NM_004048	B2M	House-keeping genes	15q21-q22.2	Junction 1-2	exon 2	163		

ribosomal protein, large, P0	NM_053275	RPLP0	House-keeping genes	12q24.2	exon 6	exon 7	144	
Hypoxanthine guanine phosphoribosyl transferase I	NM_000194	HPRT1	House-keeping genes	Xq26.2	exon 6	exon 7	87	
Transferrin receptor (p90, CD71)	NM_001128148	TFRC	House-keeping genes	3q29	exon 5	exon 6	87	

Table E3: Effect of BMP9 treatment on the transcriptional activity related to the ISR signaling pathway in PECs

Page 63 of 87

Human Integrated Stress Response (ISR)						Ref: ISR1H1			
Gene name	RefSeq	Symbol	sub-pathways	Ch. Location	Forward Primer Location	Reverse Primer location	Amplicon size (bp)	Fold Change	p-value
solute carrier family 1 member 4	NM_003038.4	SLC1A4	Amino acid transport	2p14	exon 7	exon 8	140	1,50	0,1888
solute carrier family 35 member A4	NM_080670.3	SLC35A4	Amino acid transport	5q31.3	exon 3	exon 3	146	1,79	0,2798
solute carrier family 3 member 2	NM_001012662.2	SLC3A2	Amino acid transport	11q12.3	exon 6	exon 7	134	1,29	0,3787
solute carrier family 7 member 11	NM_014331.3	SLC7A11	Amino acid transport	4q28.3	exon 10	exon 11	111	-1,14	0,7363
solute carrier family 7 member 5	NM_003486.6	SLC7A5	Amino acid transport	16q24.2	exon 5	exon 6	144	4,61	0,2854
asparaginyl-tRNA synthetase	NM_004539.3	NARS	Aminoacylation	18q21.31	exon 9	exon 10	129	1,10	0,7106
apoptotic peptidase activating factor 1	NM_181861.1	APAF1	Apoptotic process	12q23	exon 5	exon 6	109	1,30	0,3653
BCL2 binding component 3	NM_001127240.2	BBC3	Apoptotic process	19q13.3-q13.4	exon 4	exon 4	88	1,47	0,2115
BCL2, apoptosis regulator	NM_138621.4	BCL2	Apoptotic process	2q13	junction 1-2	exon 2	64	1,48	0,297
baculoviral IAP repeat containing 2	NM_001166.3	BIRC2	Apoptotic process	11q22	exon 2	exon 3	107	1,30	0,3718
baculoviral IAP repeat containing 3	NM_182962.1	BIRC3	Apoptotic process	11q22	exon 3	exon 4	123	-1,54	0,0811
baculoviral IAP repeat containing 5	NM_001012271.1	BIRC5	Apoptotic process	17q25.3	exon 2	exon 2	65	1,35	0,432
baculoviral IAP repeat containing 7	NM_139317.2	BIRC7	Apoptotic process	20q13.33	exon 1	exon 2	141	3,88	0,3351
Fos proto-oncogene, AP-1 transcription factor subunit	NM_005252.3	FOS	Apoptotic process	14q24.3	junction 1-2	exon 2	136	1,45	0,1995
NLR family apoptosis inhibitory protein	NM_004536.2	NAIP	Apoptotic process	5q13.2	exon 12	exon 13	124	-1,15	0,712
nuclear protein 1, transcriptional regulator	NM_001042483.1	NUPR1	Apoptotic process	16p11.2	exon 2	exon 2	109	1,14	0,7115
phorbol-12-myristate-13-acetate-induced protein 1	NM_021127.2	PMAIP1	Apoptotic process	18q21.32	exon 1	exon 2	95	-2,27	0,0029
siyah E3 ubiquitin protein ligase 1	NM-001006610.1	SIAH1	Apoptotic process	16q12	exon 2	exon 2	104	-1,61	0,0848
siyah E3 ubiquitin protein ligase 2	NM-005067.5	SIAH2	Apoptotic process	3q25	exon 1	exon 2	138	-1,18	0,6403
TNF receptor superfamily member 10b	NM_003842.4	TNFRSF10B	Apoptotic process	8p22-p21	Junction 5-6	exon 7	114	1,00	0,9923
X-linked inhibitor of apoptosis	NM_001167.3	XIAP	Apoptotic process	Xq25	exon 3	exon 4	138	1,10	0,7072
autophagy related 10	NM_001131028.1	ATG10	Autophagy	5q14.1	exon 8	exon 8	66	-1,37	0,1575
autophagy related 12	NM_004707.3	ATG12	Autophagy	5q21-q22	exon 2	exon 2	81	-1,33	0,1818
autophagy related 16 like 1	NM_030803.6	ATG16L1	Autophagy	2q37.1	exon 13	exon 14	135	1,10	0,7902
autophagy related 3	NM_022488.3	ATG3	Autophagy	3q13.2	exon 10	exon 11	93	-1,18	0,6513
autophagy related 5	NM_004849.2	ATG5	Autophagy	6q21	exon 2	exon 2	89	1,00	0,9986
autophagy related 7	NM_006395.2	ATG7	Autophagy	3p25.3-p25.2	exon 2	exon 3	91	3,06	0,1952
GABA type A receptor-associated protein	NM_007278.1	GABARAP	Autophagy	17p13.1	exon 1	exon 2	109	1,01	0,9705
GABA type A receptor associated protein like 2	NM_007285.6	GABARAPL2	Autophagy	16q22.1	exon 3	exon 4	122	-1,39	0,1914
NBR1, autophagy cargo receptor	NM_005899.4	NBR1	Autophagy	17q21.31	exon 11	exon 12	114	1,10	0,8046

sequestosome 1	NM_003900.4	SQSTM1	Autophagy	5q35	exon 7	exon 8	130	-2,00	0,0193
asparagine synthetase (glutamine-hydrolyzing)	NM_133436.3	ASNS	Cellular amino acid metabolic process	7q21.3	exon 7	Junction 7-8	124	-1,18	0,6622
activating transcription factor 4	NM_001675.2	ATF4	Cellular response to amino acid starvation	22q13.1	exon 1	exon 2	117	1,59	0,4619
beclin 1	NM_003766.3	BECN1	Cellular response to amino acid starvation	17q21	exon 3	exon 4	85	1,00	0,9876
eukaryotic translation initiation factor 2 alpha kinase 3	NM_002759.2	EIF2AK2	Cellular response to amino acid starvation	2p22-p21	exon 14	exon 15	98	-1,12	0,7209
eukaryotic translation initiation factor 2 alpha kinase 2	NM_004836.5	EIF2AK3	Cellular response to amino acid starvation	2p12	exon 9	exon 9	108	-1,09	0,8084
eukaryotic translation initiation factor 2 alpha kinase 4	NM_001013703.3	EIF2AK4	Cellular response to amino acid starvation	15q15.1	exon 20	exon 21	105	-1,10	0,3738
eukaryotic translation initiation factor 2 subunit alpha	NM_004094.4	EIF2S1	Cellular response to amino acid starvation	14q21.3	exon 6	exon 7	97	-1,10	0,7433
GCN1, eIF2 alpha kinase activator homolog	NM_006836.1	GCN1	Cellular response to amino acid starvation	12q24.23	exon 4	exon 5	149	1,45	0,2715
microtubule associated protein 1 light chain 3 alpha	NM_032514.2	MAP1LC3A	Cellular response to amino acid starvation	20q11.22	exon 4	exon 4	120	-1,61	0,0865
solute carrier family 38 member 2	NM_018976.4	SLC38A2	Cellular response to amino acid starvation	12q13.11	exon 11	exon 12	75	1,91	0,2127
damage specific DNA binding protein 1	NM_001923.3	DDB1	DNA damage response	11q12-q13	exon 10	exon 11	141	1,54	0,4701
damage specific DNA binding protein 2	NM_000107.2	DDB2	DNA damage response	11p12-p11	exon 3	exon 4	102	-1,34	0,1791
DNA damage inducible transcript 4	NM_019058.2	DDIT4	DNA damage response	10q22.1	exon 3	exon 3	131	2,60	0,3155
activating transcription factor 6	NM_007348.3	ATF6	Endoplasmic reticulum unfolded protein response	1q22-q23	exon 6	exon 7	111	-1,10	0,3681
heat shock protein family A (Hsp70) member 5	NM_005347.4	HSPA5	Endoplasmic reticulum unfolded protein response	9q33.3	exon 5	exon 6	140	-1,13	0,3399
nuclear factor, erythroid 2 like 2	NM_006164.4	NFE2L2	Endoplasmic reticulum unfolded protein response	2q31	exon 3	exon 4	130	1,00	0,9894
phosphatidylinositol-4,5-bisphosphate 3-kinase catalytic	NM_006218.2	PIK3CA	Protein phosphorylation	3q26.3	exon 7	exon 8	132	-1,19	0,6281
AKT serine/threonine kinase 1	NM_005163.2	AKT1	Protein phosphorylation	14q32.32-q32.33	exon 10	exon 11	128	1,60	0,418
inhibitor of Bruton tyrosine kinase	NM_015525.3	IBTK	Protein phosphorylation	6q14.1	exon 25	exon 26	108	1,02	0,9626
mechanistic target of rapamycin	NM_004958.3	MTOR	Protein phosphorylation	1p36	exon 27	exon 28	127	1,19	0,5935
actin gamma 1	NM_001199954.1	ACTG1	Protein transport	17q25	exon 2	exon 2	67	3,11	0,2015
eukaryotic translation initiation factor 2 alpha kinase 1	NM_014413.3	EIF2AK1	Regulation of translation	7p22.1	exon 12	exon 13	107	1,10	0,7112
eukaryotic translation initiation factor 2B subunit alpha	NM_001414.3	EIF2B1	Regulation of translation	12q24.3	exon 5	exon 6	98	-1,13	0,7301
eukaryotic translation initiation factor 2 subunit gamma	NM_001415.3	EIF2S3	Regulation of translation	Xp22.11	exon 5	exon 6	100	1,00	0,9949
protein phosphatase 1 catalytic subunit alpha	NM_002708.3	PPP1CA	Regulation of translation	11q13	exon 6	exon 7	88	-1,11	0,3639
ribosomal protein L7	NM_000971.3	RPL7	Regulation of translation	8q13.3	Junction 5-6	exon 6	129	-1,82	0,0029
sestrin 2	NM_031459.4	SESN2	Regulation of translation	1p35.3	exon 4	exon 5	140	2,57	0,3153
tryptophanyl-tRNA synthetase	NM_004184.3	WARS	Regulation of translation	14q32.2	exon 8	exon 9	145	-1,10	0,7743
BCL2 like 11	NM_138621.4	BCL2L11	Response to endoplasmic reticulum stress	2q13	exon 1	exon 1	129	-1,39	0,0014
CCAAT/enhancer binding protein beta	NM_005194.2	CEBPB	Response to endoplasmic reticulum stress	20q13.1	exon 1	exon 1	126	2,79	0,2449
DNA damage inducible transcript 3	NM_001195053.1	DDIT3	Response to endoplasmic reticulum stress	12q13.1-q13.2	exon 4	exon 4	137	-1,64	0,09
endoplasmic reticulum to nucleus signaling 1	NM_001433.3	ERN1	Response to endoplasmic reticulum stress	17q23	exon 19	exon 20	139	1,16	0,6866

endoplasmic reticulum oxidoreductase 1 alpha	NM_014584.2	ERO1A	Response to endoplasmic reticulum stress	14q22.1	exon 12	exon 12	119	-1,12	0,7215
protein phosphatase 1 regulatory subunit 15A	NM_014330.3	PPP1R15A	Response to endoplasmic reticulum stress	19q13.2	exon 2	exon 2	139	-1,55	0,0785
protein phosphatase 1 regulatory subunit 15B	NM_032833.4	PPP1R15B	Response to endoplasmic reticulum stress	1q32.1	exon 1	exon 1	75	1,15	0,7077
tribbles pseudokinase 3	NM_021158.4	TRIB3	Response to endoplasmic reticulum stress	20p13-p12.2	exon 3	exon 4	117	1,25	0,7352
X-box binding protein 1	NM_005080.3	XBP1	Response to endoplasmic reticulum stress	22q12.1	exon 1	exon 2	102	1,46	0,3051
ERCC excision repair 1, endonuclease non-catalytic	NM_001983.3	ERCC1	Response to stress	19q13.32	exon 6	exon 7	100	1,09	0,7248
ERCC excision repair 2, TFIIH core complex helicase	NM_000400.3	ERCC2	Response to stress	19q13.32	Junction 4-5	exon 5	99	2,65	0,1191
ERCC excision repair 3, TFIIH core complex helicase	NM_000122.1	ERCC3	Response to stress	2q21	exon 12	exon 13	108	-1,34	0,1823
growth arrest and DNA damage inducible alpha	NM_001924.3	GADD45A	Response to stress	1p31.2	exon 1	exon 2	100	-1,33	0,5134
BCL2 interacting protein 3 like	NM_004331.2	BNIP3L	Signal transduction	8p21	exon 2	exon 3	97	-1,54	0,0752
activating transcription factor 3	NM_001674.3	ATF3	Transcription regulation	1q32.3	exon 3	exon 4	124	-1,45	0,0634
activating transcription factor 5	NM_012068.5	ATF5	Transcription regulation	19q13.3	exon 3	exon 4	112	2,36	0,4017
chromobox 4	NM_003655.2	CBX4	Transcription regulation	17q25.3	exon 4	exon 5	73	1,20	0,5938
CCAAT/enhancer binding protein gamma	NM_001806.3	CEBPG	Transcription regulation	19q13.11	exon 2	exon 2	102	1,05	0,8583
egl-9 family hypoxia inducible factor 2	NM_080732.3	EGLN2	Transcription regulation	19q13.2	exon 4	exon 5	128	1,04	0,8846
egl-9 family hypoxia inducible factor 3	NM_022073.3	EGLN3	Transcription regulation	14q12	exon 3	exon 4	86	1,45	0,2087
LIM domain only 4	NM_006769.3	LMO4	Transcription regulation	1p22.3	exon 2	exon 3	86	-1,33	0,1911
nuclear factor kappa B subunit 1	NM_003998.3	NFKB1	Transcription regulation	4q24	exon 7	exon 7	67	-1,05	0,8697
transcription factor binding to IGHM enhancer 3	NM_006521.5	TFE3	Transcription regulation	Xp11.22	exon 5	exon 6	117	-1,01	0,9847
transcription factor EB	NM_001167827.2	TFEB	Transcription regulation	6p21	exon 6	exon 7	90	1,62	0,3886
thioredoxin interacting protein	NM_006472.5	TXNIP	Transcription regulation	1q11	exon 4	exon 5	104	1,25	0,5066
peptidylprolyl isomerase A (cyclophilin A)	NM_021130	PPIA	House-keeping genes	7p13	exon 1	exon 2	97		
actin, beta	NM_001101	ACTB	House-keeping genes	7p22	exon 6	exon 6	106		
TATA box binding protein	NM_001172085	TBP	House-keeping genes	6q27	exon 5	exon 6	88		
beta-2-microglobulin	NM_004048	B2M	House-keeping genes	15q21-q22.2	junction 1-2	exon 2	163		
ribosomal protein, large, P0	NM_053275	RPLP0	House-keeping genes	12q24.2	exon 6	exon 7	144		
Hypoxanthine guanine phosphoribosyl transferase I	NM_000194	HPRT1	House-keeping genes	Xq26.2	exon 6	exon 7	87		
Transferrin receptor (p90, CD71)	NM_001128148	TFRC	House-keeping genes	3q26.2-qter	exon 5	exon 6	87		
Glucuronidase, beta	NM_000181.3	GUSB	House-keeping genes	7q11.21	exon 4	exon 5	104		

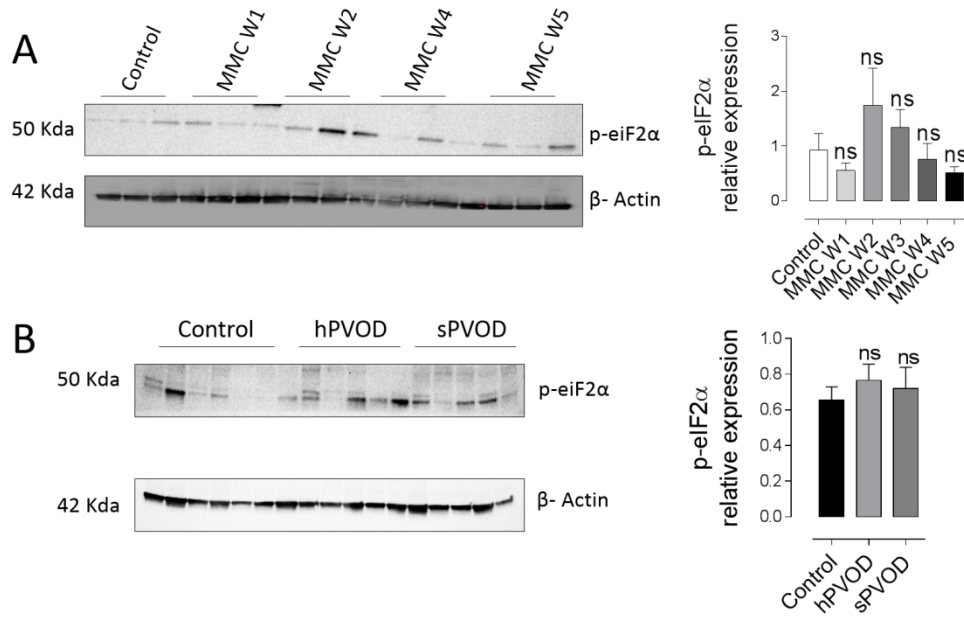


Figure E1: Analysis of p-eiF2 α in lung from hPVOD, spVOD patients and MMC-exposed rats. A, p-eiF2 α expression measured by Western blot analysis in control and MMC-exposed rats (1, 2, 4 and 5 weeks after MMC-exposure). B, p-eiF2 α in lung from hPVOD and spVOD. β -Actin was used as loading control. ns = non-significant.

432x283mm (96 x 96 DPI)

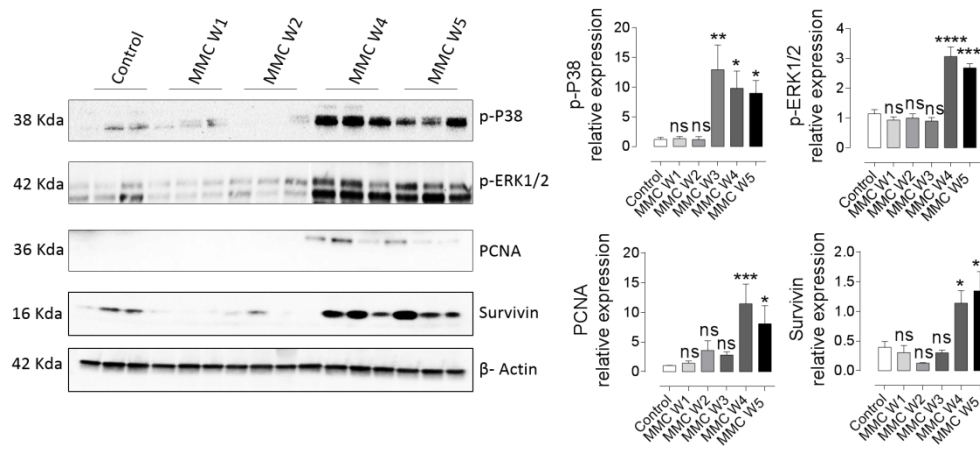


Figure E2: Upregulation of mitogenic and anti-apoptotic pathways in MMC-exposed rats: Pulmonary levels of P-P38, p-ERK1/2, PCNA and Survivin in control and MMC-exposed rats (1, 2, 4 and 5 weeks after MMC-exposure, week 3 is displayed in supplemental figure E19). β -Actin was used as loading control. * $P < 0.05$, ** $P < 0.005$, *** $P < 0.0005$, **** $P < 0.0001$

532x248mm (96 x 96 DPI)

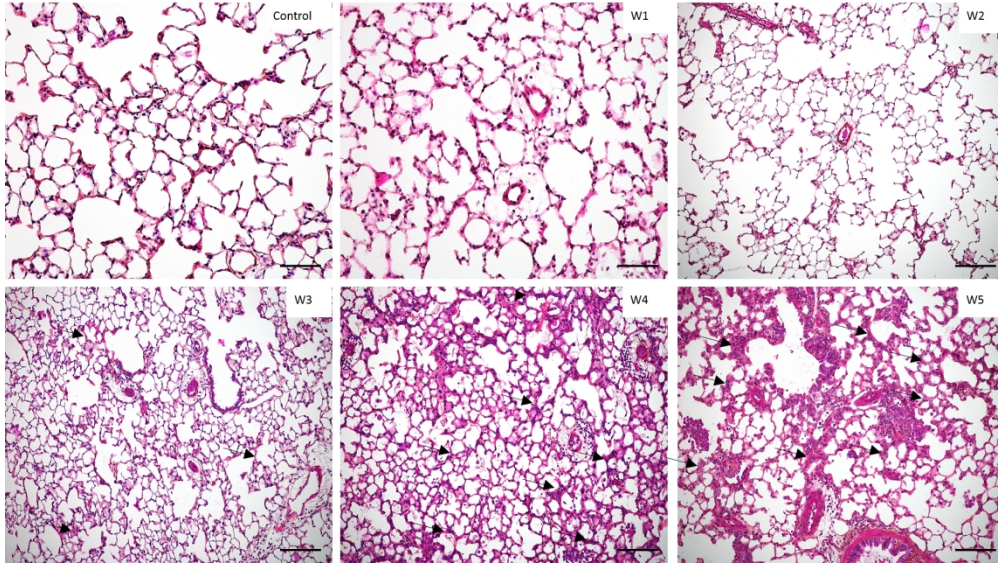


Figure E3: MMC induces progressive development of foci of alveolar wall thickening suggestive of pulmonary capillary hemangiomatosis in rats.

HE stained paraffin embedded lung sections in control and MMC-exposed rats (1, 2, 3, 4 and 5 weeks after MMC-exposure) with foci of alveolar wall thickening (arrows) suggestive of pulmonary capillary hemangiomatosis developing overtime and becoming manifest at week 3 and progressive at week 4 and 5.

509x287mm (96 x 96 DPI)

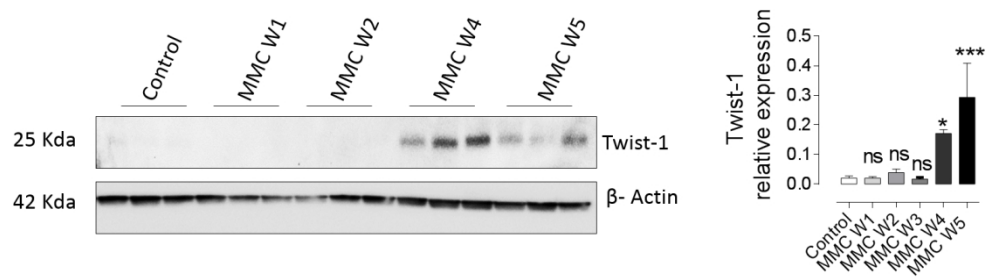


Figure E4: Analysis of protein Twist-1 expression in MMC-exposed rats. Twist1 measured by Western blot analysis (WB) in control and MMC-exposed rats (1, 2, 4 and 5 weeks after MMC-exposure, week 3 is displayed in supplemental figure E19). β -Actin was used as loading control. Quantification of the Western blots are shown close to Western blots image * $P < 0.05$; *** $P < 0.0005$.

429x131mm (96 x 96 DPI)

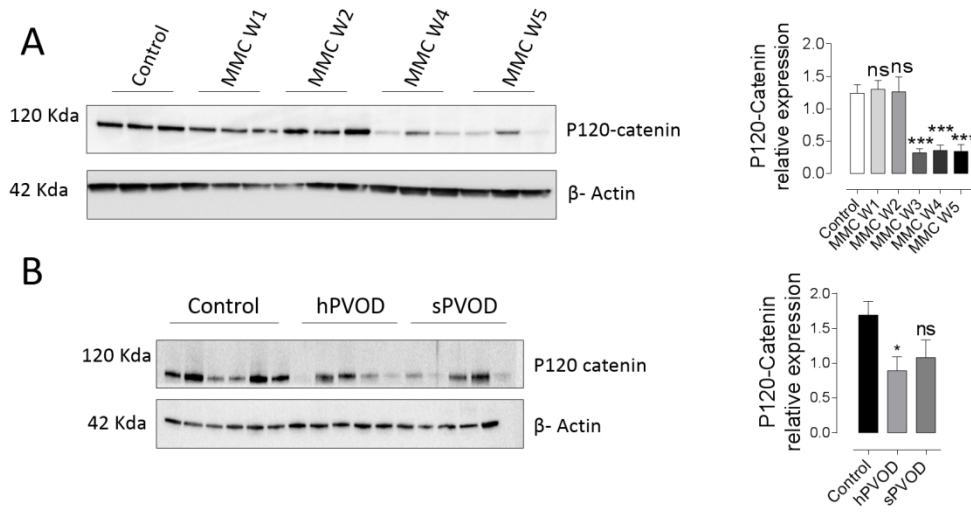


Figure E5: Analysis of protein p120-catenin expression in lung from sPVOD, hPVOD patients and in MMC-exposed rats.

Pulmonary levels of p120-catenin was analyzed by Western blotting during the development of PVOD in control and MMC exposed-rats (A) (1, 2, 4 and 5 weeks after MMC-exposure, week 3 is displayed in supplemental figure E19) and in Human (B). β -Actin was used as loading control. Quantification of Western blots is shown near Western blot image. * $P < 0.05$; *** $P < 0.0005$.

458x248mm (96 x 96 DPI)

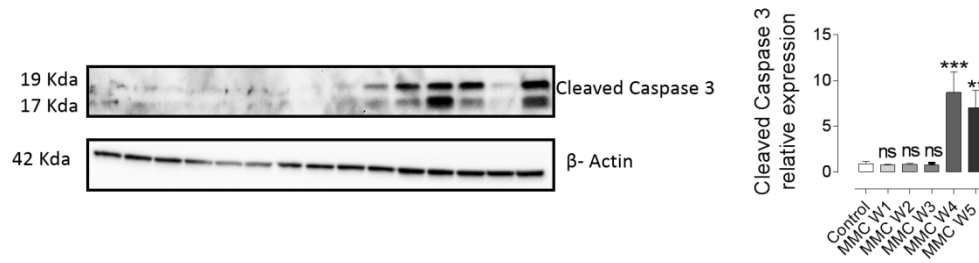


Figure E6: Apoptosis is enhanced in MMC-induced PVOD.

Pulmonary levels of cleaved-Caspase 3 measured by Western blot analysis (WB) in control and MMC-exposed rats (1, 2, 4 and 5 weeks after MMC-exposure, week 3 is displayed in supplemental figure E19). β -Actin was used as loading control. Right panel represent the quantification of the Western blots. ** $P < 0.005$. *** $P < 0.0005$.

463x129mm (96 x 96 DPI)

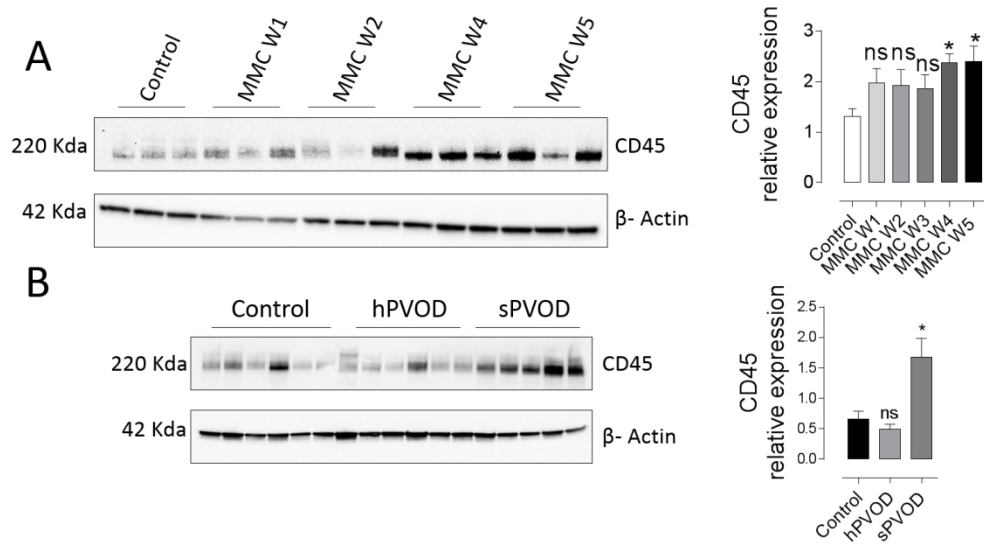


Figure E7: Inflammation is enhanced in lung from hPVOD, sPVOD patients and in MMC-induced PVOD. Pulmonary levels of CD45 measured by Western blot analysis (WB) in control and MMC-exposed rats (A) (1, 2, 4 and 5 weeks after MMC-exposure, week 3 is displayed in supplemental figure E19) and in lung from hPVOD and sPVOD (B). β -Actin was used as loading control. Right panel represent the quantification of the Western blots. * $P < 0.05$.

419x239mm (96 x 96 DPI)

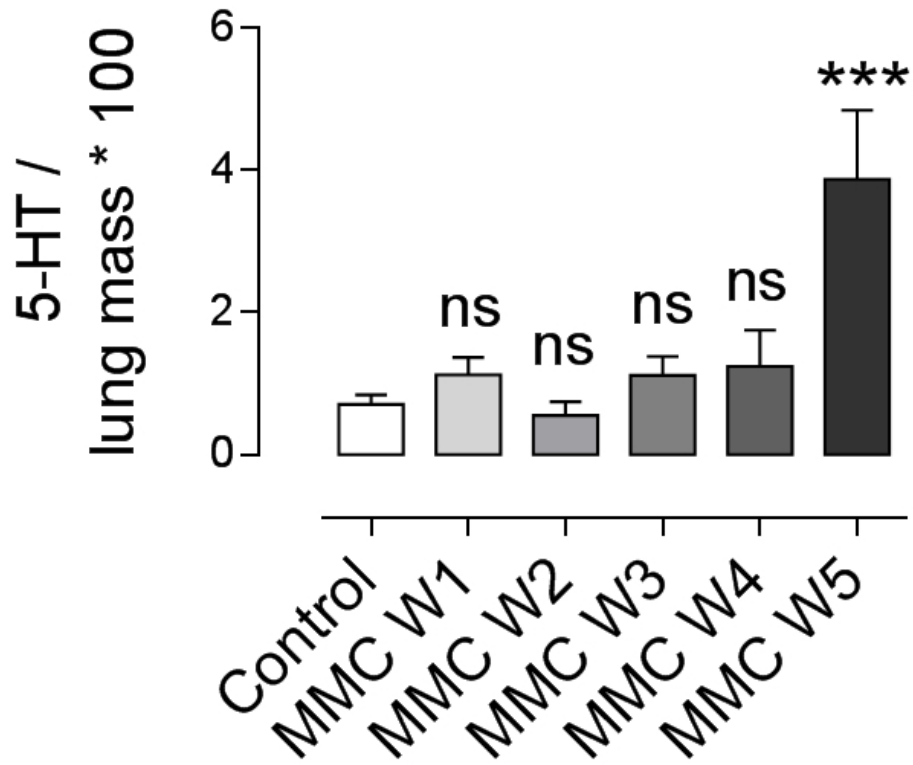


Figure E8: Dysregulation of serotonin pathway in MMC-induced PVOD. Pulmonary serotonin (5-HT) content was significantly increased at week 5. ***P<0.0005.

173x151mm (96 x 96 DPI)

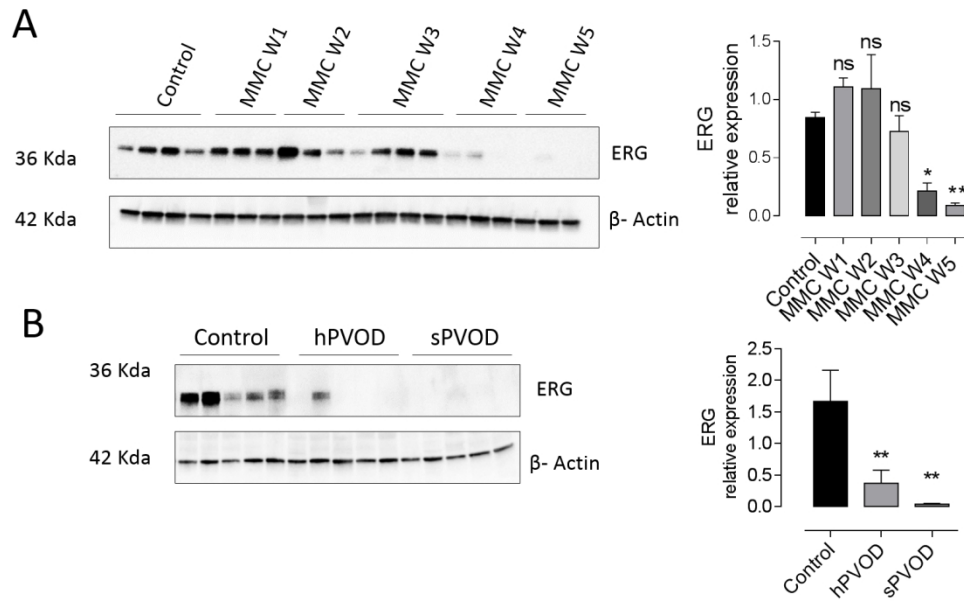


Figure E9: Analysis of ERG expression in lung from hPVOD, sPVOD patients and MMC-exposed rats. A, ERG expression measured by Western blot analysis in control and MMC-exposed rats (1, 2, 3, 4 and 5 weeks after MMC-exposure). B, ERG in lung from hPVOD and sPVOD. β -Actin was used as loading control * $P < 0.05$; ** $P < 0.005$.

439x281mm (96 x 96 DPI)

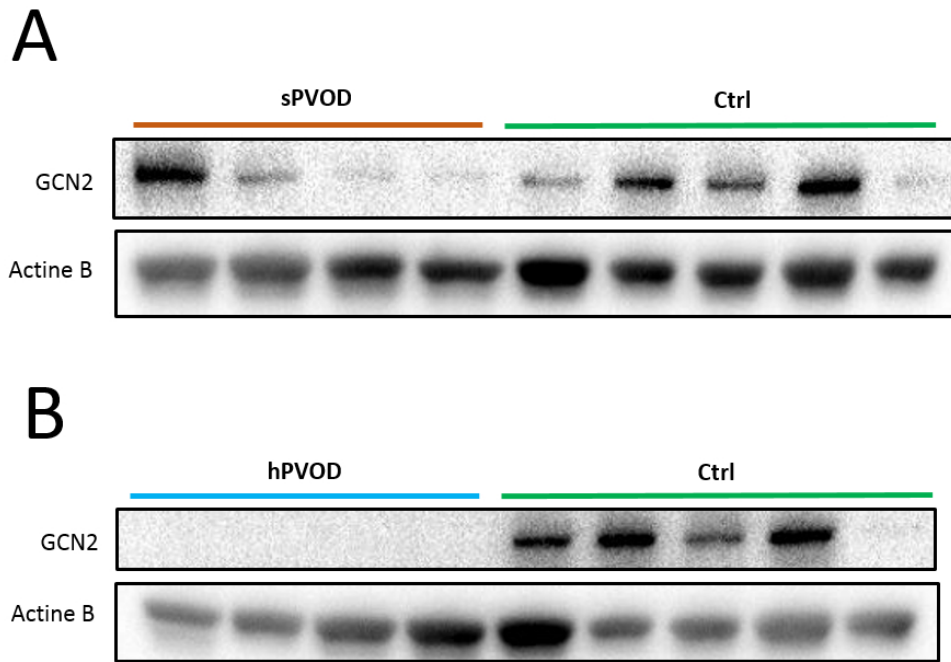


Figure 10: Additional analysis of GCN2 expression in lung from hPVOD, sPVOD patients
A, GCN2 lung expression measured by Western blot analysis in sPVOD patients. B, GCN2 lung expression
hPVOD. β -Actin was used as loading control.
hPVOD samples are originating from patients with nonsense/frameshift mutations in EIF2AK4.

241x170mm (96 x 96 DPI)

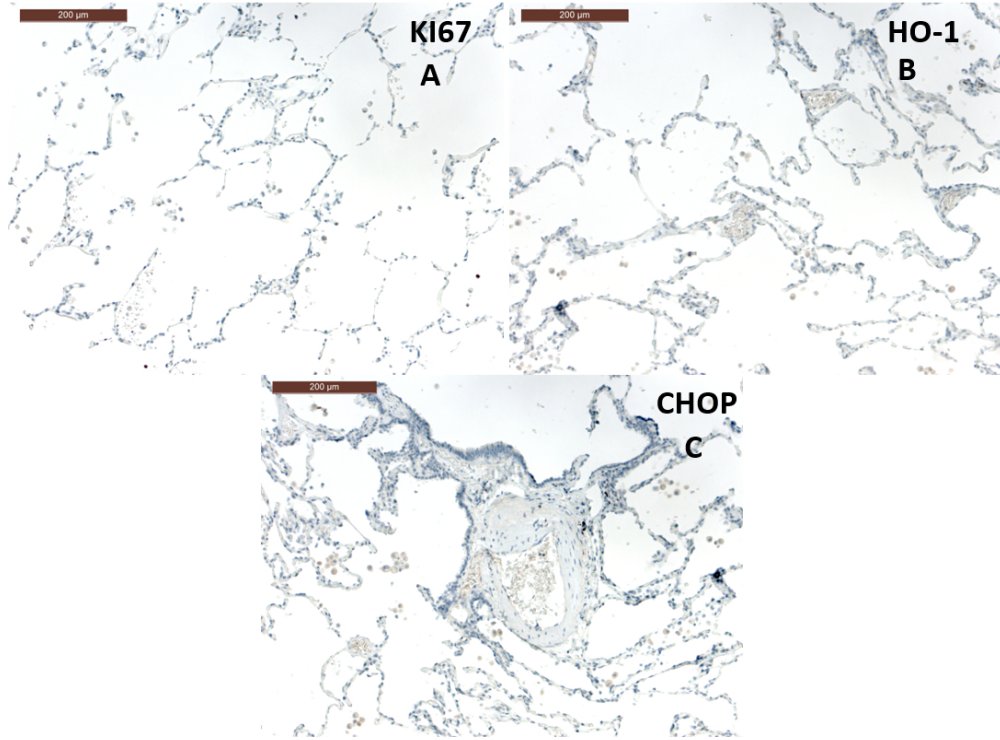


Figure E11: Analysis of Ki67, HO-1 and CHOP expression in control lung patients. Lung tissue control. No KI67 staining within the alveolar septa (A). HO-1 (B) and CHOP (C) are not expressed in lung control.

287x212mm (96 x 96 DPI)

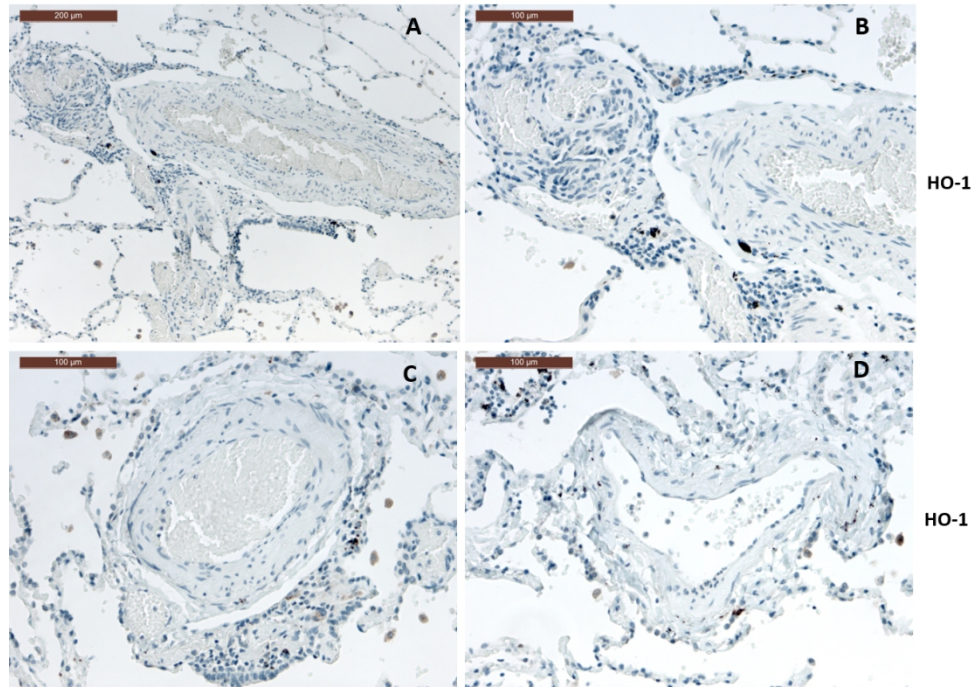


Figure E12: Analysis of HO-1 expression in PAH lung patients
HO-1 staining in lungs with pulmonary arterial hypertension. Pulmonary arteries (A, C) and pulmonary veins (B, D) do not express HO-1 staining is not found in lung explants of PAH patients.

369x253mm (96 x 96 DPI)

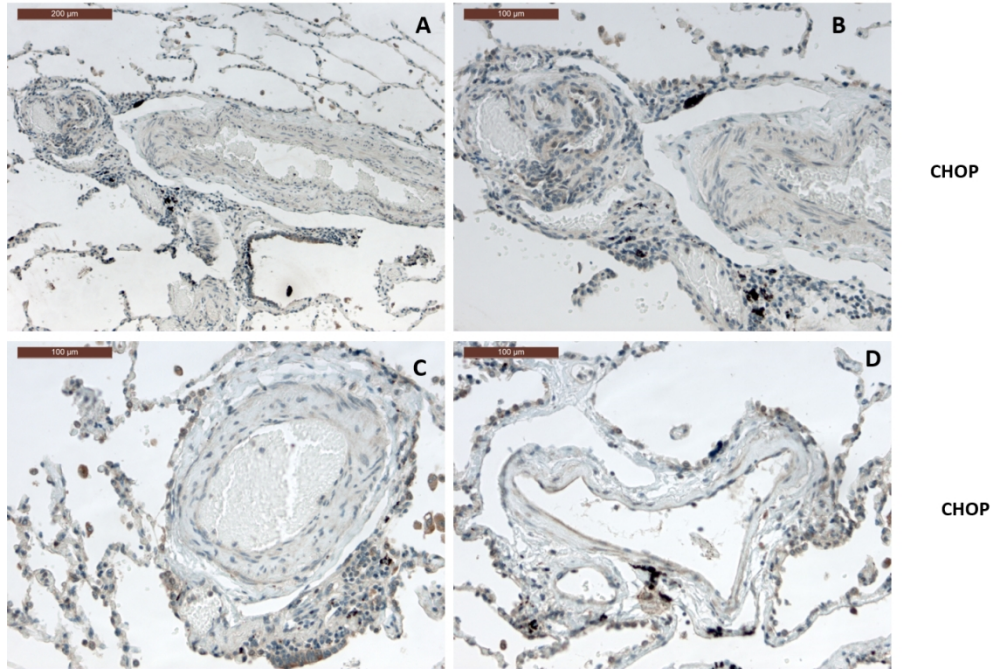


Figure E13: Analysis of CHOP expression in PAH lung patients
 DDIT3 (CHOP) staining in lungs with pulmonary arterial hypertension. Pulmonary arteries do not express DDIT3, while in plexiform lesion a very faint staining become visible within the endothelial cells (B). No staining is observed in small muscular arteries (C). A very faint staining is observed in endothelial cells of small veins (D).

375x251mm (96 x 96 DPI)

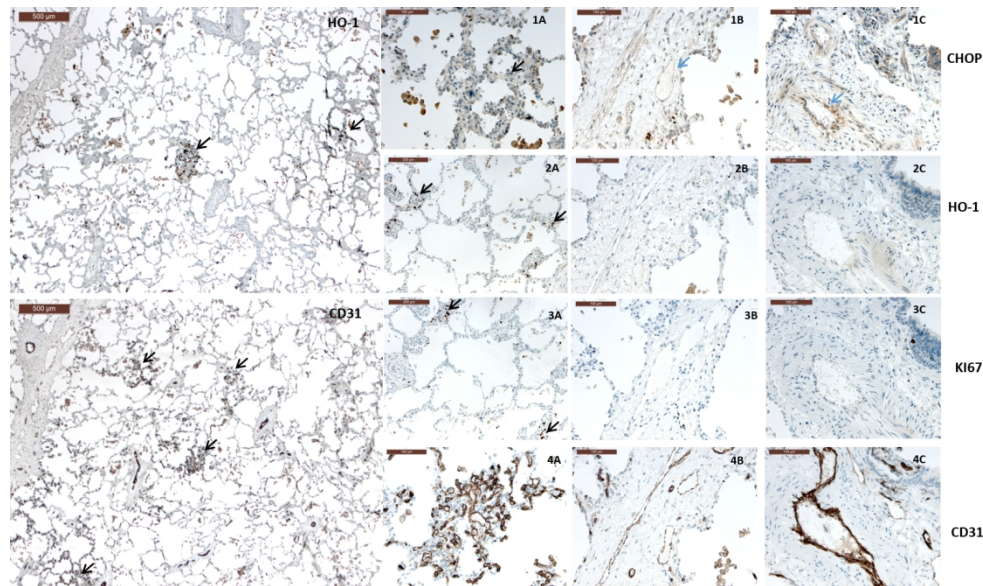


Figure E14: Analysis of Ki67, HO-1 and CD31 expression in sPVOD lung patients PVOD without EIF2AK4 mutation. DDIT3 (CHOP) staining in PVOD lung; endothelial staining is visible in both remodeled veins (1B, blue arrow) and arteries (1C, blue arrow). The staining becomes faint in smooth muscle cells whereas it is well observed in cytoplasm of bronchial cells, alveolar cells and macrophages (1A, 1B, 1C black arrows). HO-1 staining in PVOD lungs is observed in interstitial cells within alveolar septa in capillary hemangiomatosis foci (2A). The labelling is strong and highlights interstitial cells with cytoplasmic extensions. Outside these foci no staining is observed. The endothelial cells do not express HMOX. Ki67 staining highlights cells engaged in proliferation. Scant interstitial cells are labelled within capillary hemangiomatosis foci and in bronchial basal layer. CD31 staining underlines endothelial cells within alveolar septa (4A) and of pulmonary vessels (4B, 4C).

445x258mm (96 x 96 DPI)

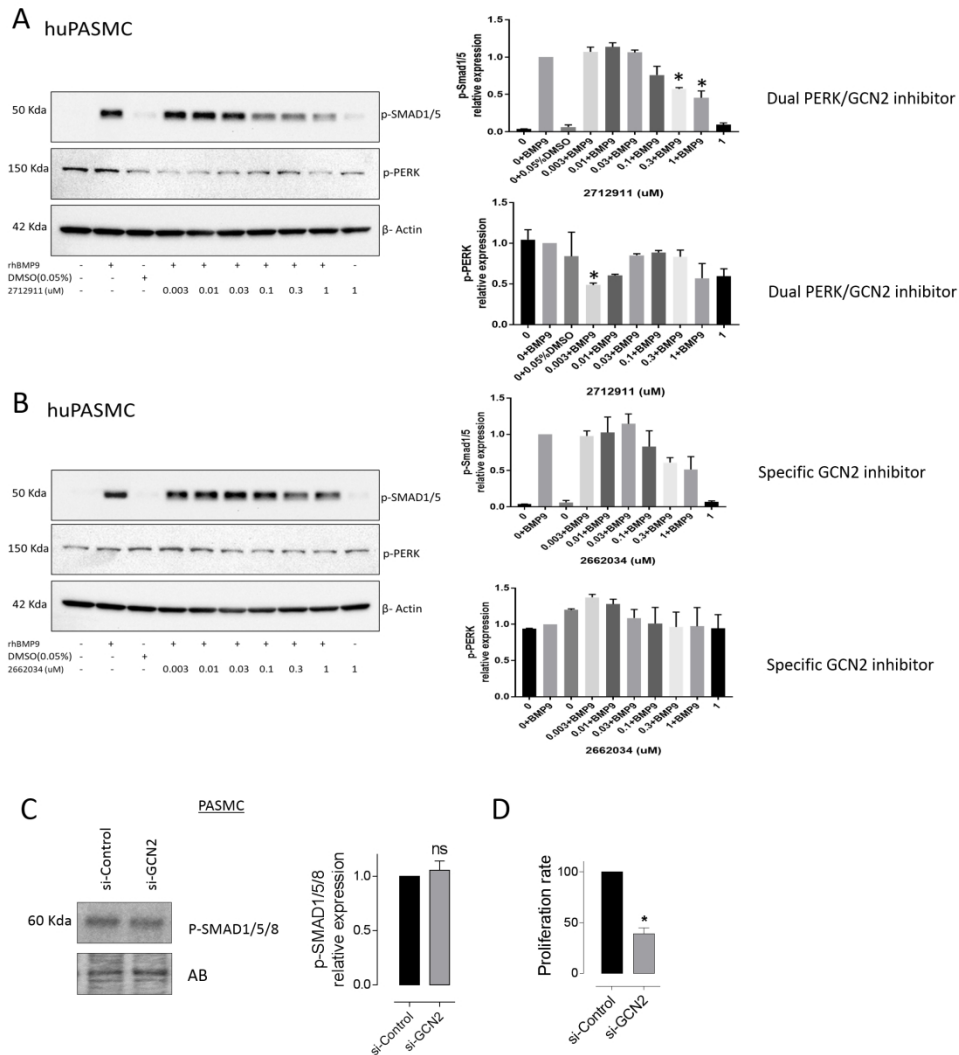


Figure E15: Effect of GCN2 and PERK/GCN2 dual inhibitor on BMP-9 signaling in huPASC cells. 2712991 is PERK/GCN2 dual inhibitor, 2662034 is GCN2 inhibitor. A, Effect of PERK/GCN2 dual inhibitor on BMP-9 signaling and PERK phosphorylation level in huPASC. B, Effect of specific GCN2 inhibitor on BMP-9 signaling and PERK phosphorylation in huPASC. C, Effect of siGCN2 on p-SMAD 1/5/8 phosphorylation in huPASC. D, Effect of siGCN2 on PASC proliferation. β -Actin (A, B) and Amido Black (C) was used as loading control. Right panels represent the quantification of the Western blots (Left panels). * $P < 0.05$.

615x665mm (96 x 96 DPI)

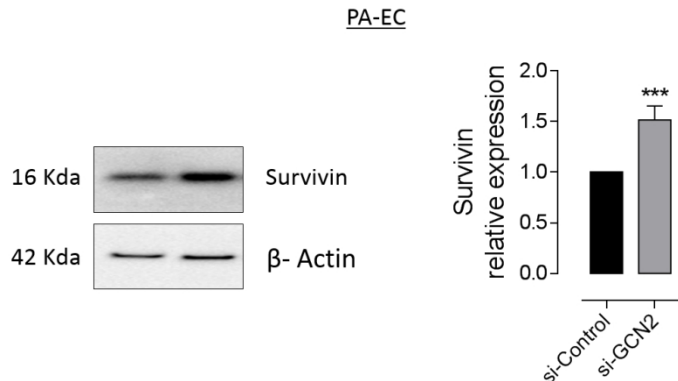


Figure E16: Knockdown of GCN2 in human pulmonary endothelial cells increases survivin expression. Consequence of GCN2 knockdown on Survivin expression in human PAEC (n=4)

388x162mm (96 x 96 DPI)

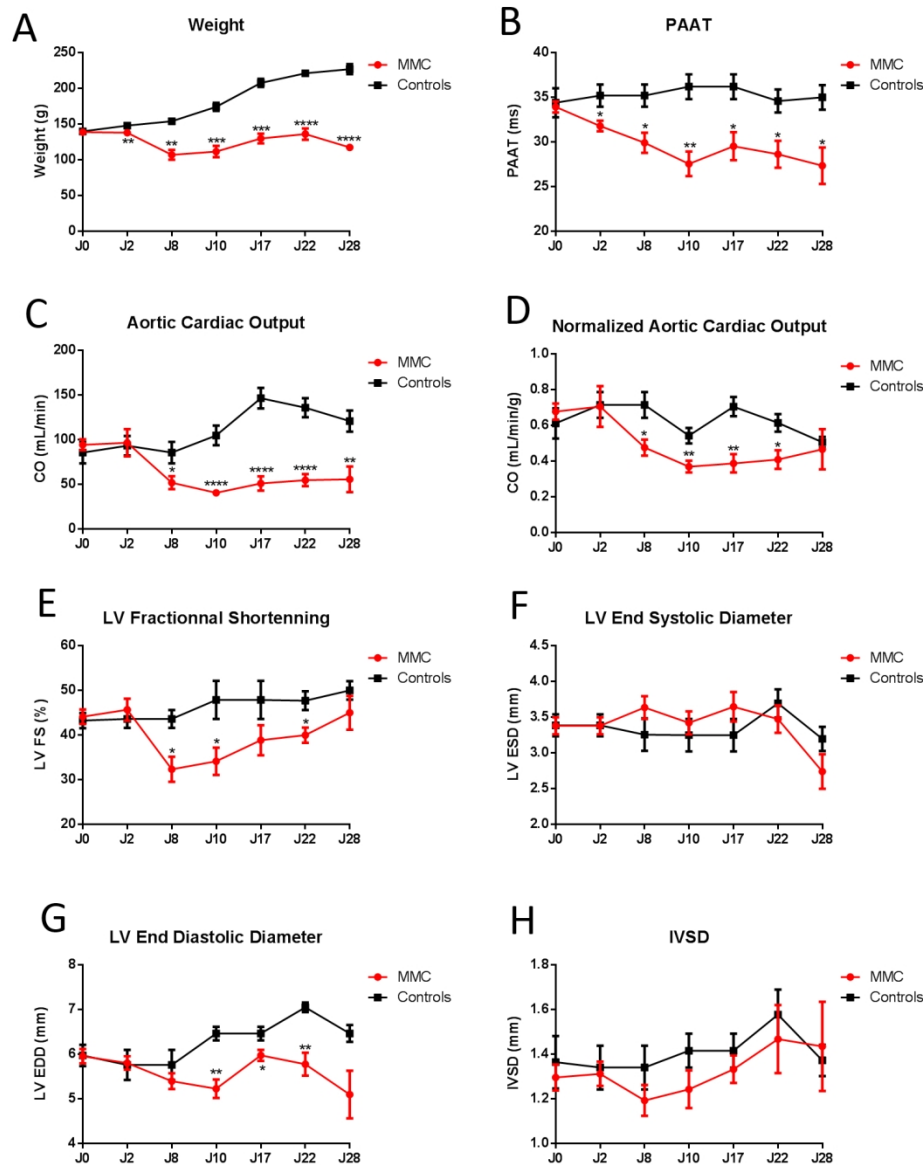


Figure E17: Effect of MMC on cardiac function in rats

Echocardiographic measurement of MMC exposed and control rats (J0, J2, J8, J10, J17, J22 and J28) of Weight (A), PAAT (B), Aortic Cardiac Output (C), Normalized Aortic Cardiac Output (D), LV Fractional Shortening (E), LV ESD (F), LV EDD (G) and IVSD (H).

Strikingly, PAAT was significantly lower in MMC exposed-rats as compared to controls, as soon as day 2 after the first MMC injection and remained lower for the whole follow-up. This was followed by a lower CO from day 8 to day 28. If normalized to the body weight, decreased CO was transient from day 8 to day 22. Interestingly, LVFS decreased following the same kinetic. Decreased LVFS was mainly attributable to lower LVEDD. IVSD was unchanged for the whole follow up indicating the absence of LV hypertrophy.

It has been shown that the use of echocardiography for assessment of cardiac anatomy, function, and hemodynamics can be consistently applied to the rat and replicates much of the information used routinely in human echocardiography. In this context, the LVFS are similar to those reported for healthy human beings (15). LVFS > 25% being the normal range, the LVFS values while decreased in MMC-exposed rat are not pathologic. Decreased CO could be linked to LV function alteration but can equally be attributed to right

ventricular dysfunction. Moreover, toxicities of chemotherapy like MMC can result in clinically significant diarrhea leading to hypovolemia, another relevant trigger of low CO. At last, cardiotoxicity of chemotherapy like doxorubicin are associated to dilated cardiomyopathy (16) that doesn't fit with the lower LVEDD we measured in MMC exposed rat.

423x533mm (96 x 96 DPI)

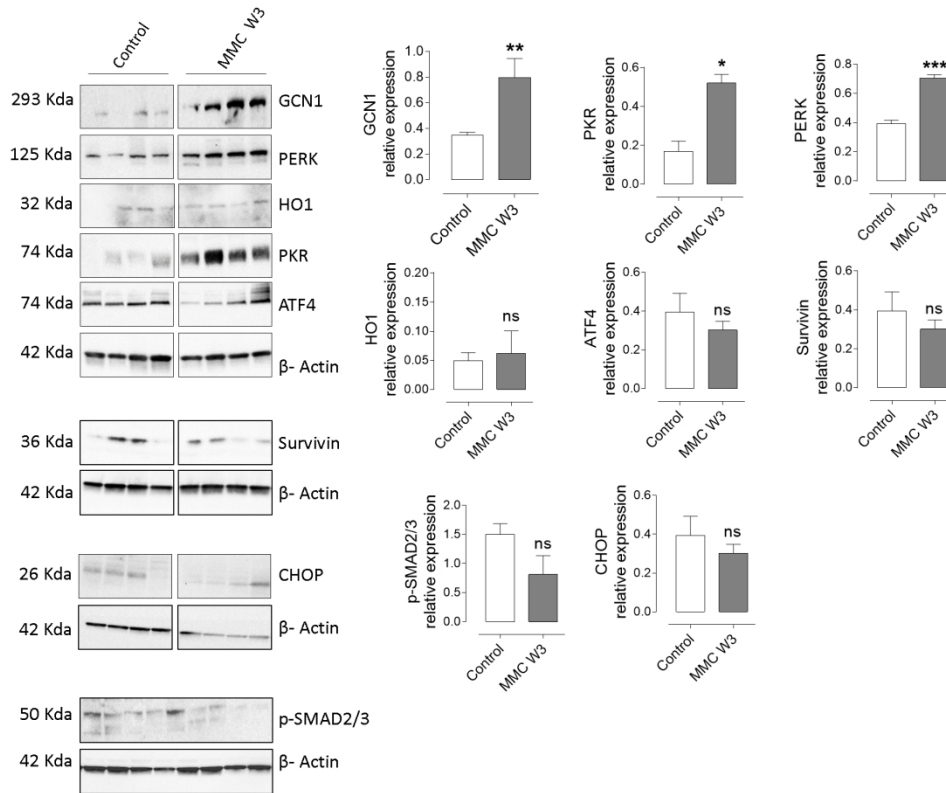


Figure E18: Pulmonary levels of p-P38, p-ERK1/2, PCNA, Survivin, GCN-1, PERK, HO-1, PKR, ATF4, CHOP, p-SMAD2/3 and Survivin in MMC-exposed rats.

A, Pulmonary levels of p-P38, p-ERK1/2, PCNA and Survivin expression in controls and MMC exposed rats (week 1, 2, 4 and 5). B Pulmonary levels of GCN1, PERK, HO-1, PKR, ATF4, CHOP, p-SMAD2/3 and Survivin in control and 3 weeks after MMC-exposure in rats. β -Actin was used as loading control. * $P < 0.05$ ** $P < 0.005$ *** $P < 0.0005$ **** $P < 0.0001$.

323x268mm (150 x 150 DPI)

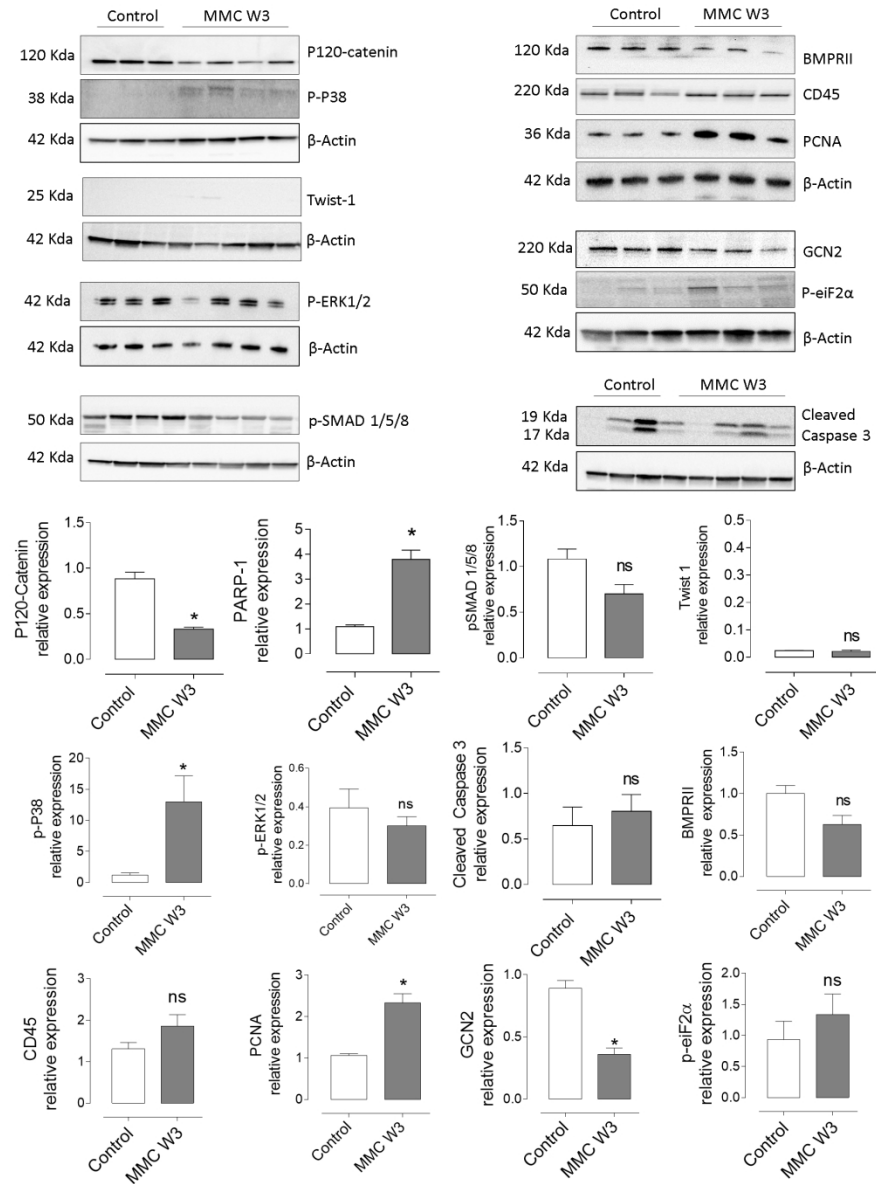


Figure E19: Pulmonary levels of P-120-Catenin, p-SMAD1/5/8, Twist 1, P-P38, p-ERK1/2, cleaved Caspase 3, BMPRII, CD45, PCNA, GCN2 and p-eiF2α three weeks after MMC-exposure. A, Pulmonary levels of P-120-Catenin, p-SMAD1/5/8, Twist 1, P-P38, p-ERK1/2, cleaved Caspase 3, BMPRII, CD45, PCNA, GCN2 and p-eiF2α in control and 3 weeks after MMC-exposure in rats. β-Actin was used as loading control. *P<0.05.

508x688mm (96 x 96 DPI)

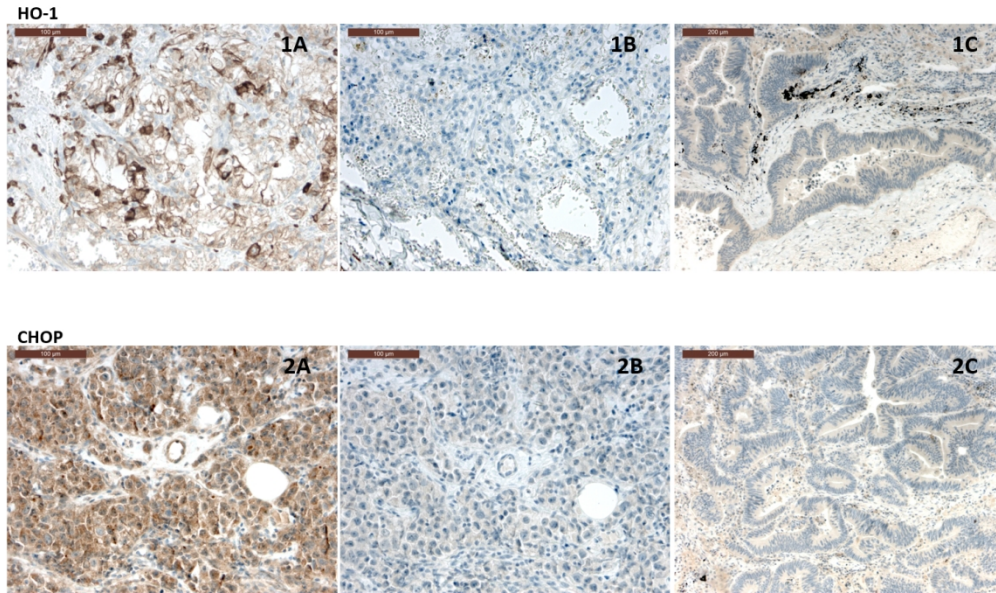


Figure E20: Positive and negative controls of HO-1 and CHOP in human lung patients. HO-1 positive and negative controls. HO-1 is expressed in membranes and cytoplasm of clear cells renal carcinoma (1A). The negative control has been performed on the same tissue by withdrawing the primary antibody (1B). HO-1 is not expressed in colorectal carcinoma [(1C) negative control]. DDIT3 (CHOP) staining appears strong within the cytoplasm of neoplastic cells (mediastinal seminoma (2A). Endothelial staining is visible in tumor associated vessels (arrow). Negative control has been assessed on the same tissue by primary antibody withdrawal. No staining is found in colorectal cancer tissue, we used as additional negative control (2C).

397x238mm (96 x 96 DPI)

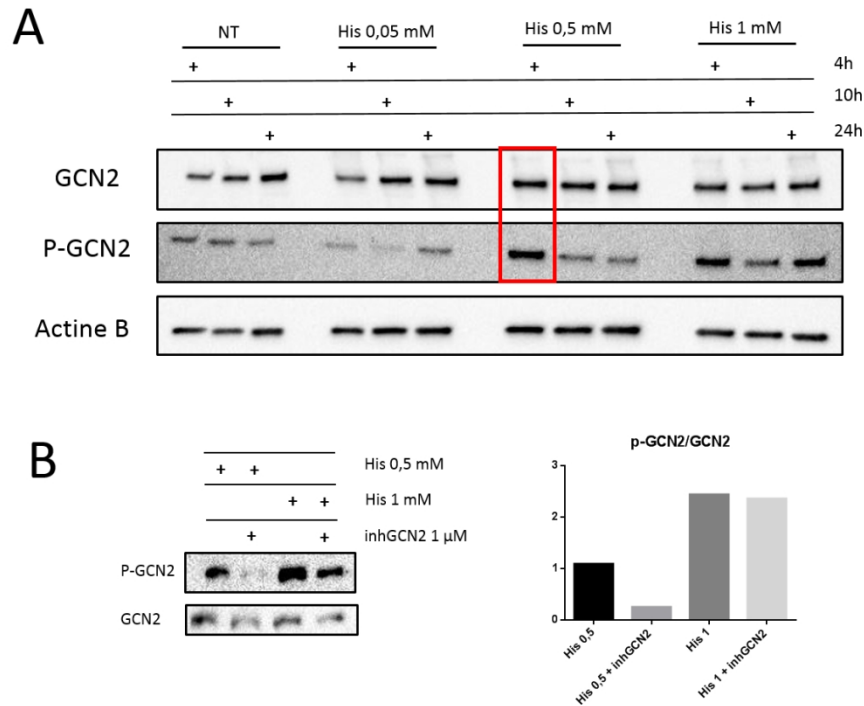


Figure E21: Determination of the histidinol concentration in in vitro experiments. Human PAEC levels of A, p-GCN2 (Thr 899) and GCN2 were analyzed by Western Blotting after treatment with several doses of Histidinol (0.05 mM, 0.5 mM and 1 mM) at several times (4h, 10h and 24h). β -Actin was used as loading control. B, p-GCN2 (Thr 899) and GCN2 were analyzed by Western Blotting after treatment with Histidinol 0.5 mM and 1 mM alone and co-treated with the GCN2 inhibitor 1 μ M (2662034) (left panel) with the quantification data (right panel).

350x267mm (96 x 96 DPI)